José Francisco da Silva Filho

EFEITOS DA ADIÇÃO DE Cr, Mo, Si E PARÂMETROS DE PROCESSOS NAS TRANSFORMAÇÕES DE FASES E PROPRIEDADES MECÂNICAS DE AÇOS BIFÁSICOS

Tese submetida ao Programa de Pós-graduação em Ciência e Engenharia de Materiais da Universidade Federal de Santa Catarina para a obtenção do Grau de Doutor em Ciência e Engenharia de Materiais.
Orientador: Prof. Dr. Carlos Augusto Silva de Oliveira
Coorientadora: Nina Michailovna Fonstein

Florianópolis
Julho de 2016

José Francisco Da Silva Filho

EFEITOS DA ADIÇÃO DE Cr, Mo, Si E PARÂMETROS DE PROCESSOS NAS TRANSFORMAÇÕES DE FASES E PROPRIEDADES MECÂNICAS DE AÇOS BIFÁSICOS
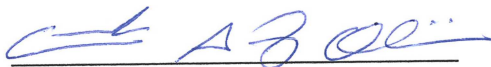
Essa tese foi julgada para obtenção do Título de Doutor em Ciência e Engenharia de Materiais, e aprovada em sua forma final pelo Programa de Pós-graduação em Ciência e Engenharia de Materiais da Universidade Federal de Santa Catarina.

Florianópolis, 19 de julho de 2016.

_____

Prof. Dr. Guilherme Mariz de Oliveira Barra
Coordenador do Curso
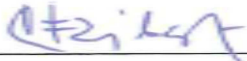
Banca examinadora:

_____
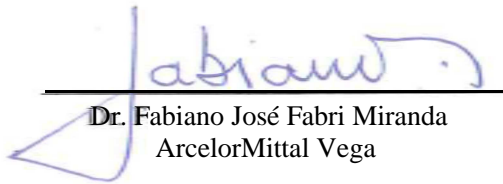
Prof. Dr. Carlos Augusto Silva de Oliveira
Orientador
Universidade Federal de Santa Catarina

Prof. Dr. Carlos Enrique Niño Bohorquez
Universidade Federal de Santa Catarina

Prof. Dr. Cesar Edil da Costa
UDESC/Joinville

Dr. Fabiano José Fabri Miranda
ArcelorMittal Vega

Prof. Dr. Kassim Shamil Fadhil Al-Rubaie
UNISOCIESC

Prof. Dr. Orlando Preti
UNISOCIESC

This work is dedicated to
GOD, Who drove and carried me on the
road of His own unique creation.
José Francisco da Silva Filho (2016)

RESUMO

Este estudo sobre os aços bifásicos (dual-phase) encontra-se alinhado com pesquisas voltadas para desenvolvimento do conhecimento sobre materiais e suas propriedades que relacionam com suas microestruturas e seus mecanismos de transformação. Em termos tecnológicos se alinha ao segmento de pesquisa voltado para a inovação dos materiais que objetiva aplicação com baixo impacto ambiental, racionalização dos recursos existentes e redução de custos.

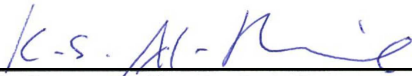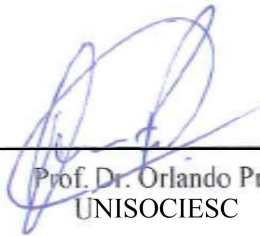Nesse sentido, foram analisados os efeitos do Cr, Mo e Si associados a diversas temperaturas de recozimento e os meios de resfriamento (ar e água) sobre as propriedades mecânicas e as microestruturas finais de aços bifásicos.

Os aços bifásicos caracterizam-se por uma matriz ferrítica macia contendo a estrutura martensítica dura (SPEICH, 1981).

Há um grande número de projetos com foco na elaboração de *design* de aços bifásicos nos diversos núcleos de pesquisa em todo o mundo, que visam a atender às restrições impostas pelas linhas operacionais, ora existentes.

Muitos trabalhos foram desenvolvidos neste sentido e, portanto, muitas dúvidas também surgiram. Desta forma, este estudo objetivou/avaliou os efeitos dos elementos Cr (0; 0,2; 0,4 e 0,6 %); Mo (0; 0,15 e 0,45 %) e Si (0 e 0,3 %) tratados em diversas temperaturas de recozimento e resfriados em dois meios (água e ar) nas propriedades finais dos aços. Isto resultou em 148 condições experimentais. Os resultados dos experimentos foram analisados quanto às propriedades mecânicas e microestruturais e permitiram esclarecer dúvidas e o melhor entendimento dos mecanismos de transformação.

O projeto de experimento para os aços deste estudo objetivou a geração de conhecimentos científicos específicos e tecnológicos aplicáveis em linhas operacionais existentes no Brasil e no exterior (Estados Unidos, França e Canadá).

A adição de cromo viabilizou a análise de seus efeitos, em solução sólida assim como carbonetos de cromo, na formação da austenita e, posteriormente, em sua temperabilidade (deslocamento da curva TTT para a direita e retardar a transformação da austenita em fases não-martensíticas indesejáveis). A adição de cromo afetou os mecanismos de transformação das fases resultando em uma microestrutura mais refinada e, consequentemente, propriedades mecânicas mais elevadas. O teor de cromo adicionado variou entre 0 e 0,6 % (em massa).

A adição de silício permitiu a análise de seus efeitos como refinador sobre a matriz e sobre o aumento da resistência mecânica do aço sem afetar, significativamente, a ductilidade. A adição de silício acelerou a nucleação e recristalização da ferrita além da transformação da austenita o que resultou no aumento da fração volumétrica de martensita. Ressalta-se que, em determinadas etapas do processo de produção dos aços, o silício apresenta efeitos deletérios como: i) altera a reatividade da superfície dos aços retardando o processo de decapagem; ii) deteriora a suas propriedades relacionadas à sua soldagem; iii) reduz a reatividade da superfície dos aços afetando negativamente a aderência do revestimento (quando galvanizado).

A adição do molibdênio aos aços inibiu condições (e.g. mobilidade da interface ferrita-austenita) que favorecem o crescimento da austenita (maior fração volumétrica), promoveu o refino da microestrutura, aumentou a temperabilidade da austenita durante o resfriamento e aumentou a resistência dos aços. Este elemento como tem sido utilizado nos atuais projetos de qualidade tornou-se a referência, neste estudo, para efeito de comparação.

As temperaturas de recozimento escolhidas cobriram a faixa de temperaturas utilizadas nas principais linhas contínuas em funcionamento no mundo.

Os aços laminados a frio utilizados para o tratamento térmico apresentaram, inicialmente, microestruturas complexas, composta por martensita, ferrita e perlita devido ao elevado teor de elementos de liga principalmente o manganês. Esta matriz "complexa" foi tratada termicamente visando produzir, predominantemente, uma estrutura bifásica final. As transformações das microestruturas iniciais ocorreram de "maneiras diferentes" em função das condições impostas (composição química e tratamentos térmicos).

Estas maneiras diferentes de transformação, causadas pela adição de Cr, Mo e Si associados aos tratamentos térmicos adequados, modificaram os mecanismos de reação o que permite vislumbrar rotas alternativas para a produção de aços bifásicos propriedades mecânicas adequadas e baixo custo, considerando as limitações físicas das linhas operacionais.

Estes conhecimentos contribuíram para viabilizar a produção deste grau aço em linhas de galvanização contínuas cujas taxas de resfriamento são moderadas (menor que 50 °C/s).

Palavras-chave: Aços bifásicos, Recristalização, Transformação de fases, Efeito de carbonetos de cromo, Efeito dos elementos de liga (Mo, Si e Cr).

ABSTRACT

The present study assessed the effect of Cr, Mo and Si in different concentrations under parameters of heating treatment and cooling media on the final microstructures and mechanical properties of dual-phase steels. The prior cold-rolled steels used in this study displayed a complex matrix composed of martensite, ferrite and pearlite which have transformed through different paths to produce a dual-phase structure (martensite + ferrite) with the appropriated mechanical properties. Additions of Cr, Mo and Si associated to specific heat treatments showed the ability to affect phase transformation and create an alternative lower cost routes. Numerous works have been developed in this area, but also some contradictions have been shown. Thereby, this study aimed to assess the effect of chemistries of steels Cr (0-0.6 %), Mo (0-0.45 %) and Si (0 and 0.30 %) heat treated on different annealing temperatures and cooled in two media (air and water). Final microstructures and mechanical properties of steels were analyzed for better understanding the mechanism and the paths of transformations undergone. The following results were observed: the investigated elements were shown to strengthen the steels through refinement and volume fraction, however by different ways. i) Cr has formed chromium carbides that supplied their interface for additional austenite grains nucleation (volume fraction) and; subsequently, many austenite in growing movement have caused collisions to each other, consequently, the restriction of austenite growth (refinement); ii) Mo increased the hardenability of austenite (volume fraction) and inhibited the movement of grains boundaries (refinement) and; iii) Si promoted higher carbon content in austenite more homogeneous by reducing its thermodynamic activity and enhancing hardenability; and (volume fraction). Besides, Si accelerated the ferrite recrystallization during heating, which in turn promoted the formation of austenite through the nucleation process, followed by grain growth.

Keywords: Dual-phase Steel, Recrystallization, Phase transformation, Chromium Carbides Effects, Mo-Si-Cr Effects.

LIST OF FIGURES

LIST OF TABLE

LIST OF ABBREVIATIONS

AHSS   Advanced high strength steel
APF   atomic packing factor
BAF   Batch annealing furnace
bcc   Body centered cubic
bct   Body centered tetragonal
CAL   Continuous annealing line
CCT   Continuous cooling transformation
CGL   Continuous galvanizing line
CTS   Cross tensile strength
Ceq   Equivalent carbon
DP   Dual-phase
FCC   Face Centered Cubic
FEG   Field-emission gun
HRC   Hardness Rockwell C
HRTEM   High-resolution transmission electron microscopy
HSLA   High-strength low-alloy steel
HSS   High strength steel
OM   Optical microscope
SEM   Scanning electron microscope
STEM   Scanning transmission electron microscope
TE   Total elongation
TS   Tensile strength
TS_M Tensile strength of martensite phase
TSS   Tensile shear strength
UTS   Upper tensile strength

LIST OF SYMBOLS

a   Area
a   Interatomic spacing
A   Atomic weight
Å   Angstrom
A_i Atomic weight of element
A   Lattice parameter: unit cell
α Ferrite
α' Martensite
at%   Atom percent
A_1 Eutectoid transformation temperature ($\gamma => \alpha + Fe_3C$)
A_3 Austenitic transformation temperature ($\gamma => \alpha + \gamma$)
Ac_1 Heating eutectoid transformation temperature ($\alpha + Fe_3C => \gamma$)
Ac_3 Heating austenite transformation temperature ($\alpha + \gamma => \gamma$)
Ar_1 Cooling eutectoid transformation temperature ($\gamma => \alpha + Fe_3C$)
Ar_3 Cooling austenite transformation temperature ($\gamma => \alpha + \gamma$)
B   Bainite
$[C]_M$ Carbon content within martensite structure
d   Interplanar spacing
Fe(Me)C   Carboneto de Ferro e Metal (Me)
f_N Function that describes the influence of the structure on the nucleation
G   Growth rate
K   Kelvin
k_1, k_2 Alloying parameters for each element
M   Amount of alloying element (M)
M_f Martensite Transformation Final Temperature
Ms   Martensite Start Temperature
n   Hardness Coefficient
Q_G Activation energy of nucleation
R   Gas constant
Rm   Tensile strength
$Rp_{0.2}$ 0.2 % offset yield strength
T   Tbsolute temperature (K)
T_s Austenite Start Formation Temperature
V_γ Volume fraction of the formed austenite
YS   Yield Strength
YS/TS   Elastic Relation
ΔT Overheating (T-Ac_1)
γ Austenite

INDEX

1 INTRODUCTION

The sustainability and the human impact on the Earth planet have been rendered discussions ever since long time ago. The issues are addressed in different directions sometimes economically and others environmental and social. Green et al. (2012) addressing it in the "triple bottom line" which include social, economic and environmental aspects, passed through the efficient use of materials, material life-cycle assessment and adequate material for support energy efficiency.

Under this context, advance of environmental and governmental laws has been pushing the automakers to continuously improve safety and fuel economy of cars with low cost. These requirements, consequently, affect design and material selection. The achievement of these goals requires a combination of high-tech materials, innovative design, advanced manufacturing processes and tight relationship among design engineers, manufacturing engineers and materials engineers (KRUPITZER & HEIMBUCH, 2005). Worldwide Institutes and research centers have been spending much effort to the development of new products leading to these goals. The AHSS group (Advance High Strength Steel) has shown to be one interesting solution, in this moment. Among the steels present in the mentioned group the class of dual-phase (DP) is one that fulfills a large amount of needs required.

High work-hardening rates in combination with excellent elongation provide to the dual-phase steels much higher formability especially with the feature of higher ultimate tensile strengths than conventional steels of similar yield strength. When compared to high-strength low-alloy steels with similar yield strength, DP steels exhibit higher initial work-hardening rate than conventional ones, higher ultimate tensile strength (UTS) and lower ratio of yield strength to ultimate tensile strength.

Advanced High Strength Steels are automotive and truck manufacturers interesting because they offer the potential for fuel economy increases through weight reduction, while maintaining an acceptable size and cost of product (DAVIES & MAGEE, 1979). Considering that the automakers are the major consumers of these advanced high strength steels and that dual-phase steels are one of the most popular among them due to their ease applicability in body-structure and body-panel applications in the last years, its importance is highlighted in this scenario.

34

2 OBJECTIVE

Literature review showed lot of efforts to find the better design of the highest strength steel to meet customers' requirements and overcome facilities restraints.

The structure-properties of dual-phase steels have been well studied; nevertheless some subjects still remain unclear; for example the effect of partial replacement of martensite by bainite, the effect of alloy elements such as chromium, molybdenum and silicon on phase transformation. Controversial discussion about the complexity of phenomena that occurs at intercritical annealing took place (interaction between recrystallization, grain growth and phase transformation) (OGAWA et al., 2010). The degree of such interplay depends firstly on the chemical composition of the steel, micro-alloying additions, for example, and processing parameters (HUANG et al., 2004; SOUZA et al., 1982).

Many researchers have carried out studies on Cr alloyed steel and observed that this element plays a very important role in dual-phase transformations associated with low cost comparing with its similar Mo. The use of Cr in the as-hot-rolled steel instead of Mo has been largely adopted (NASCIMENTO, 1981).

Molybdenum is useful element in dual-phase application since it acts as i) increasing the temperature for austenite grain growth, ii) a hardening element, iii) carbide precipitates former. However, during hot-rolled process Mo is a deleterious element in terms of increasing of demanded power for hot rolling.

Therefore, the global aim of this study was the understanding of the effect of chromium, molybdenum and silicon in association with process parameters like annealing temperatures and cooling rates on the mechanical properties and final microstructure of the designed low-carbon dual-phase steels. This study focused on the effect of such alloy elements on the transformation at heating (competition between ferrite recrystallization and austenite phase transformation) and the understanding of the additional mechanism through which the Cr hardens the steels.

The plan of investigation was developed on the basis of steels designed and latterly produced taking into account the chemical compositions, hot and cold-rolling processing, and heat treatment. Afterwards, mechanical tests and microstructures assessments were handled in the sense of bring about ideas to understand the

recrystallization phenomena and its competition with transformation ferrite/austenite (martensite) and correlation with mechanical properties.

The investigation came through the effect of chromium in 4 levels of concentration (0,0; 0.2; 0.4 and 0.6 pct. weight) followed by heat treatment at eight temperatures (720 – 860 °C); effect of Molybdenum in 3 levels (0,0; 0,15 and 0.45 %) heat treated at seven temperatures (720 – 860 ºC); and effect of silicon in 2 levels (0,0 and 0.3 %) heat treated at six temperatures (720 – 840 ºC). In this context the study brought out information about phenomena occurred under stated conditions and then found out answers for questions as competition between recrystallization and phase transformation and additional mechanism of austenite refinement.

The general objective is:
to analyze the effects of the additions of Cr, Mo and Si at different concentrations and heat treatment (temperatures of annealing) in phase transformations, recrystallization and mechanical properties of low carbon dual-phase steels produced in laboratory.

The specific objetives are:

1) to analyze the effect of chromium in 4 different concentrations (0,0; 0.2 ; 0.4 and 0.6 %) on the ferrite recrystallization and austenite transformation (overlapping);
2) to study the mechanism at which chromium strengthening the steels;
3) to analyze the effects of chromium, molybdenum and silicon on the morphology and distribution of martensite;
4) to analyze the effect of the silicon on the ferrite recrystallization (T_s and A_{e1});
5) to analyze the effect of holding temperature on the final microstructure and mechanical properties;
6) to reach a state-of-the-art in some specific steps of production of dual-phase steel;
7) to analyze the effect of molybdenum on the final microstructure and mechanical properties;
8) to analyze the effect of silicon on the final microstructure and mechanical properties;
9) to distinguish processes at heating all specimens after different annealing temperatures were water quenched to freeze microstructure developed;

10) to determine the effects of different elements on hardenability of austenite at cooling, the parallel air cooling was applied form the same temperatures.

3 LITERATURE REVIEW

3.1 INTRODUCTION

This chapter discusses the evolution of Advanced High Strength Steels contextualizing their characteristics and relationships with their applications.

The first mentioning of dual-phase steels as potential material for automotive application started with Hayami et al. (1975). At the beginning they considered the possibility by producing a dual-phase microstructure (ferrite plus martensite) based on cold rolled Mn-Si steel by heat treating it in the inter-critical temperature region, during a continuous annealing process. Steels with this microstructure showed higher strength associated with better ductility than the existing HSLA (High Strength Low-Alloy). Subsequently, Rashid et al. (1976) showed significant gain in ductility with no deleterious effect in tensile strength of dual-phase produced by inter-critical heat-treatment of HSLA vanadium alloyed. At that moment, the class of dual-phase steels appeared as a strong competitor of HSLA and to be used as high-resistances steel demanded for specific applications. Figure 3.1 displays the better properties (good performance during application since higher elongations were achieved with the strength) of dual-phase steels in comparison to HSLA.

Speich et al. (1981) studied dual-phase steels and defined them as a class of high-strength low-alloy steels characterized by a microstructure consisting of a dispersion of hard martensite particles in a soft and ductile ferrite matrix what results in some unique properties of this class:

i) continuous yielding behavior (no yield point);

ii) a low 0.2 % offset yield strength;

iii) a high tensile strength;

iv) a high work-hardening rate;

v) unusually high uniform and total elongation;

vi) high BH (baking hardenability) effect.

The high work-hardening of dual-phase steels contributes to the good formability whereas the absence of a yield point elongation eliminates Lüders band formation and assures a good surface finish after drawing. The high combination of strength, ductility and formability made them attractive for weight-savings application in automobiles.

The high level of strength results in high fatigue resistance and a good level of energy-absorption. During lasts decade cold-rolled dual-

phase steels have been successfully applied for structural and safety automotive parts as reinforcements, longitudinal bars (longerons) and traverse (crossbar); replacing and upgrading the class of HSLA steel due their characteristic of present lower yield point for similar tensile strength.

Besides relevant intrinsic characteristics of these materials, the majority of steels in this class of dual-phase present good feasibility and high yield when produced in conventional lines, what make them attractive commercially, then to the producers and inasmuch as an interesting material to be thoroughly investigated.

Figure 3.1– Uniform elongation as a function of tensile strength for standard HSLA steels and Fe-Mn-C dual-phase steel.
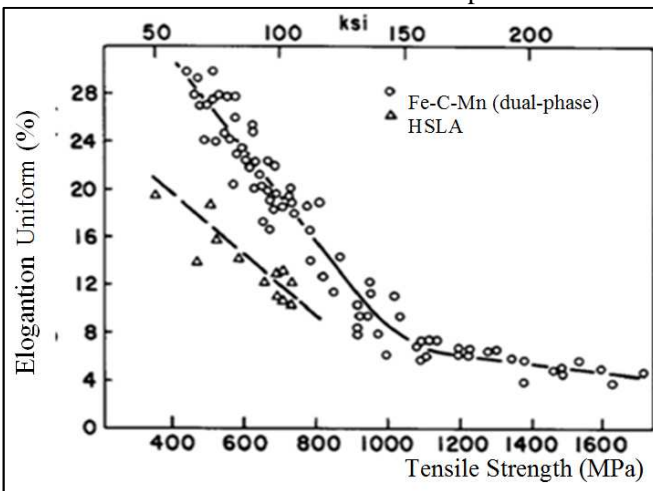
Source: DAVIES R. G., (1978).

3.2 DUAL-PHASE STEELS – DEFINITIONS, PROPERTIES AND APPLICATIONS

The dual-phase steel is a product of heat-treated steel (cold or hot-rolled), usually, with chemical composition of carbon between 0.08 and 0.15 %; manganese 1.0 to 2.5 % and others alloying elements like chromium up to around 0.5 %, molybdenum below 0.3 % and vanadium, sometimes silicon, niobium, aluminum and boron. Normally, the dual-phase microstructures as-cold rolled (before heat treatment) present a matrix composed of ferrite, pearlite, cementite and eventually

martensite. During heat treatment the microstructure of the onset matrix is subject to a sequence of dynamic transformations, what is the key to control the development of this steel grades with the desirable martensite/ferrite microstructure.

Speich et al. (1981) proposed the following sequence:

1) almost instantaneous nucleation of austenite at pearlite or grain-boundary cementite particles;
2) followed by a very rapid growth of austenite until the carbide phase is completely dissolved;
3) slower growth of austenite into ferrite at rate that is controlled by carbon diffusion in austenite at high temperature close to 850 °C and manganese diffusion in ferrite at low temperature (~750 ºC);
4) very slow final equilibration of ferrite and austenite at a rate that is controlled by manganese diffusion in austenite.

The final product presented the microstructure composed by, predominantly, ferrite and martensite and eventually small portion of bainite.

Bucher and Hamburg (1990) have proposed the ratio (r= austenite/ferrite) to reach a dual-phase steels of different tensile values strength for respective dual-phase: DP 590 (15 %), DP 780 (32 %), DP 980 (45 – 50 %) and DP 1180 (larger than 50 %), where austenite = martensite plus low bainite.

Pushkareva (2009) showed the following sequence of structural changing during the austenite to martensite transformation: Volume expansion during phase transformation from fcc austenite to bct martensite and the lattice invariant deformation accomplished by slip or twinning; which in turns introduce high density of dislocation and or fine twin. A critical amount of mobile dislocations is required to suppress the yield point elongation and this amount is produced by the fraction of transformed martensite (MARDER et al., 1981).

Pickler et al. (2000) proposed the best structure for dual-phase steel consisting of a mixture of ferrite and martensite obtained by using intermediate cooling rates; which result in the better relation of ferrite/martensite at a good carbon partitioning.

The properties of dual-phase steels are strongly related with final microstructure; which in turn are closely related to the characteristics of austenite formed in the two-phase field.

Figure 3.2 (banana curve) shows a comparison of dual-phase with others steel grades in terms of conventional elongation versus tensile

strength. Each family of steels is positioned according to its mechanical property which is in evolution with time and technologies. As earlier mentioned the aims of researchers, producers and users of steels have been to achieve a design of higher resistance associated to the higher elongation with low cost. It means moving curves upward to the diagonal direction in order to make the result, Rm x %A, the highest as possible (Figure 3.2). Dual-phase steels are well-positioned along the diagonal line and close to the class of TRIP steel. They are distinguished from the others due to the good compromise in high strength versus formability associated to its easy feasibility. This compromise comes up from the peculiar microstructures described earlier (hard phase martensite dispersed in a ductile ferrite matrix).

Figure 3.2 - Ductility-strength relationship of several high-strength cold-rolled steels; IF - interstitial-free; TRIP - transformation-induced plasticity; DP; PM - Partially Martensitic.
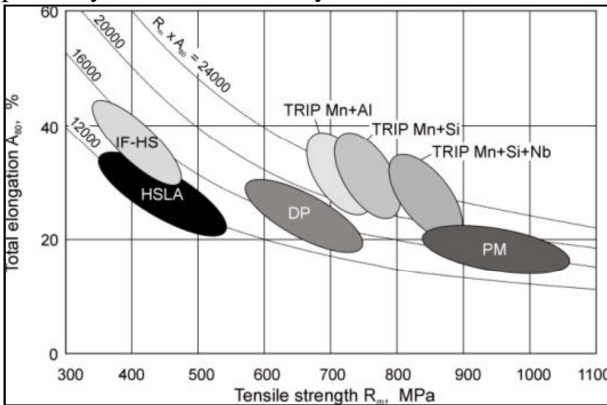
Source: BLECK et al., (2002).

Considering the good performance and acceptance of DP steels under applications by automakers some required properties are discussed in sequence.

3.2.1 Formability and Crashworthiness of DP Steels

Considering the importance of automotive industry as a consumer of steels of this class and their main requirement is the conformability, it is worth to know the behavior of dual-phase considering the importance of automotive industry as a consumer of steels of this class and their

main requirement is the formability, it is worth to know the behavior of dual-phase under mechanical loading (stamping).

Numerous studies have been presented results of investigations on the formability of dual-phase steel grades since the strength increases. Bending test is important for users in operation lines for structural parts; thus advanced high strength steels have to show good bendability.

The formability of a higher resistant dual-phase 980 was studied in comparison with a less resistant dual-phase 780 using a V-type bending test machine. Bendability results were similar due to the effect of refinement of microstructure of DP 980 which compensated the deleterious effect of resistance increases (Figure 3.3), (TAKAKURA & TAKAGI, 2005).

Figure 3.3 - Microstructure of (a) DP 780 and (b) DP 980.
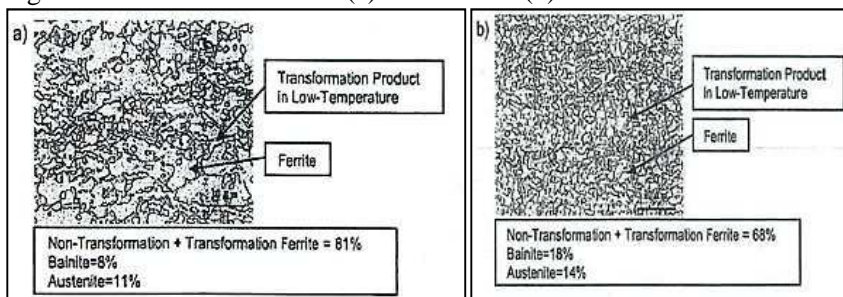
Source: TAKAKURA & TAKAGI, (2005).

Another important property for the steels with shock-resistant behavior is the mechanical crashworthiness that is measured through the collision absorbed energy (Energy absorption calculated as the area under the curve stress x strain).

Figure 3.4 displays the collision absorbed energy strain rate of different steel grades and their dependence on the static tensile strength measured at a low strain rate. The replacement of DP 780 by DP 980 resulted gain of absorbed energy around 40 MJm^{-3} (OSAWA et al., 2003).

Figure 3.4 – Relationship between tensile strength at a low strain rate and collision absorbed energy at a high strain rate.
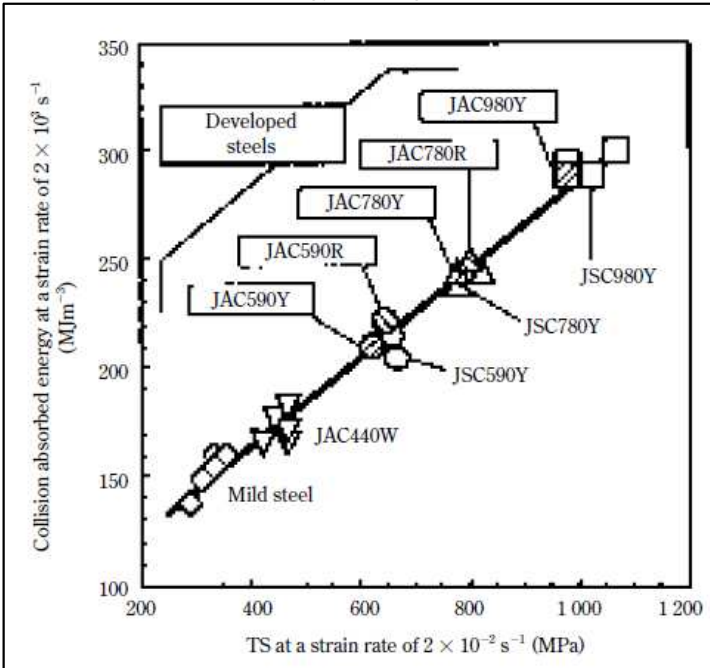
Source: OSAWA et al., (2003).

The absorbed energy was studied by using a drop weight test. Results obtained were important to explain weight reduction ratio as a result of application of the DP 980. Curves presented in Figure 3.4 show levels of absorbed energy for various thickness and DP grades.

Fracture of dual-phase steels is associated with either non-metallic inclusions (e.g. aluminum oxides and manganese sulphides) or martensite voids initiation mechanisms. Considering the enhancement of cleanliness of steels, the point turns to martensite-related void initiation effect (AVRAMOVIC-CINGARA et al., 2009; KRAUSS G., 2001). Void initiation at martensite occurs mainly by either the fragmentation of the martensite or decohesion at the ferrite-martensite interface mechanisms. Martensite fragmentation develops at low strains (3 to 5 %) whereas decohesion of the ferrite-martensite interface takes place at higher strains or even at the onset of plastic deformation (STEINBRUNNER et al., 1988; HE et al., 1984).

Study of micromechanisms of DP fracture observed that the preferential sites for void initiation are mainly associated to the martensite. Finally, it is observed that shear bands are responsible for the final stage of fracture by acting as nucleation sites for cracks (GARCIA O. L., 2013).

3.2.2 Hardenability

Hardenability is the capacity of steel in delay the time required for the decomposition of austenite into ferrite and pearlite (PORTER & EASTERLING, 2004).

Krauss et al. (2010) incorporated various factors in hardening and defined hardenability as "the capacity of steel to transform partially or completely from austenite to some percentage of martensite at a given depth when cooled under some given conditions". On the different view "hardenability is the transformation of austenite to martensite by preventing the diffusion-controlled formation of microstructures with lower hardness than martensite during quenching".

Figure 3.5 displays the effect of alloying elements and their amount on the hardenability (multiplying factor).

Figure 3.5 – Multiplying factors as a function of concentration of several alloying elements on steel.
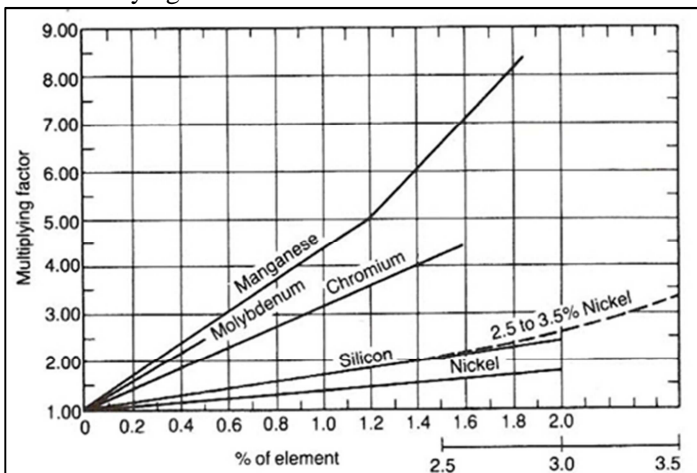
Source: KRAUSS et al., (2010).

3.3 PHASE TRANSFORMATION DURING PROCESSING AND MICROSTRUCTURE OF DUAL-PHASE STEELS

In the current study samples were undergone on several heat treatments (heating, holding and cooling) aiming to develop different microstructures and, consequently, mechanical properties related to the difference in phase transformations and recrystallization. Evolutions of microstructures associated with process conditions were analyzed to assist the development of hypothesis to explain part of the phase transformations. Therefore, a discussion on phase transformation is appropriate.

Rapid cooling of steel from the ferrite/austenite field, with no sufficient time for eutectoidal diffusion-controlled decomposition processes to occur, resulted in the steel transformation to martensite (heterogeneous reaction) – or in some cases martensite with few percent of retained austenite. In case of dual-phase steel a mixture of ferrite + martensite is predominately (PORTER & EASTERLING, 2004).

The main feature of obtaining this dual-phase (ferrite-martensite) structure in the prior, low alloyed carbon steels (usually ferrite-pearlite cold-rolled structured) is by heating up to inter-critical region where initial portion of austenite becomes substantially enriched by carbon which has the dominant effect on hardenability of austenite and retard transformations others then martensite.

Martensite is a diffusionless transformation product, i.e. transformation manner occur by associated movement of atoms called *military* (it means that from start to the end of the transformation individual atomic movements are less than one interatomic space). The martensite in steel is formed because of cooling rate is such fast that the majority of carbon atoms in solution in fcc γ-Fe remain in solution in α-Fe phase. Steel martensite is simply a supersaturated solid solution of carbon in α-Fe phase. The martensitic phase (α') is often in the shape of a lens and spans initially an entire grain diameter. Its structure depends on carbon content: i) low carbon (lath or lamellar); ii) medium carbon (plate or twinned).

The content of carbon in austenite in combination with the following cooling system (water-quenching, mist or gas cooling) will define whether the all austenite transforms to martensite or part of that transforms to "new ferrite" or/and bainite. Controlled heating-treatment and stoichiometric addition of alloying elements such Mo, Mn and Cr are usual to avoid transformation back to ferrite, bainite and pearlite (PORTER & EASTERLING, 2004).

Martensitic transformation as a displacive solid state structural and diffusionless changing, which is dominated in kinetic and morphology by deformation energy from shear dislocations. In a displacive transformation, atoms move organized in coordination with their neighbors named "military" reaction. Generally, this displaciveness can be described as a combination of homogeneous deformation and slip displacive ("shuffle"). In a diffusionless reaction atoms do not play any random movement or jump through the interface interphase, so the phase transformed has the same chemical composition, atomic organization and point defects of prior phase. Dislocations move conservativeness during martensitic reaction, therefore without generation or annihilation of point defects (COHEN & WAYMAN, 1981).

Martensitic transformation was described as the result of water-quenched of steel samples to below a particular temperature (about 220 °C) it is no longer possible to retain all of the original austenite. This is considering that the incubation time for bainite formation was too long as the temperature falls and preservation of austenite phase gets easier. When rapid quenching suppresses the diffusion processes necessary for the formation of cementite in the steel and the temperature continues to fall, the free energy can be reduced by transforming the iron solvent from the fcc structure. Iron tries to become bcc but it is distorted to bct by the super saturation of carbon that remains in solid solution. Austenite can transform to bainite and the martensite can decompose into ferrite and carbides. The bct martensite is a phase that does not appear on the phase diagram, because it is a metastable phase that readily transforms when held at temperatures above a couple of hundred degrees Celsius (MEYRICK et al., 2001).

Martensite can have within its structure defects (dislocations) and carbides precipitates (MIAO et al., 1993).

Microstructures of martensite were related with properties of steels. These morphologies and distribution of martensite on the structure of the steels affect their properties. Whether the structure presents martensite islands almost isolated in the ferrite matrix, dual-phase steel shows relatively low yield strength and yield ratio. Nevertheless, when martensite appears as a continuous network along the ferrite grain boundaries, the yield strength and yield ratio will increase. The ductility is related to the microstructure and morphology of martensite. Over-ageing or tempering process will impel the solute atoms diffusing to the phase interface, making the ferrite purer. Meanwhile, quenched martensite will be tempered, improving the

comprehensive mechanical properties. On the other hand, martensite without tempering has low ductility, which causes the increase of yield strength and decrease of ductility, even inducing brittle fracture. The morphologies of martensite have been mentioned by numerous authors such as i) martensite island, ii) massive martensite and iii) solid martensite. The martensite island usually shows smooth surface when investigated by scanning electron microscopy, but the morphology of massive martensite is complex due to higher hardenability (HAN et al., 2011).

Since quenched martensite has low toughness then its tempering is required to enhance such property, however the highest strength is only preserved by low-temperature-tempering (KRAUSS, 2010).

3.3.1 Transformation of Austenite at Cooling

Since the final structures of dual-phase steels are controlled by austenite transformation an overview of phase transformation of austenitic at cooling is relevant.

According to Bain (1945), the decomposition of the solid solution (austenite) does not begin instantaneously when its temperature is lowered to that at which, in time, it would transform, instead, there is a definite period of lag, which is presumably occupied by nucleus formation or the chance association of sufficient atoms of the new constituent to form a permanent crystallite. At any rate, this reluctance is very definite and constant for any particular austenite, and a degree of undercooling is possible which, quite necessarily, depends upon the rate of the cooling. These conditions of time and manner of arrangement interferer of γ/α interface formation (on the structure and properties) that affect the ferrite nucleation, which in determine final morphology of ferrite (YEN et al., 2011).

Porter and Easterling (2004) showed in Figure 3.6 the equilibrium diagram and discussed the step by step of partially transformation of austenite to ferrite, at various temperatures below A_3 after austenitization and quenching.

Figure 3.6 - Holding temperatures for steel.
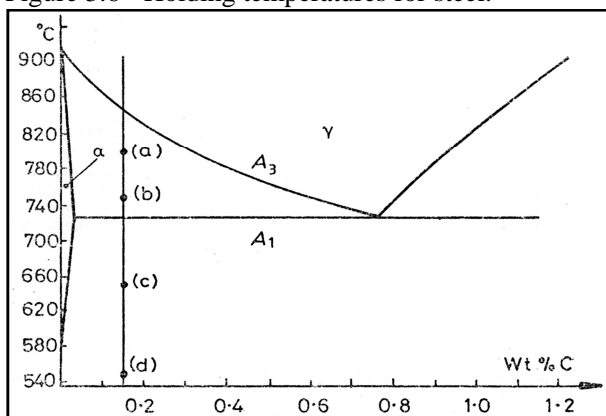
Source: PORTER & EASTERLING, (2004).

Figure 3.7 displays the resultant microstructures as a function of undercooling, where the grey areas are martensite that formed from the untransformed austenite (γ) during quench.

At small undercooling below A_3 the ferrite nucleates on austenite grain boundaries and grows in a blockey manner to form what are known as grain-boundary allotriomorphs (Figure 3.7 - a) At larger undercooling, there is an increasing tendency to ferrite to grow from the grain boundaries as plates, so-called Widmanstätten side-plates, which become finer with increasing undercooling (Figures 3.7 - b, c, d) (PORTER & EASTERLING, 2004).

Figure 3.7 also shows microstructure in smoothly curved due to incoherent interface; and faceted (planar) due to coherent (or semicoherent) interface.

At small undercooling, it is proposed that both incoherent and coherent interfaces move at similar rates creating equiaxed morphologies.

At larger undercooling, only incoherent interfaces can make full use of the increased driving force creating plate-like morphologies.

It can be seen in Figure 3.7 also that ferrite can precipitate within the austenite grains (intergranular ferrite). This precipitates are generally equiaxed at low undercooling and more plate-like at higher undercooling.

Other relevant point is the effect of austenite grain size on carbon concentration: i) in fine-grained austenite the ferrite that forms on grain boundaries will rapidly raise the carbon concentration within the middle

of the grains reducing the undercooling and making nucleation even more difficult; ii) in a large-grained austenite, it takes a longer time for the carbon rejected from the ferrite to reach the center of the grain and meanwhile there will be time for nucleation to occur on the less favorable intragranular sites.

Figure 3.7 – Microstructure of an alloy Fe - 0.15 % C. The specimens were austenitized, held at an intermediate temperature and then quenched to room temperature.
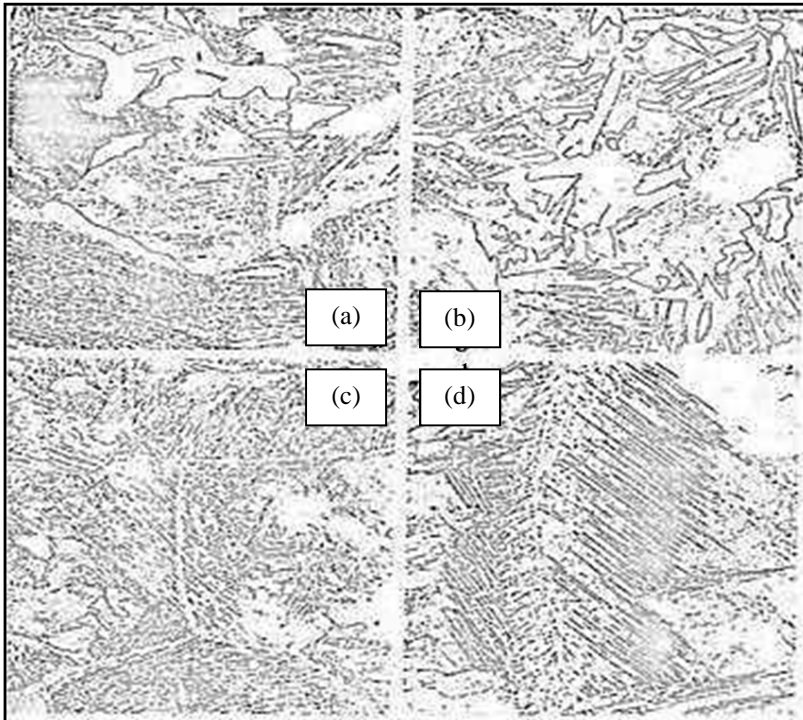
Source: PORTER & EASTERLING, (2004).

Pushkareva et al. (2009) observed that the ferrite formed from austenite during cooling (epitaxial ferrite = new ferrite) presented no structural interface between them (epitaxial and retained ferrite) but the new ferrite was an extension of the retained ferrite.

3.3.2 Transformation of Austenite from Ferrite + Pearlite at Heating

In continuous annealing line of any type the relatively fast heating of deformed cold-rolled steels takes place; especially if steels contain some elements retarding of recrystallization, austenite formation can differs – starting from either, recrystallized or non-recrystallized initial structure. This kind of competition was considered in some details (HUANG et al., 2004).

Transformation which occurs in non-recrystallized ferrite during ultrafast heating (> 1000 °C/s) leads to more refined grains (HUANG et al., 2004).

Studying C-Mn-Si steel, Yang et al. (1985) showed that the formation and distribution of austenite are strongly affected by the "ferrite recrystallization" and "rapid spheroidization of cementite in deformed pearlite". In this way, austenite forms initially at grain boundary of elongated ferrite, and after completion of recrystallization, on carbide in the ferrite matrix.

In time, the development of new technologies allowed the uses of equipment of more capabilities as faster heating and cooling with better performance; which in turns leveraged the changes in the concepts and design of steels.

Controversial explanations, in literature, are found for the mechanism of phase transformation and recrystallization. For instance, Huang et al. (2004) showed that austenite forms initially at grain boundary of ferrite; while Speich et al. (1981) proposed earlier a sequence at which austenite forms initially at pearlite or grain-boundary of cementite particles.

3.4 EFFECT OF CHEMICAL COMPOSITION ON STRUCTURE FORMATION AND PROPERTIES OF DUAL-PHASE STEELS

Considering that study is focused on the effect of chemical elements Cr, Mo and Si in the steels containing Mn, B, Al, P, Ti, Nb a discussion about the role of the elements is appropriate.

The primary aim of adding alloying elements to steels is to increase the hardenability. This allows slower cooling rates to produce more martensitic phases. Alloying elements can reduce the rate of austenite decomposition by reducing the "growth rate" or "nucleation rate" of ferrite, pearlite or bainite. Some elements are considered austenite stabilizers (e.g. Mn, Ni, and Cu) and ferrite stabilizers (e.g. Cr,

Mo, and Si) (PORTER & EASTERLING, 2004; SILVA & MEI, 1988). According to Aaronson et al. (1962) the "nucleation" delaying is caused by the presence of thin layer of precipitates of carbides, nitrides or carbonitrides formed and covering the austenite grain surface hence, inhibits temporarily the ferrite nucleation. The "growth" delaying is caused by i) partitioning of alloying elements which have low diffusion rates comparing to the carbon, then retard ferrite grain growth. (e.g. Mn, Ni, Pt) (AARONSON, 1962); ii) the segregation of alloying elements in the interface austenite/ferrite reducing C activity (AARONSON, 1966); iii) "solute drag effect" caused by inertia of interface for dragging the alloying elements to move itself (HONEYCOMBE, 1980; PURDY, 1978; SONG at al., 2004); iv) carbide partitioning which precipitates at grain boundary retarding ferrite grain growth; and finally v) combined mechanisms as the precipitation in the interface (γ/α) associated to solute drag resistance.

The alloying elements classified as ferrite stabilizers tend to restrict the austenitic field and raise the eutectoid temperature. The opposite occurs with the austenite stabilizers (NASCIMENTO, 1981). These effects on eutectoid transformation temperature and consequently on the austenitic field are shown in Figure 3.8.

Figure 3.8 – Effect of substitutional alloying elements on eutectoid transformation temperature.
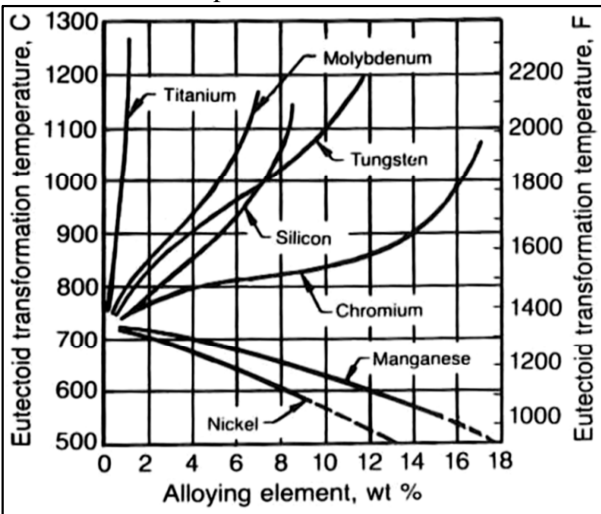
Source: BAIN, (1945).

The question is how come ferrite elements such as chromium, molybdenum, silicon (used in the design of these study), besides titanium, niobium, vanadium, zirconium, phosphorus are ferrite stabilizers and; in spite of shrinking the austenite region, they retard the austenite decomposition and favor more martensite transformation? Garcia et al. (1995) explained that this effect is due to the strong reduction on the diffusivity of carbon in austenite and by the partitioning of the elements within the product phases offering a strong diffusive drag on the phase transformations.

All these elements are substitutionally dissolved in austenite and ferrite. At the equilibrium, an alloying element will be partitioned between phases: carbide-forming elements such as Cr, Mo and Mn will concentrate in the carbide, while elements like Si will concentrate in the ferrite structures (PORTER & EASTERLING, 2004).

Figure 3.9 displays the effect of some chemical elements on the phase transformation during continuous annealing of advanced high strength steel (TRIP). The TTT diagram shows that, on cooling, the Cr, Mo, C and Mn push α-curve to the right side delaying the austenite to ferrite transformation. Inversely, Si, Al, P, V and Nb push the same curve to the left side accelerating the austenite to ferrite transformation. Both phenomena will affect hardenability, the first increasing and the second decreasing. Similarly, for bainite region C-curve can be pushed to the right side by addition of C, Mn and Nb, delaying austenite to bainite transformation (BLECK et al., 2002).

Figure 3.9 – Effect of chemical elements on the border of regions of phase transformation.
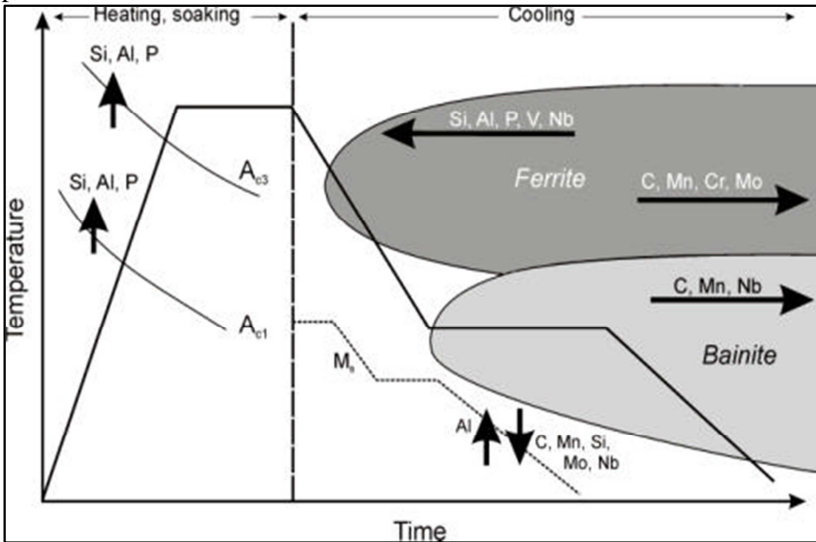
Source: BLECK et al., (2002).

According to Merck et al. (2001), the alloying elements cause the appearance of additional phases within the steels what includes alloy carbides and intermetallic compounds, thereby affecting the whole balance of the phases. These alloying elements can be divided into groups according to their propensity to form carbides.

Carbide Formers: these elements either do not object to the presence of cementite, e.g. Mn dissolves in cementite, or they form carbides themselves, e.g. Ti. They are ranked according to the stability of their carbides in the iron matrix.

Moderate carbide formers...Cr, Mo
Strong carbide formers...W, Ta, Nb
Very strong carbide formers... V, Ti, Zr

Graphite Stabilizers: some alloying elements dissolve in ferrite and thermodynamically prevent the formation of cementite. This enhances the formation of graphite, the reason they are called graphite stabilizers (e.g. Si, and Ni).

Bain et al. (1945) studied the partitioning of the elements between ferrite and carbide and observed that Si, Ni, Al and much of the Mn in the steel were dissolved in the ferrite regardless of the C content, however, Ti, V and Nb were combined in the carbide phase, as far as the

excess of C permits. Sundry elements occupied the intermediate position. Chromium was somewhat dissolved in ferrite even with high carbon, while only a moderate portion of Mo, Ta and W was found in ferrite under similar conditions.

Considering the relevant effect of alloying elements on the steel hardenability, it is worthy note the understanding how does the element is incorporated in the steel.

When the addition of alloying elements affect the structure of steel, the enhance in strengthening is more effective than when does not affect the structure but only keeps dissolved as solid solution in ferrite (BAIN et al. 1945).

Meyrick et al. (2001) mentioned that the alloy element cannot directly raise the hardenability whether it is not dissolved within the austenite, but it might, indirectly, lower it. The elements present in low alloy steels primarily for increasing the hardenability are: Cr, Mo, Ni, Mn and B; being Mo and Cr carbide formers.

During production of dual-phase steels in industrial lines which have the disadvantage of restricted cooling rates, the use of alloying elements also play beneficial role. To overcome the mentioned disadvantage stoichiometric addition of alloying elements have been practiced, nevertheless with balancing for reaching (low cost; availability, strategy, etc.). Alloying elements such as Cr, Mo, Mn and V are used to enlarge the window work and allow feasibility of facilities.

The alloying elements change thermodynamic stability of the phases and the kinetics of transformation whereby the transformation temperatures are shifted, the transformations are either promoted or hindered and the phase distribution is altered. Additionally, the elements might act as solid solution or precipitation hardeners and affect the grain size. Figure 3.10 shows that, among the elements below at 1 % addition, Mn and Si are more effective in higher the tensile and yield strength, values, nevertheless balancing of all of them are practiced since other properties are also desirable (IRIE, 1981; MEYRICK et al., 2001).

Figure 3.10 – Effect of alloying elements on tensile and yield strength of cold rolled.
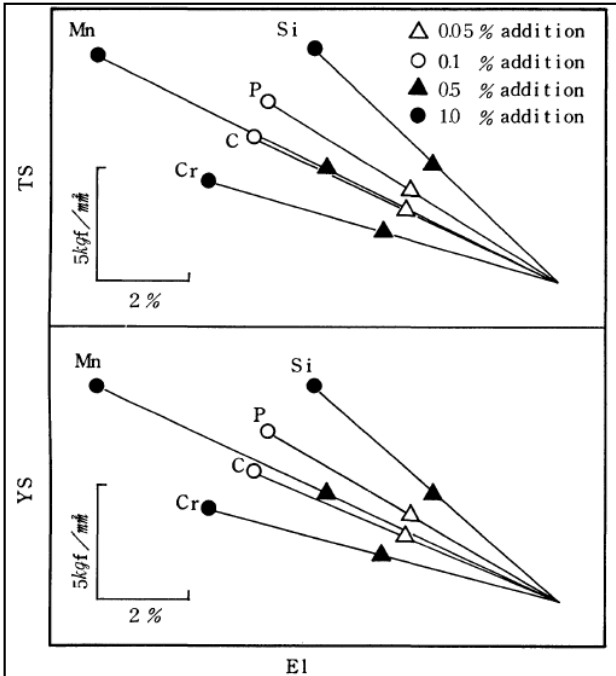
Source: IRIE, (1981).

The effect of chemical composition on final properties of dual-phase steels is also explained by their impact on:

a) critical points that define the fraction of austenite at given temperatures.

b) grain sizes of ferrite and martensite due to effect on recrystallization of deformed matrix and following grain growth.

c) intrinsic properties of ferrite due to solution or precipitation hardening.

Studies have been performed to show the effect of chemical elements on the kinetics of transformation at heating to two-phase region.

A pioneer study conducted by Speich (1981) showed that the Mn and C are elements which enrich and control the austenite phase formation. It means that for any inter-critical temperature the amount of austenite will increase with carbon content in steel and consequently the amount of martensite.

Alloying elements on dual-phase steels must have the 3 main features to be suitable:

    i)   it should not cause a solid solution hardening in ferrite;

    ii)   it should delay the points of start and finish bainite (favoring the austenite to martensite transformation);

    iii) it should be an austenite forming element which promotes the partitioning of C between austenite and ferrite resulting in a decrease in the carbon concentration of ferrite (TANAKA et al., 1979)

3.4.1 Effect of Carbon

In continuous annealing lines the process speeds are extremely high what demand significant low levels of carbon in solid solution to prevent steels from premature natural aging. So, carbon must be precipitated somehow. One way is the presence of MnS (greater than 0.05 µm) which behave as preferential nucleation sites of Fe_3C during the overaging step (HAYASHIDA, 1994).

Carbon is considered as the main alloying element by which all transformations are noticeably affected and, by which the final microstructure and the mechanical properties are controlled. Carbon stabilizes the austenite leading to the formation of martensite in the case of dual-phase steels and to the retention of austenite in the case of TRIP steels. However, other requirements for steel applications such as weldability and coatability limit the use of carbon to around 0.2 mass % (BLECK et al., 2002).

Fonstein and Girina (2005) showed that steels with different amounts of carbon and annealed at the same temperature at inter-critical region, resulted in a different volume fractions of austenite ($V\gamma$), and consequently, different amounts of martensite after direct quenching (Figure 3.11). The amount of carbon in martensite $[C]_M$ affected tensile strength like: the increase of 0.20 to 0.44 % of carbon in martensite (respectively for steels of 0.10 % and 0.22 % C at V_M=50 %) resulted an increase in tensile strength of low tempered martensite from 1300 to 1900 MPa.

For one given inter-critical temperature, the amount of austenite will increase with increasing carbon content in steel, becoming 100 % at a carbon content corresponding to the $\gamma/\alpha+\gamma$ boundary.

Figure 3.11 - Fe(Me)C diagram illustrating various [C] - content of carbon in austenite depending on different alloying at the same temperature of annealing.
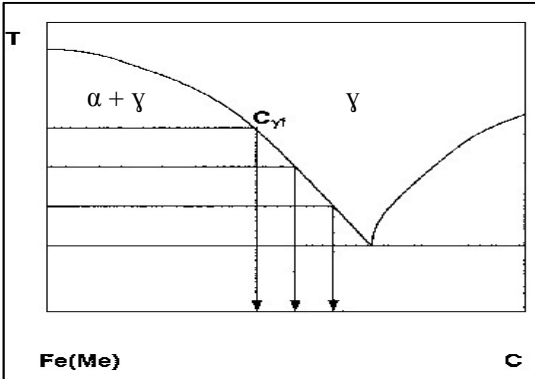
Source: FONSTEIN & GIRINA, (2005).

The increase in carbon content of steel from 0.09 to 0.12 % led to an increase in both tensile and yield strength (Figure 3.12 and 3.13), however without any significant deterioration of the strength-ductility balances (Figure 3.14). Evidently these changes resulted in the increase in YS/TS ratio (Figure 3.15) (affects the structure and mechanical properties of cold-rolled dual-phase and TRIP steels. Changes in carbon contents from 0.09 to 0.12 % led to an increase in both tensile and yield strength (POTTORE et al., 2006).

Figure 3.12 - Effect of carbon content in the steels on tensile strength.
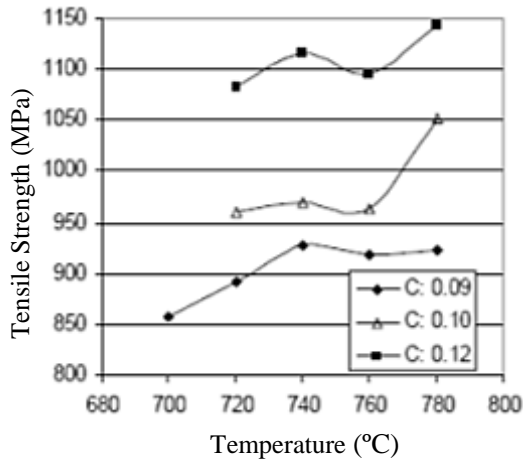
Source: POTTORE et al., (2006).

Figure 3.13 – Effect of carbon content in the steels on yield strength.
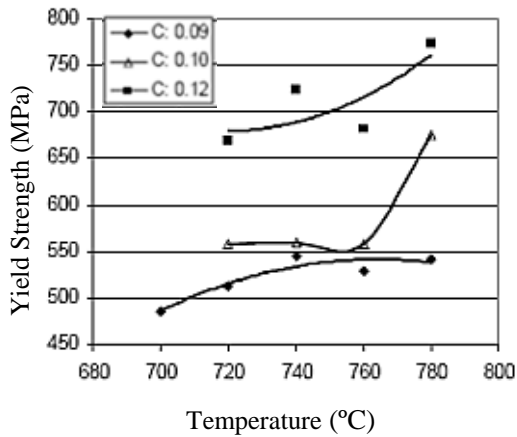
Source: POTTORE at al., (2006).

Figure 3.14 - Effect of carbon content in the steels on the total elongation/tensile strength ratio.
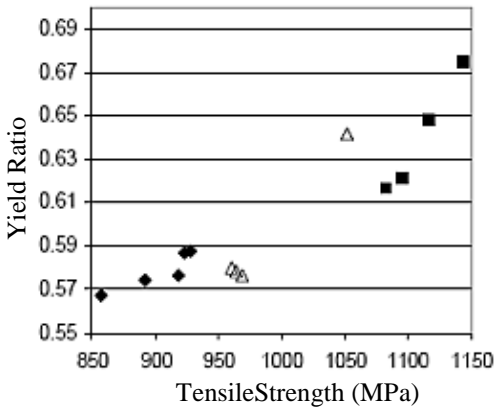
Source: POTTORE et al., (2006).

Osawa et al., (2003) showed that carbon favors fracture in the grain boundary, thereby low carbon martensite enhances the ductility of steels because of cracking of the martensite particle or de-cohesion of the martensite/ferrite interface becomes more difficult.

3.4.2 Effect of Silicon

It has been known that the addition of Si in high strength steels, dual-phase steels in particular, is very effective in improving the balance of strength and ductility through critical changes in the microstructure. On the other hand, Si oxide on the steel surface causes deleterious effects such as bare-spot of coating layer and delays galvannealing reaction (reaction between Fe and Zn to form zinc coating) (HIRONAKA et al., 2006).

Hironaka et al. (2010) showed that the addition of 0.01 to 1.6 mass % Si to the dual-phase steels affected significantly their mechanical properties and microstructure. Tensile and yield strength increased with increasing Si content, however tensile increased more than the yield strength, thereby decreased the YS/TS ratio, Figure 3.15. However, the decrease of uniform elongation with Si content increasing was very small; as a result, tensile strength and total elongation balance were improved. The improvement in of tensile strength and total

elongation balance by Si addition was due to the increase of work hardening rate.

Figure 3.15 – Effect of silicon content on the tensile x yield strength.

High Si (1.2 % Si) steel exhibited higher work hardening rate than low Si (0.01 % Si) steel in all strain region due to the effect of Si on retarding the formation of dislocation cell structures during tensile deformation. Furthermore, high Si steel exhibited increasing ratio of dislocation density in ferrite during tensile deformation larger than low Si steel. These abilities of Si on retarding the formation of dislocation cell structures and increase the ratio of dislocation density in ferrite makes the work hardening increases; which in turn improves the balance tensile strength x total elongation (HIRONAKA et al., 2010).

A controversial effect of Si on martensite volume fraction was observed in studies of Hironaka et al. (2010) and Nouri et al. (2010) as shown in Figures 3.16 and 3.17, respectively.

Figure 3.16 – Effect of silicon content on the volume fraction of martensite.
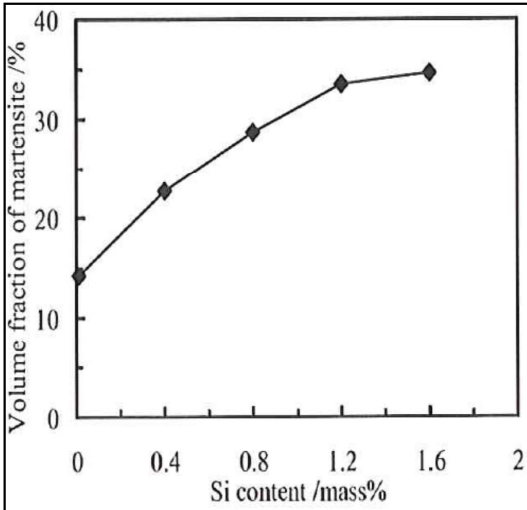
Source: HIRONAKA et al., (2010).

Some authors also explained the effect of Si on acceleration of ferrite recrystallization to the initial structure (CABALLERO et al., 2001; MOHANTY et al., 2011).

Pottore and Fonstein (2004) studied the effect of silicon on the Hole Expansion (HE) value. HE represents the ability of steel to resist the initial cracking (fissures) during strain deformation. It is expressed by the relation between strengths of ferrite and martensite. This element acts on decreasing the disparity of strength between ferrite and martensite through the strengthening of the ferrite via solid solution.

Speich (1981) studied the effect of Si on the hardenability of austenite through the acceleration of polygonal ferrite that rejects carbon to austenite. Silicon as a ferrite forming element can be preferentially partitioned to the ferrite phase during inter-critical annealing and during slow cooling it accelerates the polygonal ferrite formation. It also minimizes carbide precipitation, enabling austenite retention until room temperature. In the equilibrium diagram, silicon acts on widens the α+γ phase field (HUANG et al., 2004).

As mentioned before, Nouri et al. (2010) observed an opposite effect of silicon with respect to the formation of martensite when studying C-Mn steel with addition of 0.34 to 2.26 % Si. Their study showed the reduction of volume fraction of martensite with silicon

content in the steel (Figure 3.17). The explanation comes from the ferrite effect of Si which increases the Ac_1 and Ac_3 temperatures pushing up the intercritical region ($\alpha + \gamma$), which in turns will increase the volume fraction of ferrite at a given annealing temperature, and consequently lowering the volume fraction of austenite (martensite) (NOURI et al., 2010).

Figure 3.17 - Variation of volume fraction of martensite with silicon content.
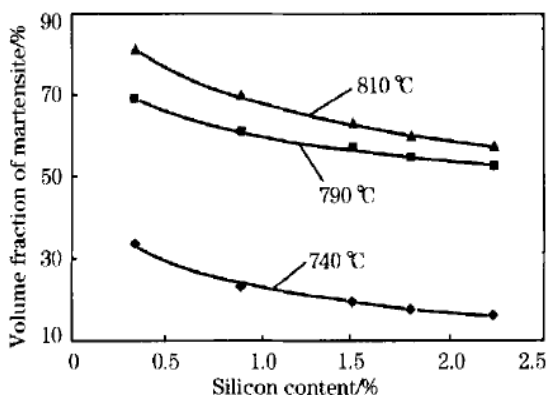
Source: NOURI et al., (2010).

Silicon inhibited the formation of cementite due to its low solubility at this stage. The kinetics of nucleation and growth of carbides become controlled by diffusion of silicon what delays the reaction of precipitation. It allows the austenite to enrich in carbon, and consequently, increases its thermodynamic stability. On the other hand, Si showed detrimental effect on surfaces characteristics (slivers, poor wettability) that deteriorated also coatability of steels (SOUZA et al., 2009).

3.4.3 Effect of Chromium

In the last years Cr becomes rather a traditional element in the alloying of coated dual-phase steels replacing Mo, partially (NASCIMENTO, 1981).

The austenite pools are favored to form, firstly, at regions of localized Cr concentration (alloying element) which improves the

hardenability of the austenite. Addition of 0.5 % of Cr to dual-phase steels suppressed the yield point elongation (% YPE) even at low cooling rates (MARDER et al., 1981); what is positive for dual-phase producers since high cooling rates demand very expensive equipment.

Maalekian et al. (2007) observed the tendency of Cr and Mo to precipitate in high volume fraction in ferrite, since their solubility in austenite is very high.

Figure 3.18 displays the effect of Cr as ferrite stabilizer, thus shrinks the austenite field (FONSTEIN, 2015; KRAUSS, 1995; BAIN, 1945).

Figure 3.18 – Effect of chromium content on size of austenite field.
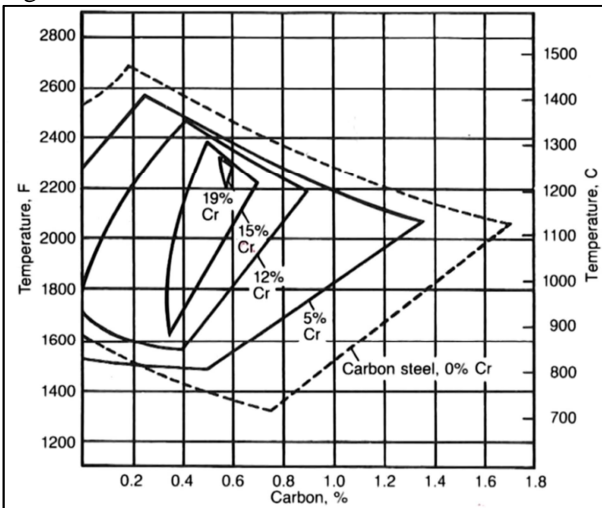
Source: BAIN, (1945).

Pickering et al. (2000) mentioned Cr not as a ferrite strengthener but as an additional alloying that contributes to improve hardenability of dual-phase steels by the retarding transformation reactions of austenite to pearlite and bainita. Consequently, it increases the hardenability of the remaining austenite even at slow cooling rates.

According to Inamura et al. (1977), Kato et al. (1981) and Bramfitt et al. (1981) the Cr in steels, at levels below 8 %, acts as an austenite stabilizer delaying the critical temperatures, therefore, extending the available time for partitioning of C from ferrite into the austenite, hence increasing the hardenability. Cr attracts C and reduces the activity of C for diffusion process (ZHUKOV & KRISHTAL, 1975).

Goldenstein et al. (1978) explained that Cr affects the cross-diffusion coefficient of a ternary alloy steel (Fe-C-Cr) through the retarding of C diffusion in austenite, and consequently the enhancement of austenite hardenability.

Lee et al. (2004) proposed an empirical expression (equation 10) for explaining the way that Cr affects the carbon diffusivity (D) in austenite through the terms of diffusivity coefficient (Do) and the activation energy (Q).

However, the effect of Cr on activation energy (Q) is much higher than on the diffusion coefficient (Do) which favors the increases in carbon.

$$D = \{0.146 - 0.036C \ (1 - 1.075Cr) + \Sigma K1M.\left[\exp - \ (\frac{144.3 - 15C + 0.37C^2 + \Sigma K2M}{RT})\right]\}$$

(10)

Where:

D = carbon diffusivity (cm^2/s)

Do = [0.146 – 0.036C (1-1.075Cr) + $\Sigma k1M$] = Diffusivity coefficient

Q = $-144.3 - 15C + 0.37C^2 + \Sigma k2M$ = Activation energy of carbon diffusion in austenite

M = amount of alloying element (M)

R = gas constant

T = absolute temperature (K)

K_1, K_2 = alloying parameters for each element

Lee et al. (2004) studied the influence of Cr addition on the mechanical properties of two advanced high strength steels. Table 3.0 summarizes the Cr effect on the mechanical properties.

Table 3.0 – Effect of Cr addition on the mechanical properties of AHSS

	Cr-Free		0. 4 % Cr-Addition	
	TS (MPa)	YS (MPa)	TS (MPa)	YS (MPa)
Steel 1	817	505	990	425
Steel 2	838	486	1066	436

Addition of 0.4 % Cr increased the tensile strength but decreased the yield strength with reduction in elongation. Cr also increased the volume fraction of martensite in expensive of retained austenite. Cr

stabilized ferrite at the inter-critical annealing temperature and consequently the austenite (equilibrium). Afterwards, during transformation the austenite hardenability was enhanced by the diffusion of C atoms from ferrite to austenite. Thus, at fast cooling rate, most austenite was transformed to martensite and atoms of carbon were pinned inside martensite (LEE et al., 2003).

According to Meyrick et al. (2001) carbides formers like Cr and Mo also lower the Ms temperature and would be expected to enhance the driving force for transformation. Presumably, these alloying elements cause changes in media, which make the non-martensitic transformation more difficult. It is not obvious what these changes are, but it is possible that their presence affects the initiation sites.

Fonstein et al. (2006) observed that addition of 0.4 % Cr to DP steel facilitate the carbides spheroidization.

Chromium as carbide precipitates increases the strength by means of precipitation strengthening. Secondary chromium carbides pin the grain boundaries and inhibit the grain growth. This results in the grain refinement and the presence of second phase particles also makes dislocation movement more difficult. Second phase particles like chromium carbide in the matrix increases the energy required for elastic/plastic deformation, hence creating higher strength in the alloy (RAZZAK, 2011).

In some cases, when sufficient quantity of alloying elements such as Cr are present in the steels, the solubility limit exceeds and some phases other than cementite may form. Small additions of Cr to Fe-C alloys at 890 °C maintain the cementite structure, M_3C (M standing for a combination of chromium and iron atoms); larger additions cause the M_7C_3 carbide to form; and still larger additions produce the $M_{23}C_6$ carbide (KRAUSS, 1995).

Figure 3.19 shows the effect of Cr on increasing tensile and reducing yield strengths.

Figure 3.19 – Effect of Cr content in the associated with cooling rate on mechanical properties.
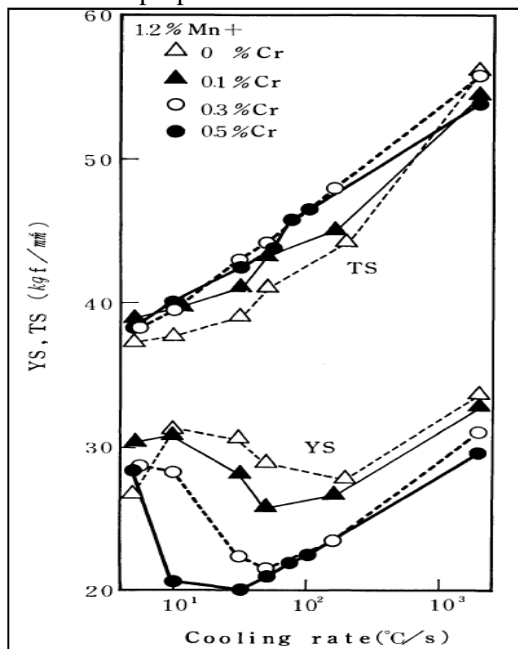
Source: IRIE, (1981).

3.4.4 Effect of Manganese

Manganese is an element that plays a very important role on the hardenability of γ-phase.

Leslie et al. (1961) and Huang (2004) developed studies focused on the effect of Mn in steels. It delayed the growth of new recrystallized grains due to solute drag on migrating boundaries. Mn prevented pearlite formation, decreased M_s and retarded bainite formation. Increasing the concentration Ac_1 moves down, and volume fraction of austenite increases for the same temperature of inter-critical annealing. Figure 3.20 shows the increase in total elongation for the same strengthening with the addition of Mn in the steel.

Figure 3.20 - Relationship between total elongation and tensile strength in medium-C-Mn-Si-Al steels.
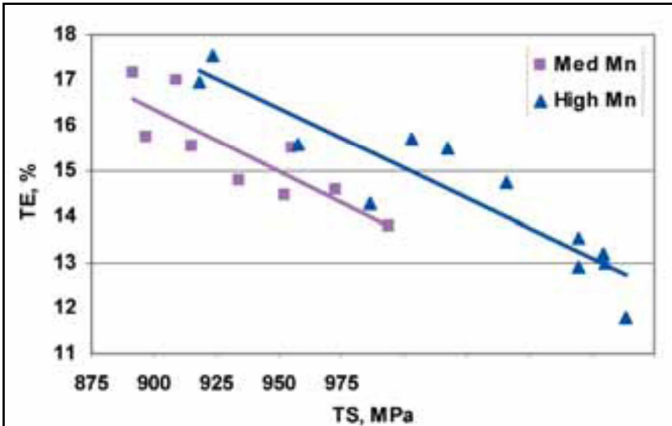
Source: POTTORE et al., (2006).

Mn decreases the Ar3-temperature and stimulates the formation of low-temperature constituents (massive ferrite and bainite). Its ability in strengthening steels comes through both mechanism solid solution and transformation hardening. Despite these good characteristics, Mn can drop the spot weldability, deteriorate galvanizing properties of surface and become negative influence on texture when concentration is above 2.5 %. Therefore, whether the steel application requires deep-drawability properties then addition of Mn has to limit to below 1,5 % weight (WATERSCHOOT et al., 1999).

Speich et al. (1981) showed that the additions of 1.5 % Mn to a plain carbon steel, under equilibrium conditions, lower the solubility of carbon from 0.2 to 0.05 percent (at 760 °C).

Based on phase equilibrium in the ternary Fe-Mn-C system the austenite enrich in both C and Mn if true equilibrium is achieved during inter-critical annealing. Beneficial effect of Mn is also attained when it is added to steels to smooth out the negative effect of Al on temperatures of phase transformations.

Manganese influences the kinetics of austenite growth:

i) at low temperature (~750 °C), Mn diffuses in the ferrite (or along grain boundaries) and controls the rate of growth of austenite into ferrite.

ii) the final balance between austenite and ferrite is controlled by Mn diffusion in austenite.

iii) The control of the austenite growth by Mn diffusion in the ferrite at low temperatures implies that Mn enrichment of the austenite phase may occur.

Manganese carbide is not found in steels, but instead, as an element Mn enters readily into solid solution in Fe_3C.

Addition of 1.8 % manganese promotes the attainment of optimal mechanical properties in terms of lower yield strength, reasonable total elongation, and enhanced hole expansion coefficient (hole expansion is an ordinary test in the industry used to measure the ability of steel to resist to the initiation and propagation of cracks from the border of a punched hole).

Manganese is added to steel to improve the machining performance by ensuring that all the sulphur is present as MnS rather than FeS, which causes hot shortness (cracking) during hot working. The MnS inclusions deform plastically during chip formation into planes of low strength which facilitate deformation in the primary shear zone. The MnS inclusions also exude into the tool-chip interface, acting as a lubricant and also forming a protective deposit on the tool. The net effect is a reduction in cutting forces and temperatures and a substantial reduction in the tool wear rate (LLEWEUYN & HUDD, 1998).

3.4.5 Effect of Phosphorus

Waterschoot et al. (1999) discussed the relevance of finding a satisfactory equilibrium between Si, P and Mn when both strength and formability targets must be achieved. In spite of, individually, P has no effect on texture. Combined addition of Si to P and Mn steels results in a stronger γ-fiber.

3.4.6 Effect of Molybdenum

Molybdenum is known as an effective element used for suppressing pearlite transformation without preventing the formation of polygonal ferrite during the continuous cooling and, consequently develops a microstructure appropriate for the dual-phase steels (SPEICH, 1981; HAN, 2010; HAN et al., 2010). Mo also is added to the low-alloy carbon steels to attain better combinations of strength, toughness, fracture resistance, fatigue resistance and wear resistance (KRAUSS, 2010). However, Mo is not always a desirable alloying element due to its negative effect on hot rolling (increase in necessary loads) and some scrap separation issues (GIRINA & FONSTEIN, 2005).

As shown in Figure 3.21 Mo delays the growth of newly recrystallized grains retarding the recrystallization. It is due to the Mo ability to drag the solute during migrating boundaries (LESLIE, 1961; HUANG et al., 2004).

Figure 3.21 – Effect of molybdenum on delaying the kinetic of recrystallization for any temperature.
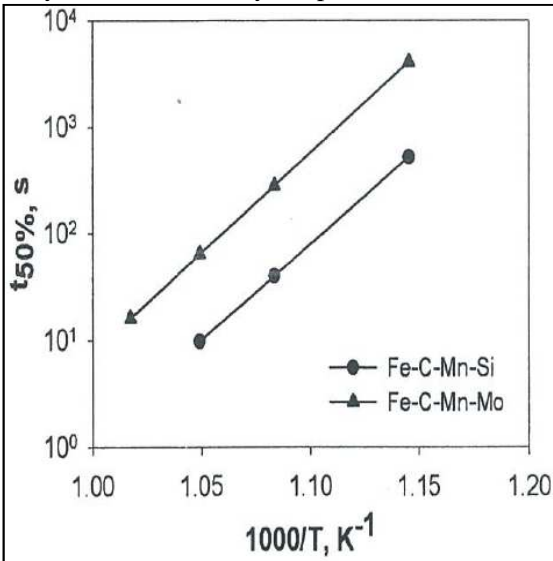
Source: HUANG et al., (2004).

Molybdenum interacts with carbon reducing the diffusion rate of C into austenite, so affects phase transformation. Another possible contribution could be the Mo segregation to the ferrite/austenite interfaces reducing the migration rates of those interfaces (MEYRICK, 2001).

Krauss (2010) observed that Mo retards the formation of pearlite and bainite during the cooling since its diffusion coefficient in austenite is low. It is explained because Mo is an element that tends to concentrate in ferrite and carbides phases, whose formation requires Mo diffusion.

Molybdenum in the steel promotes interaction between heterogeneous atoms such Fe, C as well as alloying elements what changes the phase stability (microstructures) and favors the appearance of new stable phases. The origin of these changes is the difference in

atomic structure, atomic size and crystal lattice between Mo and C or others alloying elements (Han et al., 2010).

Sun and Yong (2010) observed the following effects of Mo on the steels: Mo retards the pro-eutectoid ferrite transformation allowing the transformation of acicular ferrite and bainite; which in turn improve the strength and toughness of low-alloy low-carbon steels. Also acts on increasing the solubility of micro-alloying elements (Ti, Nb, V) in austenite and retarding the precipitation of micro-alloying carbonitrides, so that more micro-alloying elements can be preserved at relatively low temperature and then precipitated from ferrite, which can result strong precipitation hardening effect. Mo delays the recrystallization of austenite and expands the areas of non-recrystallization of austenite in the rolling process. It also occupies a fraction of lattice sites of micro-alloying precipitated from ferrite to form precipitates with chemical formula of (M, Mo) (C, N) (M is the micro-alloying element). This can increase the volume fraction of precipitates and refine their sizes, so its precipitation hardening effect is improved remarkably.

According to Sun and Yong (2010), Mo delays the process of precipitation of carbides and nitrides, because as-dissolved in austenite it reduces the activity of microalloying, C and N, increases their solubility product and decreases the supersaturation of precipitation and the driving force of nucleation of precipitates. Thus, more microalloying elements are held and precipitates during ferrite transformation. The precipitates in ferrite are small and hold semi-coherent relationship with neighboring ferrite, resulting in a greater strengthening.

Pottore et al. (2006), studied the effect of Mo on the mechanical properties of cold-rolled dual-phase steels with base composition 0.08 % C, 1.6 % Mn, 0,0020 % B. They concluded that Mo led to the increasing of the tensile and yield strength values especially at lower gas-jet cool temperature (Figure 3.22 a and b); increased the total elongation (Figure 3.23) and no evident effect on the yield/strength ratio (Figure 3.24).

The expression "gas-jet cool" was used by authors to describe a system of cooling in which "air is sprayed at surface of strip steel by a set of nozzles".

Figure 3.22 - Effect of Mo addition on strength of steels (a) tensile and (b) yield.

(a)

(b)
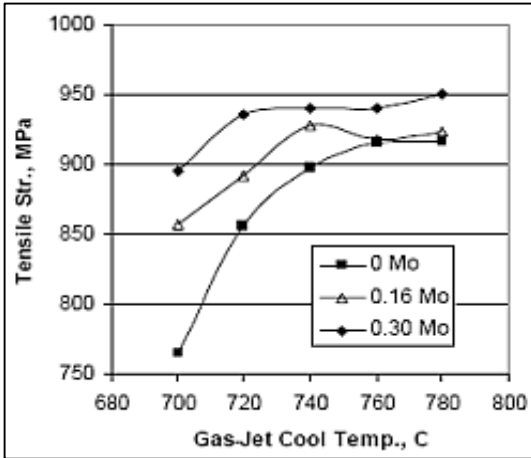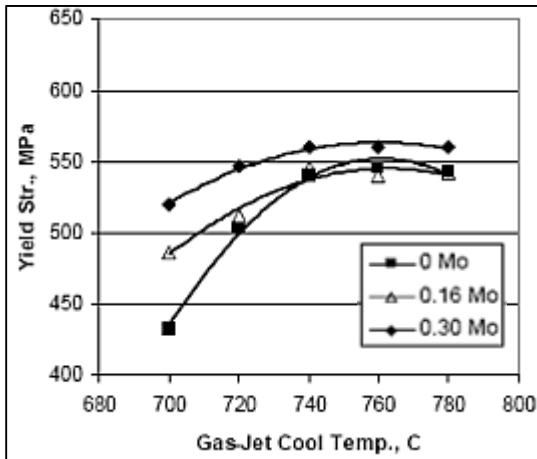
Source: POTTORE et al., (2006).

Figure 3.23 - Effect of Mo addition on balance of total elongation vs. tensile strength.
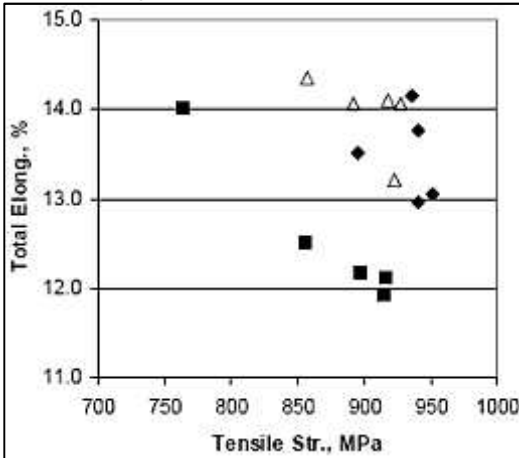
Source: POTTORE et al., (2006).

Figure 3.24 - Effect of Mo addition on the ratio of yield strength to tensile strength.
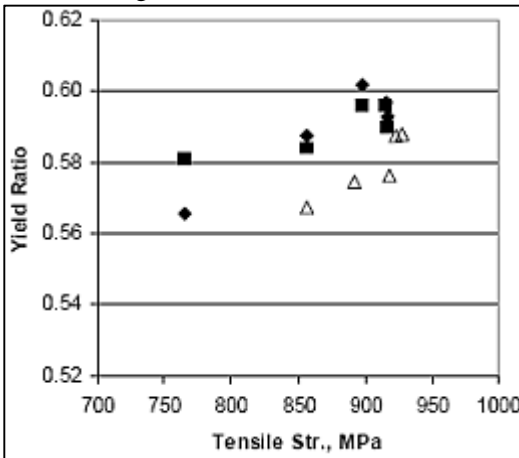
Source: POTTORE et al., (2006).

When steels have route of galvanizing lines, the use of Mo for dual-phase steels is of fundamental importance to improve the performance since the zinc pot acts as "post-treatment" affecting the transformation of austenite.

Controlled addition of Mo prevents formation of non-martensitic structures into the zinc pot, since Mo shifts the field of pearlite/bainite transformation to longer time in CCT diagram, preventing the formation of these undesirable products and, consequently, favoring the production of dual-phase steel in galvanizing lines (OSAWA et al., 2003). Besides, Huang et al. (2004) showed that Mo can reduce the austenite recrystallization rate as well as transformation of austenite to ferrite during cooling of Fe-C-Mn-Mo steel.

Figure 3.25 displays a schematic thermal profile typical of continuous annealing line (dashed curve) and a continuous galvanizing line (solid curve) with respective microstructures formed at each zone.

Figure 3.25 – Schematic illustration of formed microstructure on continuous annealing line (CAL) and continuous galvanizing line (CGL) of conventional C-Mn steels.
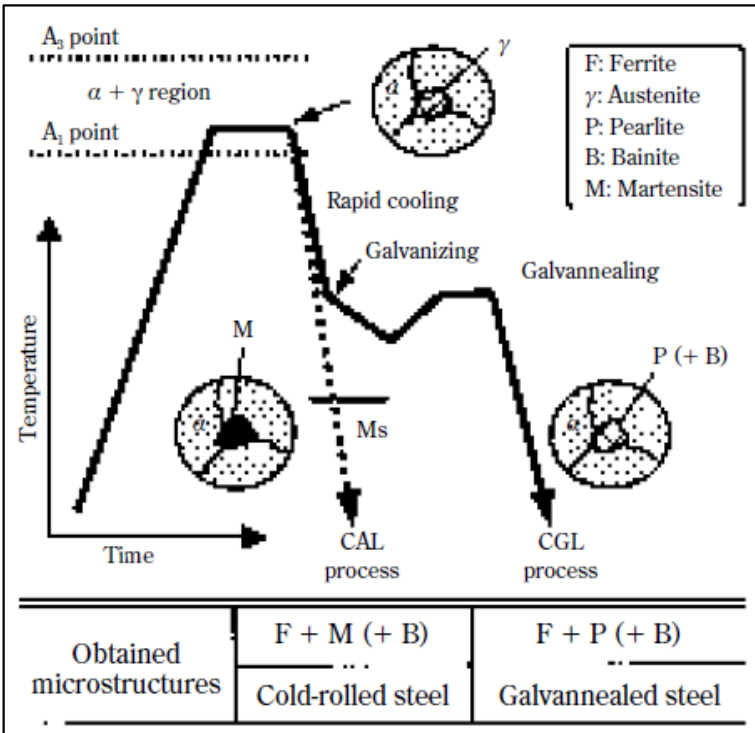
Source: OSAWA et al., (2003).

The addition of Mo in dual-phase steel increased the volume fraction of austenite and promoted the refinement of martensite islands and favored their formation in the vicinity of ferrite grain boundaries as shown in Figure 3.26 (OSAWA et al., 2003).

Figure 3.26 - SEM micrograph of steels DP 590 Mo-added.
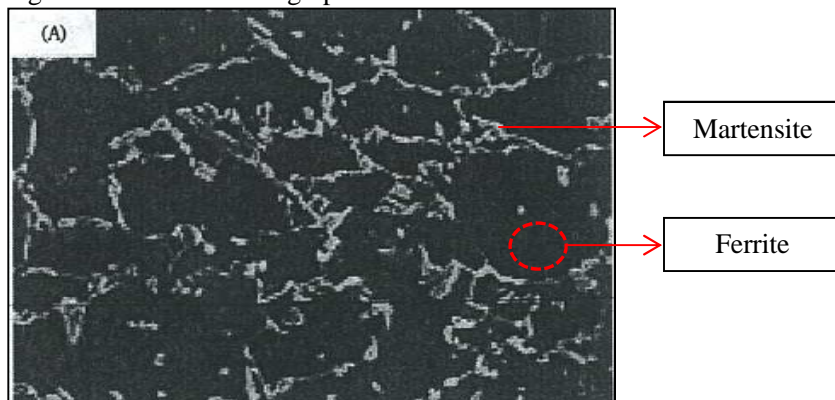
Source: OSAWA et al., (2003).

Study developed by Han et al. (2008) compared the effects of Mo and Cr in steels pointed out:

i) molybdenum has a more substantial effect on the improvement in hardenability of the boron-added steel than chromium. This indicates a synergistic effect between molybdenum and boron.

ii) the addition of 0.2 wt. % molybdenum to the boron- added steel nearly suppresses the formation of polygonal ferrite even at low cooling rates around 0.5 ºC/s. On the other hand, the addition of 0.5 wt. % chromium does not prevent the formation of polygonal ferrite until the cooling rate exceeds 3 ºC/s.

iii) the synergistic effect of the combined addition of molybdenum and boron on the hardenability enhancement is likely due to the suppression of $M_{23}(C, B)_6$ precipitation at austenite grain boundaries. It is due to the reduction of carbon diffusivity and the deterioration of phase stability by molybdenum.

Additions of Mo in the hot-rolled steels favor the formation of martensite in the ferrite structure which induces a number of mobile dislocations in the ferrite, which suppresses the yield point elongation in tensile stress-strain curves (HAN et al., 2011).

3.4.7 Effect of Boron

Boron is well known as an element that increases hardenability of austenite, reducing the sensitivity of final microstructure and tensile properties to the cooling rate or to temperature of annealing in the inter-critical region (FONSTEIN, 2015).

Shen and Priestner (1990) showed that it acts on preventing the ferrite nucleation and growth in steels cooling from γ-field but does acts when cooling from $(\alpha+\gamma)$-field.

According to Han et al. (2008), boron as an interstitial element diffuses very rapid into austenite to segregating at grain boundaries, which in turns retards the diffusional transformation (austenite to ferrite) by lowering the interfacial energy at the austenite grain boundaries during cooling. Thereby, small amount of boron dramatically increases the hardenability of steels. The addition of Mo, simultaneously, creates a synergic effect that makes this inhibition of the proeutectoid ferrite transformation more pronounced (SUN & YONG, 2010). Nevertheless, there is a critical boron content, at which the excesses will induce the precipitation as $M_{23}(C,B)_6$ borocarbide at the austenite grain boundaries, which acts as a preferential nucleation site for ferrite and thus deteriorates.

Boron is effective in retardation bainite reaction and lowering Bs temperature (FONSTEIN, 2015).

The beneficial effects of boron occur when it is in solid solution in the austenite, where its solubility is very low. Boron is chemically reactive with other alloying elements in steel, particularly carbon and nitrogen. The usual practice is to add boron within the range of 0.0005 to 0.003 wt. %, and add small quantities of titanium and zirconium to react with nitrogen and to keep more of the boron in solution. If more than 0.003 wt. % boron is added, the hardenability begins to decrease again and, at about 0.004 wt. %, iron boride precipitates on the austenite grain boundaries and causes a reduction in the final toughness. It has been suggested that boron segregates at the grain boundaries because it is able to reduce the grain boundary energy which in turns makes the austenite grain boundaries less effective as heterogeneous nucleation sites. An alternative explanation suggests that borocarbides, $Fe_{23}(C, B)_6$, precipitate at the grain boundaries and inhibit the nucleation of ferrite and cementite (SHEN, 1990). Maybe both phenomena participate. It is generally accepted that the austenite grain boundaries are affected in some manner because the transformations begin at the boundaries.

Pottore et al. (2006) showed the effect of boron additions on strengthening of cold-rolled dual-phase steel: i) Additions of Boron led to increases in both tensile and yield strength in a whole range of temperature (Figures 3.27 a, b); ii) No significant effect on the yield/strength ratio (Figure 3.28).

Figure 3.27- Effect of boron addition on (a) tensile strength and (b) yield strength.
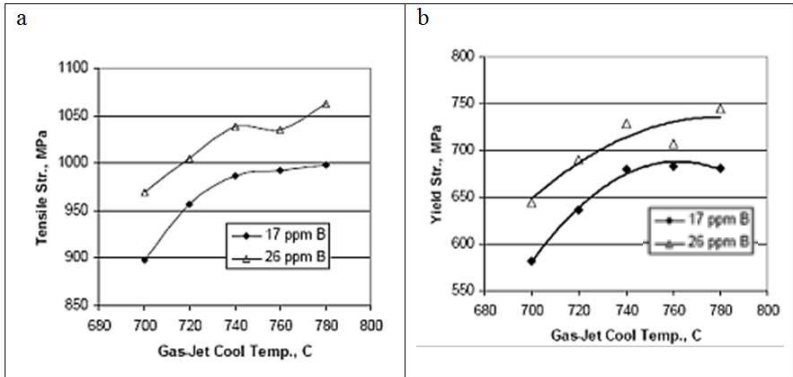
Source: POTTORE et al., (2006).

Figure 3.28 – Effect of Boron content on the ratio of Yield Strength to Tensile Strength.
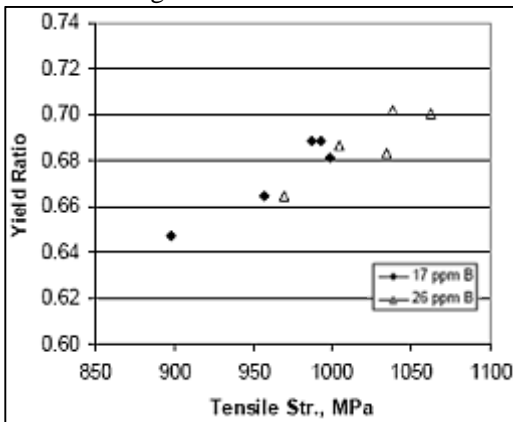
Source: POTTORE et al., (2006).

3.4.8 Effect of Niobium

Niobium is an alloying element that can control efficiently the behavior of the austenitization, recrystallization, grain growth, phase transformation, and precipitation and thereby can vary the mechanical properties in a wide range. It interacts strongly with C and N to form a dispersion of NbC and NbN, which can dissolve as the austenite phase grows into the ferrite during intercritical annealing (BLECK et al., 2002; SPEICH, 1981).

Niobium in the solid solution retards the recrystallization (static and dynamic) during hot deformation as well as the austenite to ferrite transformation. Small particles of niobium-carbonitrides also delay the recrystallization due to their effect as obstacle to the grain growth which results in significant strengthening of steels (BLECK et al., 2002).

Sundry studies have shown that the presence of Nb in steel exerts a pinning force either as a solute or precipitates or as a combination of both, retarding the recrystallization of austenite or ferrite and to prevent grain coarsening (CHO et al., 2011).

The addition of Nb to dual-phase steels provides noticeable grain refinement with improvement in ductility, besides an additional holding step in the temperature range of maximum ferrite formation (ferrite formation involves carbon enrichment of the austenite thus retarding pearlite and bainite formation and facilitating martensite formation). Any static recrystallization within the finishing mill is suppressed, due to the solute drag effect caused by the presence of soluble niobium which raises the temperature at which recrystallization can occur above the entry temperature to the finishing mill (BLECK et al., 2002).

Osawa et al. (2003) added Nb to cold-rolled dual-phase steels and observed the effect on properties:

   i)   small increase in TS (20 ~ 40 MPa) (Figure 3.29);
   ii) large increase in yield strength (50 ~ 70 MPa) (Figure 3.30);
   iii) increase in the yield ratio (0,60 ~0,70) (Figure 3.31);
   iv) a small deterioration in total elongation (Figures 3.32).

Figure 3.29 - Effect of Nb addition on Tensile Strength.
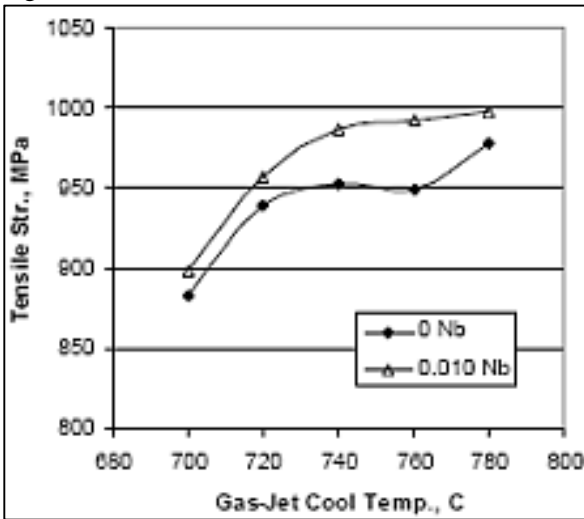
Source: OSAWA et al., (2003).

Figure 3.30 - Effect of Nb addition on Yield Strength.
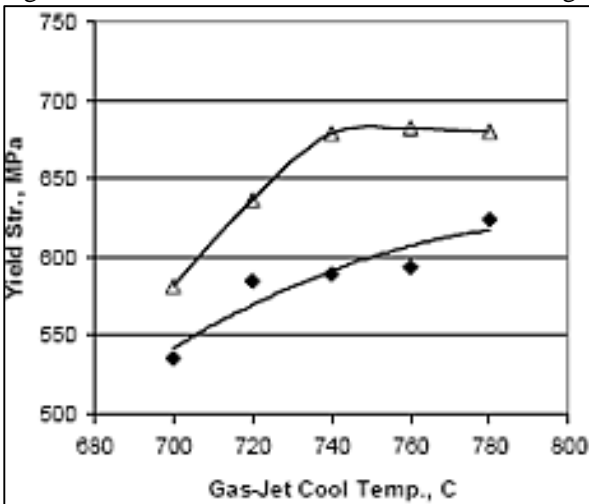
Source: OSAWA et al., (2003).

Figure 3.31 - Effect of Nb addition on the Yield Ratio to Tensile Strength.
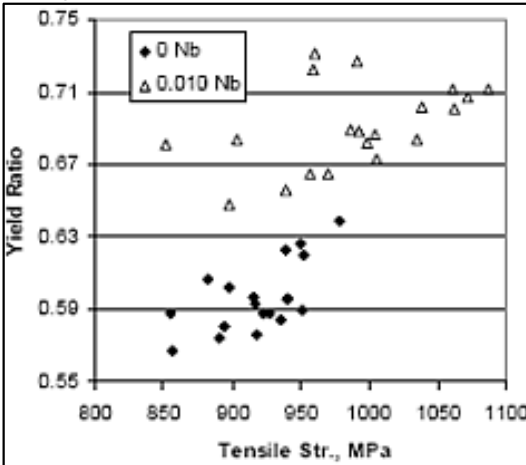
Source: OSAWA et al., (2003).

Figure 3.32 – Effect of Nb addition on balance of Total Elongation vs. Tensile Strength.
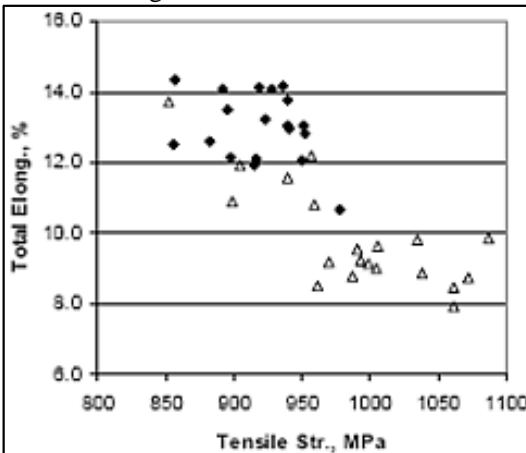
Source: OSAWA et al., (2003).

On dual-phase steel Figure 3.33 shows the effect of grain refinement due to the addition of 0,1 % Nb (WEY, 1981).

Figure 3.33 - Effect of Nb on the grain size of dual-phase steel maintained at 1100 °C for 100 h.

Source: WEY, (1981).

Girina et al. (2007) showed that addition of Nb from 0 to 0.030 % wt. increases the strength level up to around 200 MPa and total elongation throughout the whole range of annealing temperatures, as shown in Figure 3.34.

Figure 3.34- Mechanical properties as a function of annealing temperature.
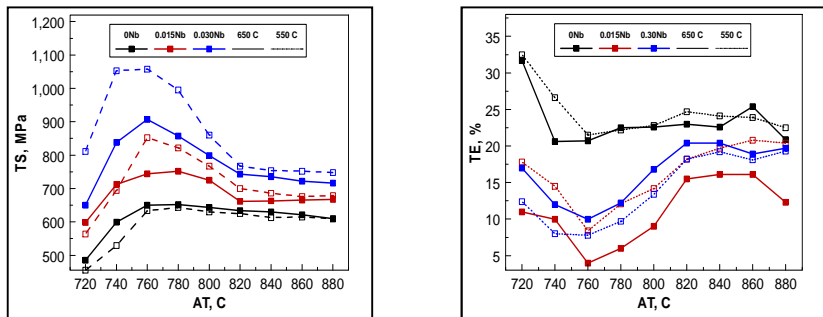
Source: GIRINA et al., (2007).

The additions of Nb to steels lower the start annealing temperature of austenite formation during heating. The effect of Nb on austenite formation temperature (Ttr), the temperature of full transformation of pre-existing (prior to heating) carbon-containing phase

to austenite, is shown in Figure 3.35. Additions of 0.015 % of Nb decrease the austenite transformation temperature by ~10 °C.

Figure 3.35 - Effect of Nb on austenite formation temperature – Ttr.
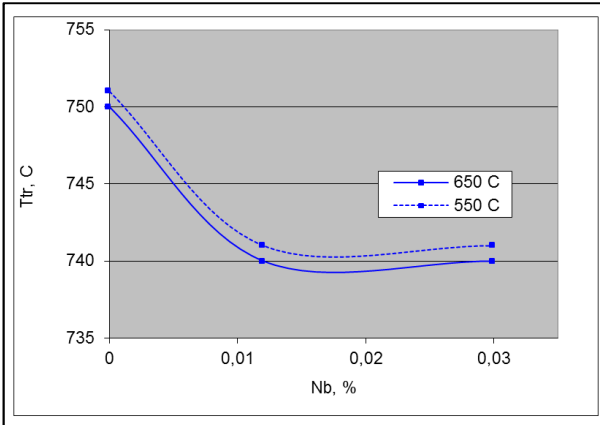
Source: GIRINA et al., (2007).

3.4.9 Effect of Titanium

The presence of excess titanium may be beneficial for the mechanical properties. For instance, the presence of Ti during hot rolling avoids the supersaturation of carbon in solution and reduces the precipitation of more soluble elements such as Nb or V. These ones control the microstructure at lower temperatures.

3.4.10 Effect of Carbides on Steel

As shown before alloying elements play very important role on mechanisms of phase transformation and recrystallization, mainly as solid solution. However, depending on the concentration and associated conditions it can appear also as precipitates and exert an additional effect on mechanisms.

Schneider and Inden (2004) highlighted that the metastable phases (precipitates/carbides), during their temporary presence exert strong influence in kinetics of the other phases.

Considering the important role of precipitates and that the chemistry of steels used in this study favors the formation of

precipitates, a consistent discussion about this issue is developed hereafter.

Hu et al. (1982) reported that the grain boundaries of carbides can be a site for the formation of a pool of austenite, at the intercritical temperature, since they are high carbon content regions and these areas would transform to martensite during rapid cooling.

Studies developed by Bain (1945) showed that i) undissolved carbides retard the coarsening of grain size of steels; which in turns affect their strengths; ii) in many steels the grain size quite increases with the disappearance of most of the carbide particles; thus whether the composition provides a moderate dispersion of carbide particles still undissolved (after desired austenite composition is achieved) the microstructure of austenite is fine-grained. Such steels are naturally regarded as being inclined toward fineness of grain as properly heated. Thus many steels containing Mo, Cr, W and others alloying elements are automatically fine-grained as ordinarily heated.

It will be appreciated that in most instances a considerable portion of the carbide-forming element is dissolved in the austenite while a smaller portion remains in the carbide maintaining its reluctance or inability to dissolve. The influence of such elements is therefore dual in nature. We have seen how fine-grained austenite alone contributes toughness to its products of transformation; accordingly carbide-forming elements may at once influence austenite transformation characteristics by being in part dissolved and contribute toughness through restriction of grain growth.

Molinder et al. (1956) observed, through the thermodynamic experiments, that alloying elements affect significantly the disintegration of cementite, which in turns affect the total rate of carbon diffusion in austenite. Considering the frequent practice of addition of alloying element in the new generation of steels, other kinds of carbides also appears on the structure and should affect the dissolution rate.

Yefei et al. (2011) noted that the chromium carbides affect steel properties (mechanical, corrosion, and hardness) due to their properties such as high hardness, high melting point, excellent resistance to chemical corrosion, high moduli and super wear resistance what affect the properties of final steel.

Chromium carbide (precipitates): Chromium carbides (Cr_3C_2, Cr_7C_3 , Cr_3C , $Cr_{23}C_6$ and CrC) influence significantly the properties and behavior of Fe-Cr-C. All these carbides are considered as paramagnetic and their enthalpies of formation are negative indicating that they are thermodynamically stables, except for CrC which has positive formation

enthalpy and is considered as metastable precipitate. Compounds of chromium carbides have covalent bonds type p and d hybridization between Cr and C.

Yefei et al. (2011) determined the stability and hardness of chromium carbides:

- stability sequence: $Cr_3C_2 > Cr_7C_3 > Cr_3C \sim Cr_{23}C_6 > CrC$
- Hardness values for chromium carbide phase sequence: $CrC > Cr_3C_2 > Cr_7C_3 > Cr_3C > Cr_{23}C_6$.

Miao et al. (1993) observed that mechanical properties of steels under study could be related to chromium carbides particles found within ferrite matrix. Those particles were identified and their size measured: $Cr_{23}C_6$ as a blocky feature (10 ~ 300 nm) and the Cr_7C_3 as bamboo-leaf-like feature (up to 200 nm long). They concluded that the these very fine carbides has led to the improvement in the hardness and tensile properties of the steel due to tetragonal distortion and high densities of dislocations, while coarser $Cr_{23}C_6$ and Cr_7C_3 dropped down the beneficial effect of these carbides on the mechanical properties.

Lleweuyn and Hudd (1998) added Cr and Mo into high-speed steel and identified the following types of carbides $M_{23}C_6$ and M_7C_3 for Cr; and M_6C (called eta-carbide and has low solid solubility in steel) for Mo. Table 3.1 displays the enthalpy of formation for some chromium carbides.

Table 3.1- The enthalpy of formation of some Chromium carbides/precipitates at 25 °C.

Chromium Carbide	Cr_3C_2	Cr_7C_3	$Cr_{23}C_6$	Cr_3C	CrC	Fe_3C
Formation Enthalpy (kJ/mol)	-72.3	-144	-344	-	-	+ **19**

Xiao et al. (2007) showed quite better stability and mechanical properties for the Cr_7C_3 than other carbides like Fe_3C and Fe_2B; and explained this better stability of Cr_7C_3 by its attractive interactions in the whole crystal.

Maalekian et al. (2007) mentioned in their study that additions of Cr to the steels up to 4 wt % favored the mechanism of nucleation at the interface of Fe_3C/ferrite for governing the reaction of transformation of Fe_3C to Cr_7C_3. Chromium diffuses in ferrite more rapidly than most metallic alloying elements.

Atomistic simulation on the structural properties and phase stabilities of carbides demonstrated through the "lattice constant" and

"cohesive energy" that the Cr_7C_3 is more stable than $Mn_{23}C_6$ (XIE et al., 2006).

Carbides with complex crystal structures and low heats of formation, e.g. M_7C_3, M_6C and $M_{23}C_6$, generally form relatively coarse dispersions (PORTER & EASTERLING, 2004).

M_7C_3 was formed through *in situ* transformation of cementite and the $M_{23}C_6$ inhibited the cementite formation by precipitation (OLIVEIRA et al., 1985)

Literature reviewing showed the possibility for existence of chromium carbides in a finite time (in some cases at similar condition used in this study) and some mentioning about the relation mechanical property and carbide presence in steel.

3.5 EFFECT OF PROCESSES PARAMETERS ON MECHANICAL PROPERTIES OF COATED DUAL-PHASE STEELS

The industrial production of dual-phase steels depends on specific details of facilities to meet the specific demands of this steel, what is dependable of cold-rolled conditions and chemical composition. Figure 3.36 shows a schematic heat cycle to produce dual-phase steels.

Figure 3.36 - Temperature-time-schedule for cold rolled dual-phase.
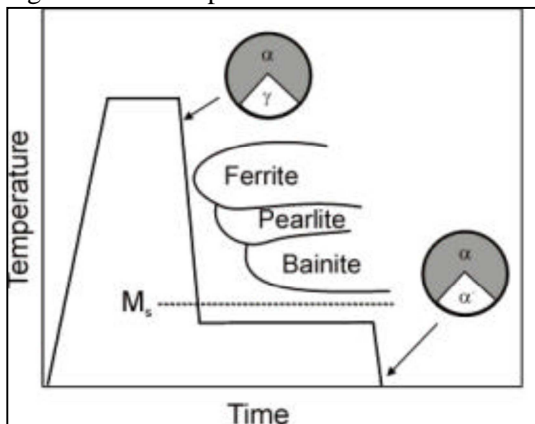
Source: BLECK et al., (2002).

3.5.1 Effect of Heating Rate on Phase Transformation

Fonstein (2015) mentioned the heating temperature as the key factor controlling the volume fraction of austenite and its average

carbon content and, consequently the final microstructure. Equation 3.5 describes the velocity of austenite phase boundary (the phase growth rate):

$$v = D \frac{dC}{dx} \left[\frac{1}{\Delta C(\gamma - \alpha)} + \frac{1}{\Delta C(p - \gamma)} \right]$$

(3.5)

Where:

D = diffusivity of carbon in austenite (cm^2/s)

dC/dx = gradient of carbon in austenite grain

$\Delta C^{(\gamma-\alpha)}$ = difference between carbon concentration on austenite-ferrite

$\Delta C^{(p-\gamma)}$ = differences between carbon concentration on carbide particle-austenite

v is proportional to the diffusivity of carbon in austenite (D) and the gradient of carbon dc/dx in austenite grain; but inversely proportional to the diffusion path x as well as to differences between the carbon concentration on austenite-ferrite $\Delta C^{(\gamma-\alpha)}$ and carbide particle-ferrite $\Delta C^{(p-\gamma)}$ (WYCLIFFE et al., 1981)

The formation and distribution of the austenite can be strongly affected by ferrite recrystallization and spheroidization of cementite during heating. Austenite forms initially on grain boundaries of elongated ferrite grains and later, after complete recrystallization, on the carbides in the ferrite matrix, which determines the distribution of island of austenite (YANG et al., 1985).

Huang et al. (2004) studied the effect of heating rates on the austenite morphology of Fe-C-Mn-Mo steel heat-treated at (1 °C/s, 10 °C/s and 100 °C/s) up to holding temperatures of 750, 775 and 800 °C:

i) the volume fraction of austenite was twice as high when the heating rate changed from 1 to 100 °C/s;

ii) at 1 °C/s some highly elongated austenite islands and a number of smaller islands on ferrite grain boundaries have been formed; while at 100 °C/s a relatively low density of large, highly elongated austenite islands formed;

iii) at higher heating rate there is a significant overlap between ferrite recrystallization and austenite formation.

Figure 3.37 shows the effect of heating rate on the percentage of recrystallization that completes up to the temperature of the start of

austenite formation. At 100 °C/s were found 90 % of ferrite in non-recrystallized condition; whereas at 10 °C/s only 50 % of ferrite was non-recrystallized when austenite formation in ferrite is first observed.

Figure 3.37 – Effect of heating rate on the percentage of recrystallization at onset of austenite formation.
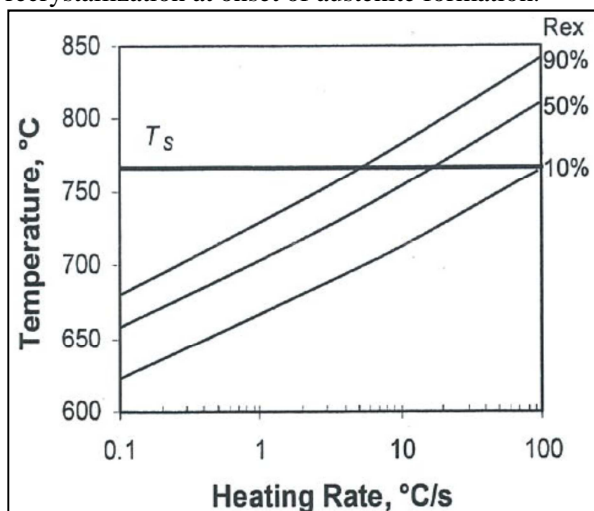
Source: HUANG et al., (2004).

Comparing the Fe-C-Mn-Mo versus Fe-C-Mn-Si it was observed that the latter chemistry reached the complete ferrite recrystallization before austenite formation for all heating rates, indicating no overlap. It suggests that Mo delays the recrystallization process and decreases the Ts temperature; while Si accelerates the recrystallization process (HUANG et al., 2004).

In the current study the steel chemistry considered several concentrations of Cr, Mo and Si and high heating rate ~150 °C/s to better understand the final effect on microstructure and mechanical properties when element with opposite effects on recrystallization and phase transformation were added. These particular chemistry and process produced microstructures that allowed better comprehension of recrystallization phase transformation and their competition.

3.5.2 Effect of Annealing Temperature on Dual-Phase

It seems, however, that the final changes in austenite stability depend on numerous other factors: alloying content, initial microstructure, heating rate, cooling rate and annealing temperature. In fact, all listed parameters define the homogeneity of the formed austenite composition, which should be considered as the most important factor.

The inter-critical temperature affects the amount of austenite (Figure 3.38) which in turns determines its own carbon concentration that determines the hardenability of austenite.

Figure 3.38 – Effect of annealing temperature on austenite volume fraction.
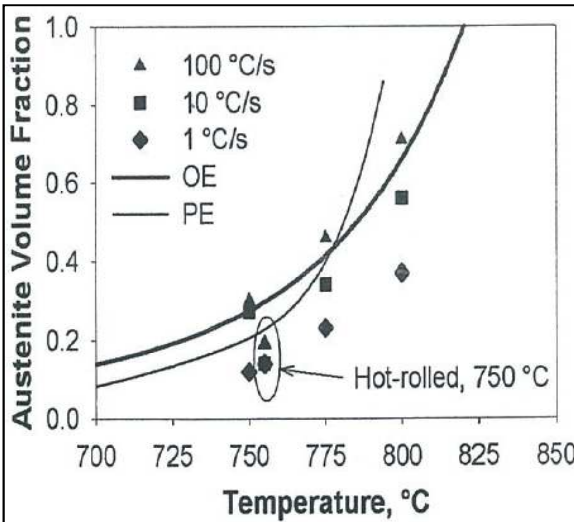
Source: HUANG et al., (2004).

Annealing temperature defines also the content of carbon soluble in ferrite and consequently its ductility and further aging/baking hardening behavior. The maximum of carbon solubility is at Ac_1 temperature, the higher is the annealing temperature in two-phase region, the "cleaner" ferrite (FONSTEIN & GIRINA, 2005).

3.5.3 Effect of holding time

Holding time is important stage in determining the properties of steel since the grain growth over recrystallization process develops in.

Longer holding time in two-phase region results in bigger volume fraction of austenite up to a determined time when the material will reach the equilibrium austenite volume fraction at an intercritical temperature. Above that time volume fraction of martensite keeps constant with the time, Figure 3.39.

Figure 3.39 – Effect of Isothermal Holding Time and Heating-Rate on the Kinetics of Austenite Formation (cold-rolled Fe-C-Mn-Mo steel).
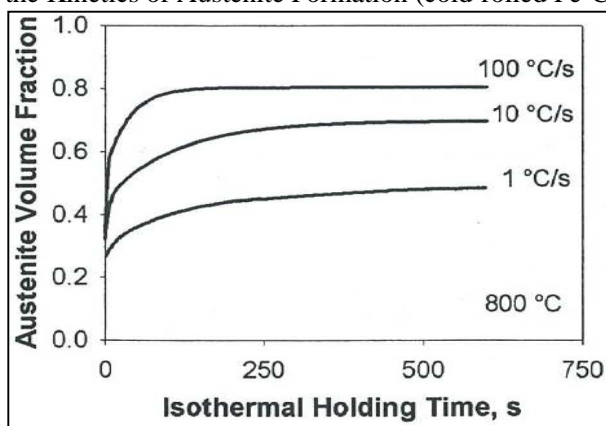
Source: HUANG et al., (2004).

Consequently, we should have decreasing the mean carbon concentration since carbon diffuses from austenite with time,

$C_\gamma = Cst/V_\gamma$:

C_{st} = Carbon content in the steel;

V_γ = Volume fraction of austenite.

Fonstein et al. (2015) confirmed the decreasing in the austenite stability with the holding times 30 to 60 or 120 s (FONSTEIN & GIRINA, 2005).

3.5.4 Effect of cooling rate

Figure 3.40 shows the effect of cooling systems on the microstructure of final products.

Figure 3.40 - CCT diagram for steels illustrating the transformation behavior under different cooling rates (WQ, oil quench and air cooling).
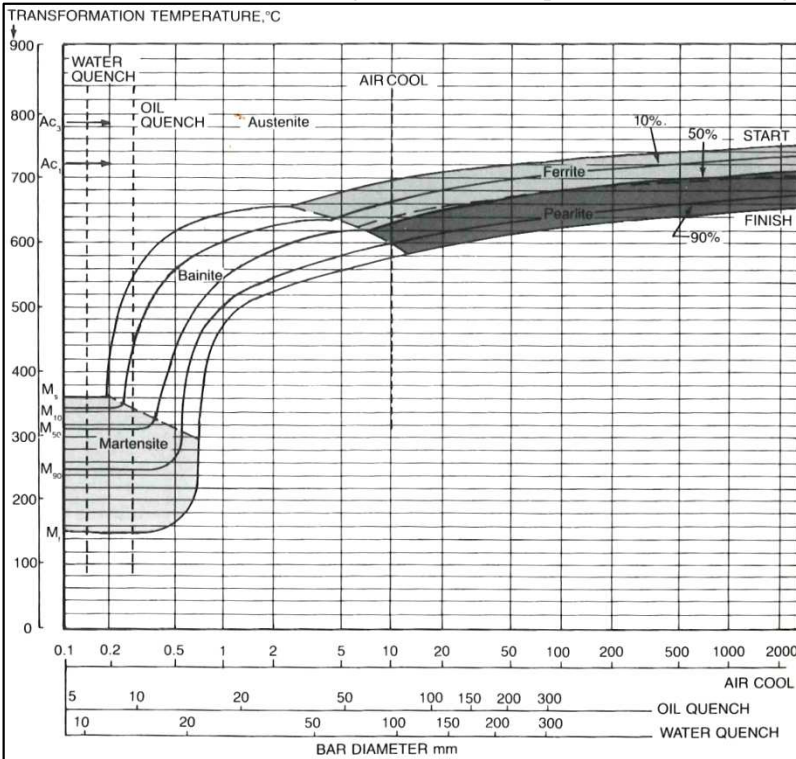
Source: KRAUSS, (1990).

Cooling rate from two-phase temperature region has a fundamental effect on the structure and properties of dual-phase steels. It controls the dominant transformation type, the fraction of austenite transformed to martensite, the martensite characteristics and ductility of ferrite, which depends on the contents of interstitial atoms and possible precipitations.

For the same specific steel composition, the required minimum cooling rate and the heating temperature in the inter-critical range are interrelated. The lower annealing temperature in the $\alpha+\gamma$ region and higher the $C_\gamma = C_{st}/V_\gamma$ the slower an acceptable is the cooling rate which displays martensite transformation. Where C_γ = carbon content in austenite; C_{st} = carbon content in the steel; V_γ = volume of austenite (GIRINA & FONSTEIN, 2005).

In fact, the choice of annealing temperature and/or of chemical composition of steel at given requirements to the strength of steels is completely dependent on achievable cooling rate.

At very low cooling rates cementite may precipitate in the ferrite saturated with carbon. Sometimes the "new" epitaxial ferrite is formed from austenite at slower cooling rates which is facilitated by existing inter-phase boundaries.

The production of dual-phase steels on continuous galvanizing lines (CGL) presents some difficulties because of initial relatively slow cooling and necessity to preserve at least the portion of austenite up to completion of galvanizing/galvannealing zone. Nevertheless some general observations published earlier for uncoated steels can be related to CGL processing as well.

According to Speich et al. (1981) at high cooling rate (240 ºC/s) essentially all the austenite transforms into martensite. At the lower cooling rates, part of austenite transforms into ferrite or ferrite-carbides. If high cooling rate is applied, at higher intercritical temperature, the fraction of austenite that transforms into nonmartensitic products is very large, whereas at the lower intercritical temperature this fraction is small.

Traint et al. (2005) showed the effect of cooling rate on the microstructure of a dual-phase steel: Rapid cooling (water quenched) resulted in a microstructure of ferrite and martensite with the appearance of substructure. However, lowering the cooling rate to 90 K/s (363 ºC/s) the volume fraction of martensite decreases and the substructure became more homogeneous. For the cooling rate 10 K/s (283 ºC/s), the bainite structures appear at the expense of fraction of martensite.

Increasing the cooling rate from 10 K/s (283 ºC/s) to 70 K/s (343 ºC/s) decreases the amount of austenite transforming during cooling (non-martensitic structures) and shifts the beginning of transformation to lower temperatures. The tensile strength, decreases when cooling rate shifted from water quench to 90 K/s (363 ºC/s) due to the formation of pronounced amount of ferrite, since tensile strength is sensibly affected by the amount of non-ferritic phases (martensite, bainite, pearlite) (Figure 3.41) (TRAINT et al., 2004).

Figure 3.41 – Yield and tensile strength as a function of the quench temperature for various cooling rates.
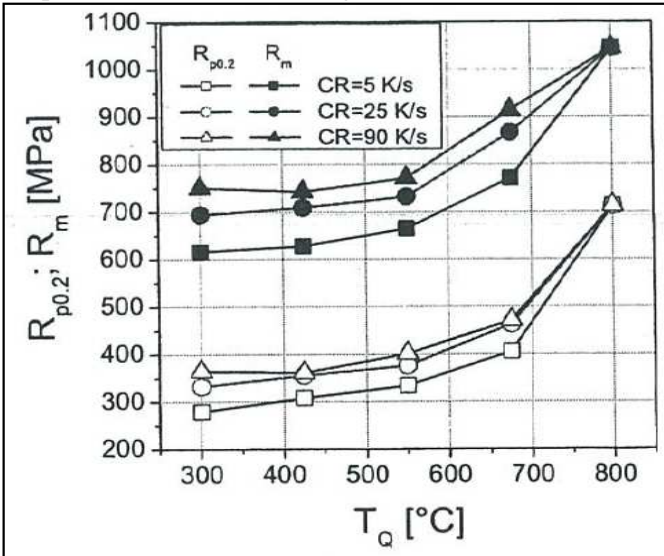
Source: TRAINT et al., (2004).

Depending on chemical composition quenching rates greater than 100 °C/s is sufficient to prevent any transformation of austenite back to ferrite, and thus, the austenite volume fraction and distribution at intercritical temperature are considered the same as those observed form martensite at room temperature.

Pickler et al. (2000) studied the effect of cooling rates (50 K/s; 10 K/s and 0.5 K/s) on final microstructure of dual-phase steel. The lowest cooling rate (0.5 K/s) resulted ferrite, pearlite and a minor fraction of martensite. The intermediate cooling rate (10 K/s) resulted polygonal ferrite, acicular ferrite with martensite and bainite and a significant amount of martensite at the grain boundary of polygonal ferrite. The highest cooling rate (50 K/s) produced less polygonal ferrite, an increasing amount of acicular ferrite and some block martensite. Significant amounts of martensite and bainite were situated between the acicular ferrite plates.

4 EXPERIMENTAL PROCEDURE

4.1 MATERIAL

The use of these steels aimed to investigate the effect of chromium (Cr), silicon (Si) and molybdenum (Mo), and their synergic effect with different annealing (holding) temperatures on microstructure and mechanical properties of dual-phase cold-rolled steel. Water quench treatment aimed to freeze ferrite + austenite structures straight from inter-critical range.

Table 4.1 displays the chemical composition of the steels used in this study. It was chosen one chemistry (see Table 4.1) as a base steel or reference (sample code 0). In order to investigate the effect of one specific element, it was added or suppressed from the base steel as shown in Table 4.1.

Table 4.1 - Chemical Composition of Steel under investigation (% weight) -* Boron concentration in ppm

	Sample Code	Combination	C	Mn	Cr	Mo	Si	Nb	Ti	B * (ppm)	Temperature Ac_1 (ºC)	Temperature Ac_3 (ºC)
	0 = (**0.2 % Cr**)	**Base Steel**	0.082	2.07	**0.22**	0.15	0.007	0.016	0.031	11	705	805
Cr Effect	1 = (**0 % Cr**)	**Base Steel - 0.2 % Cr**	0.079	2.08	**0**	0.16	0.010	0.015	0.031	12	701	808
	2 = (**0.4 % Cr**)	**Base Steel + 0.2 % Cr**	0.088	2.08	**0.41**	0.15	0.014	0.016	0.030	14	708	800
	3 = (**0.6 % Cr**)	**Base Steel + 0.4 % Cr**	0.091	2.10	**0.62**	0.15	0.018	0.013	0.019	12	712	792
Si Effect	4 = (**0.3 % Si**)	**Base Steel + 0.3 % Si**	0.086	2.12	0.21	0.14	**0.314**	0.012	0.020	14	713	811
Mo Effect	5 = (**0 % Mo**)	**Base Steel – 0.15 % Mo**	0.089	2.07	0.22	**0**	0.007	0.017	0.032	14	705	798
	6 = (**0.30 % Mo**)	**Base Steel + 0.15 % Mo**	0.086	1.94	0.22	**0.30**	0.010	0.016	0.03	9	706	812
	7 = (**0.45 % Mo**)	**Base Steel + 0.30 % Mo**	0.085	2.06	0.21	**0.43**	0.015	0.016	0.03	12	705	813

According to Andrews (1965), the Ac_1 and Ac_3 temperatures for the steel in question may be calculated by the following equations:

$$Ac_1 = 723 - 10.7\,Mn - 16.9\,Ni + 29.1\,Si + 16.9\,Cr + 290\,As + 6.38\,W$$

(4.1)

$$Ac_3 = 910 - 203\,C^{0.5} - 15.2\,Ni + 44.7Si + 104V + 31.5Mo + 13.1W - 30Mn - 11Cr - 20Cu + 700P + 400Al + 120As + 400Ti$$

(4.2)

Table 4.1 shows the Ac_1 and Ac_3 temperatures calculated for all compositions.

The addition of Mn was limited to 2.10 % to prevent deleterious effects on the texture formability, weldability and coatability; and Mo limited to 0.45 % in order to avoid negative effects on the hot rolling process (high loading demands).

The addition of 14 ppm of boron in these steels aimed the inhibition of ferrite nucleation at the grain boundaries of austenite and; thus, increasing austenite hardenability.

Nb was added to the base steel to meet the requirements of high yield strength and to promote better balance of strength and elongation due to structure refinement.

Elements such as Mn, Mo and Cr were added to avoid the austenite transformation to non-martensitic structures (ferrite, pearlite and bainite).

Such elements as Si and Al were added to reduce the rate of variation of austenite volume fraction with temperature, thereby providing robustness to the product design. However, Si additions were limited to 0.3 % to prevent the formation of silicon-oxides on the steel surface, which cause poor weldability to the steels, deteriorates the scales pickling yielding and delays the galvannealing reactions and bare-spot in the coating layer.

The addition of Ti aims to keep B in solid solution to maximize its effects as an inhibitor. The role of Ti is to react with N to form TiN instead of BN.

Residual levels of elements such as sulphur, phosphorus, copper and nickel were present.

This study were produced in the Laboratory of ArcelorMittal R&D Chicago – U.S. and processed up to rolling mill (as-cold rolling samples).

Vacuum-induction-melted heats, with the chemistries (Table 4.1) were cast. The slabs were reheated and hot-rolled into plates using a research laboratorial hot mill. Plate's parts were reheated and processed into hot bands, which were slow cooled in a controlled atmosphere furnace, simulated coiling conditions. The ingots were hot rolled using a slab reheating temperature of 1250 °C, finishing temperature of 880 °C and coiling temperature 650 °C. Hot band sections were straightened and surface grounded on both sides to ensure a decarburized-free surface. Then cold reduced by about 55 % until 1.25 mm thickness and cut into 410 samples (called as-full-hard).

Afterwards, samples were brought to Brazil for heating treatment.

4.2 PLAN OF EXPERIMENTS

Table 4.2 shows the combination of samples for the heat treatment. At each treatment condition, 3 samples were used.

Table 4.2 - Matrix of experiments planning combining chemical composition (Cr, Mo and Si), holding temperature and cooling media.

Alloying Element on Dual-Phase Steel	Alloy Content (%)	Heat Treatment		Cooling System
		Temperature (°C)	Holding Time (s)	
1) Cr-Containing	1.1) Base Steel - 0.2%Cr	720°C		Water Quench and Air Cooling
	1.2) Base Steel	740°C		
	1.3) Base Steel + 0.2%Cr	760°C		
	1.4) Base Steel + 0.4%Cr			
2) Si-Containing	2.1) Base Steel + 0.3%Si	780°C	60s	
		800°C		
3) Mo-Containing	3.1) Base Steel – 0.15%Mo	820°C		
	3.2) Base Steel + 0.15%Mo	840°C		
	3.3) Base Steel + 0.45%Mo			
		860°C		

Figure 4.1 shows part of a Fe-C diagram indicating the annealing temperatures used in this study.

Figure 4.1 - Fe-C diagram indicating the annealing temperatures used in this study.
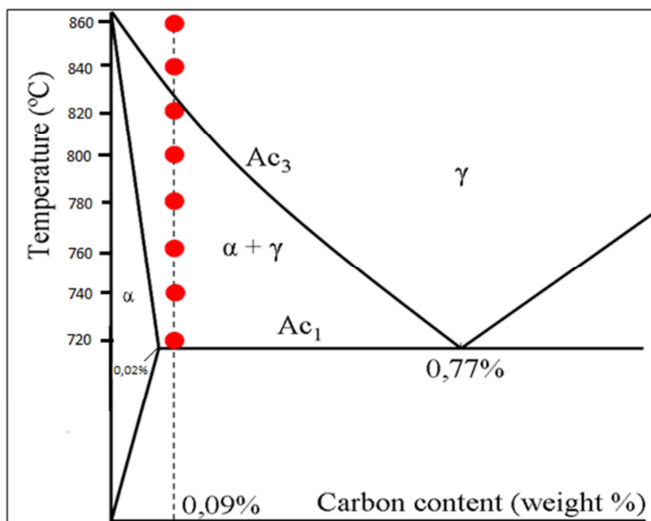
Source: Original, (2014).

4.3 HEAT TREATMENT

From the total of 410 samples (cold rolled), 390 were heat treated to cover 130 conditions (combinations of composition x temperatures x cooling media) and 20 samples were kept as reference (full hard).

4.3.1 Equipment Used for Experiments

Heat-treatment was carried out by using a laboratory salt pot (Figure 4.2) followed by water-quench or air cooling.

Pot was internally equipped with thermocouples for continuous monitoring the instantaneous temperatures and loading the computers system, in the cabinet, with data.

Figure 4.2 – Schema of salt bath furnace configuration - side view.
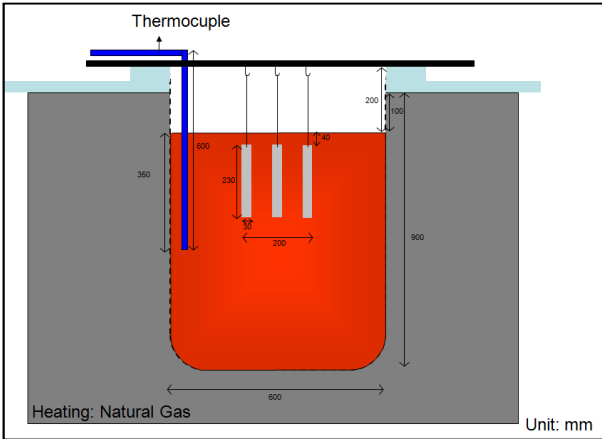
Source: Original, (2014).

4.3.2 Parameters of Heat Treatment

Holding times of 60 seconds were chosen based on continuous galvanizing lines CGL furnace dimension and industrial line speed typically (~150 mpm).

Since eight annealing temperatures were used in this study, the strategy was to move down the temperatures from 860 ºC to 720 ºC to attain the better stability inside the salt bath.

Bath was filled up with barium chloride salt ($BaCl_2$) and heated with natural gas (see Figure 4.2, side view and Figure 4.3 top view). Bath temperature, during annealing, was controlled (plus or minus 2 °C) by heat/cooling system coupled in 8 thermocouples. These thermocouples were installed in the walls of the cylindrical pot.

During the immersion time, the specimens were positioned just in front (height) of thermocouples (it means at same depth), assuring that the bath temperature found around the samples was accurate with temperature registered on the computer system data base.

Once the set of heating source was positioned in the internal surface of the furnace's wall, then the isotherm lines might appear. The use of straight support for the six specimens would result in gradient of temperature among them, what could result differences in the temperature among specimens of the same batch. To overcome this problem it was built a circle device in stainless steel with 200 mm diameter, which was placed concentric to furnace diameter. It allowed

fitting specimens of same batch in just one temperature's line (Figure 4.3).

Figure 4.3 – Schematic Configuration of Salt bath furnace - Top View.
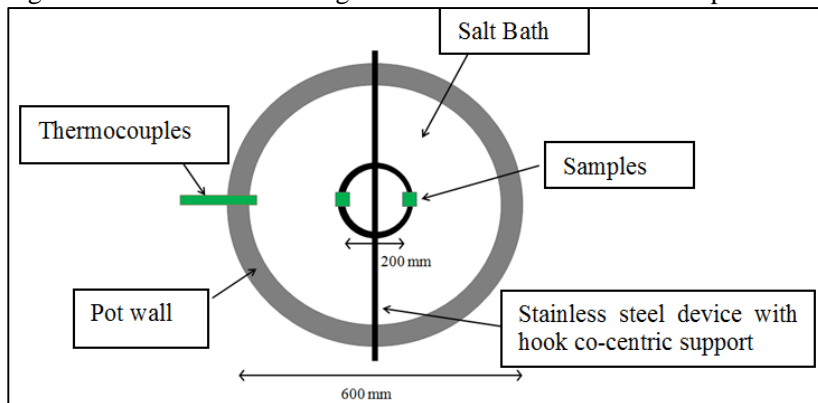
Source: Original, (2014).

For keeping similarity among samples, when handling and preparing material, all the cold-rolled samples, were cut as the same size (30 x 230 x 1.25 mm), in the same direction of cold rolling, i.e. on the longitudinal direction (LD).

For each batch annealing treatment, 3 samples of each chemical composition were assembled together at the same hook device for immersion in the bath. It resulted in 27 samples per batch annealing.

The detailed proceedings of heat treatment at bath pot are described hereafter:

Each set of 27 samples were heated simultaneously up to the pre-determined annealing temperature. The eight annealing temperatures under investigation fitted in the range (860 – 720 °C). Samples were held at these temperatures for 60 seconds; then were transferred to water tank or air cooling (2 seconds transferring time).

4.4 MICROSTRUCTURE / MECHANICAL CHARACTERIZATION

The products of heat treatment were separate into groups for further analysis.

4.4.1 Optical and Scanning Electron Microscopy

These samples were evaluated by light microscopy and scanning electron microscopy; and the microstructures were, subsequently, subjected to the specific image analysis system (Optical Microscope Zeiss AXIO) for the quantification of phases under investigation.

It is important to highlight that phase's quantification were obtained only with the standard magnification of microstructure 2500x.

SEM (Scanning Electron Microscopy) used to assess the ferrite recrystallization level; to identify and quantify precipitates (carbides and nitrites) and also to characterize substructures developed in the grain. Sample preparation is described in appendix A.

Samples for microstructural analysis were previously mounted in baquelite resin, ground and polished using the conventional methodology (appendix A), and subsequently were etched.

The amount of martensite was measured on the microstructures using the magnification of 2500x in microscope in agreement with the methodology of R&D Chicago Laboratory for the sake of comparison. The grid is shown in appendix B.

4.4.2 Transmission Electron Microscopy (TEM)

TEM (Transmission Electron Microscopy) was used to identify the phases and precipitates present in the products by handling and analyzing the lattice parameters of the crystalline and recrystallization evolution. See appendix C.

4.4.3 Electron BackScattered Diffraction (EBSD)

EBSD was used to develop microstructure features (recrystallization and orientation). See appendix D.

4.4.4 Dilatometry

The complementary technique of dilatometry analysis was also used in this study, for investigating the effect of Cr and Mo additions on the microstructures and kinetics of steels. The conditions at which this experiment was carried out consisted of heating the steels at $\alpha + \gamma$ region, holding isothermally for 60 sec and; afterwards cooling at different rates. These paths allow the analysis of phase's transformation.

Table 4.3 shows the equipment and laboratories used to assessment the heat-treated samples.

Table 4.3 - Laboratory/equipment used on the characterization (original).

Test	Equipment	Laboratory
Mechanical Tests (Tensile and hardness)	Universal Instron 5585 machine	AM Vega
	Hardness tests using a Taylor Robson	AM Vega
Volume Fraction of Martensite (Austenite) after Quench	Scanning Electron Microscope Jeol 6360	AM Vega
Characterization of volume fraction of recrystallized ferrite	Scanning Electron Microscope Jeol 6360	AM Vega
	Optical Microscope Zeiss AXIO	AM Vega
Characterization of martensite and bainite after cooling	Scanning Electron Microscope Jeol 6360	AM Vega
	Optic Microscope (OM)	AM Vega
Characterization of volume fraction of "new ferrite"	Scanning Electron Microscope Jeol 6360	AM Vega
Characterization of Recrystallization level; Characterization of type of Precipitate;	Transmission Electron Microscope (TEM)	UDESC/UFSCar/ArcelorMittal R&D Chicago
	Electron Backscatter Diffraction (EBSD)	ArcelorMittal R&D Chicago/ UFC
Characterization of chromium carbides	Field Emission Gun Scanning Electron Microscopy (FEG) and Scanning Electron Microscopy (SEM)	ArcelorMittal R&D Chicago/SENAI Joinville

Figure 4.4 shows the flow diagram of materials and methods used in the study.

Figure 4.4 – Diagram below the materials and methods used for the study.
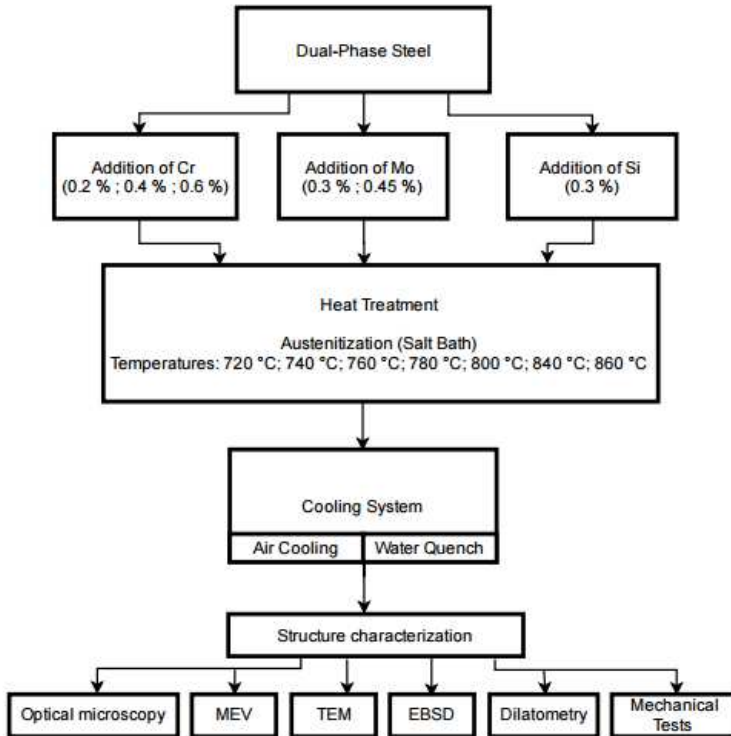
4.4.5 Mechanical Tests

Tensile tests were carried out using an Instron universal machine 5585 (100 kN maximum loading) at room temperature. Samples were cut in the longitudinal direction of rolling and the essays performed according to DIN-EN 10002 (length of the useful part = 50 mm). Yield strength was measured at 0.2% strain.

5 RESULTS AND DISCUSSIONS

Results and discussions are presented first as microstructures of cold rolled samples, afterwards the heat treated samples. The results of heat treated samples are presented separately per alloying elements and cooling media. Mechanical properties are shown just after the sections of microstructures of steels air cooled.

Sections were organized according to subject as:

Results of cold rolling samples => section 5.0

Effect of Cr => sections 5.1 (Quench) and 5.2 (Air Cooling)

Effect of Mo => sections 5.3 (Quench) and 5.4 (Air Cooling)

Effect of Si => sections 5.5 (Quench) and 5.6 (Air Cooling)

An overall panel (containing all microstructures) was shown at the beginning of each section (5.1 - 5.6) aiming to give a general viewing of the experiment. Nevertheless, detailed microstructures are also displayed along the text.

It is worth to highlight that samples used on "water quenching" or "air cooling" media were heat-treated together (in the same hook shown in section 3). Thereby, the amount of austenite transformed up to the inter-critical region is similar for both conditions and the difference in the final amount of martensite was due to the effects of cooling media and alloying elements.

Whereas the quench treatment resulted predominantly in ferrite + martensite structures, the air cooling, as being slower cooling, allowed the formation of non-martensite constituents (e.g. bainite).

5.0 COLD ROLLING SAMPLES RESULTS

Figures 5.1 to 5.3 display the microstructure of full hard used on heat treatment. Cold rolling reduction didn't transform the phases or constituents (from hot rolling), but elongated pearlite structure and ferrite grains.

Cold rolled steels have already shown in the microstructure the ferrite matrix, carbon content constituents like (martensite, pearlite) and carbides (Figure 5.1 - 5.3) due to presence of many alloying elements, mainly the Mn. In this stage of process it was observed the effect of alloying elements on the microstructures; it means that the amount and

size of carbon-containing constituents (martensite/bainite, pearlite) increased with the additions of Cr, Mo and Si.

Figure 5.1 – Effect of Cr on the microstructures of full hard steels.

Cr-Free	0.2 % Cr	0.4 % Cr	0.6 % Cr
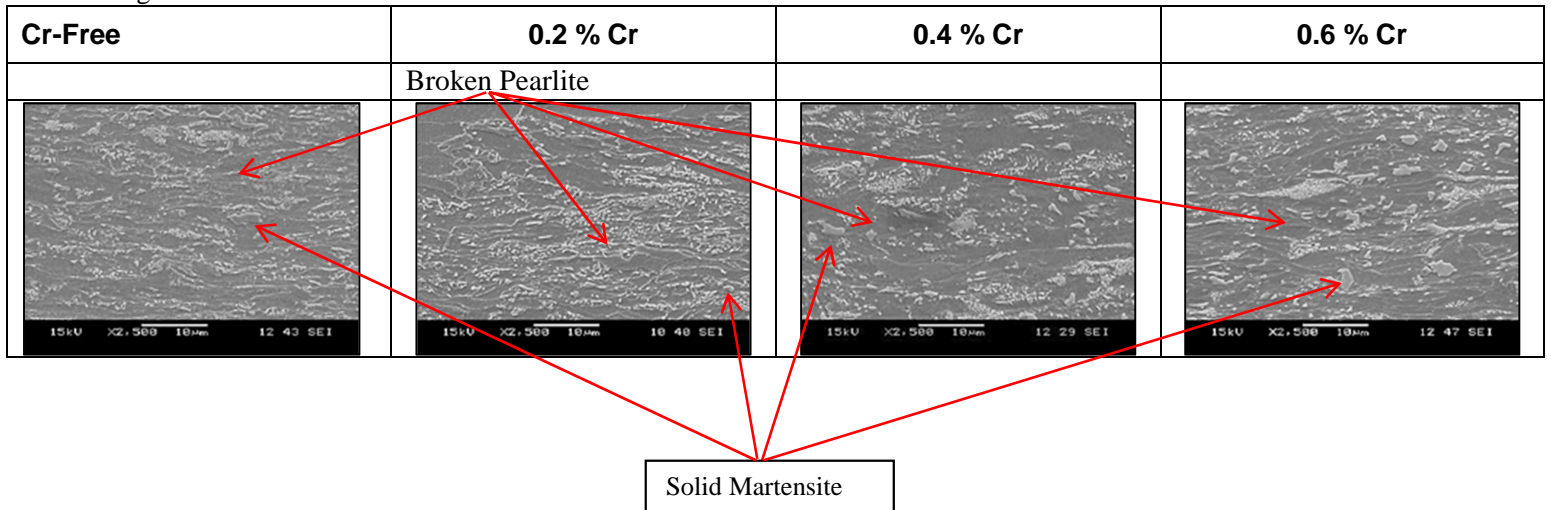
Source: Original, (2014).

Figure 5.2 – Effect of Mo on the microstructures of full hard steels.

Mo-Free	0.15 % Mo	0,45 % Mo
	Broken Pearlite	
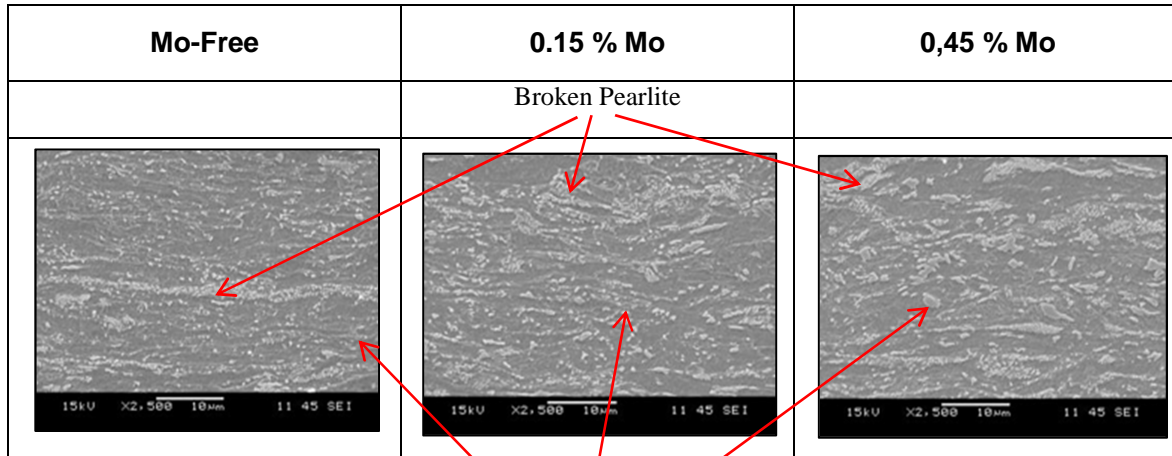
Source: Original, (2014).

Solid Martensite

As far as Si rejects C to austenite it enhances the hardenability, favoring the formation of more martensite in the full hard.

Figure 5.3 – Effect of Si on the microstructures of full hard steels.

	Si-Free	0.3 % Si
		Broken Pearlite
(5) 30 °C (Full hard)		

Solid Martensite
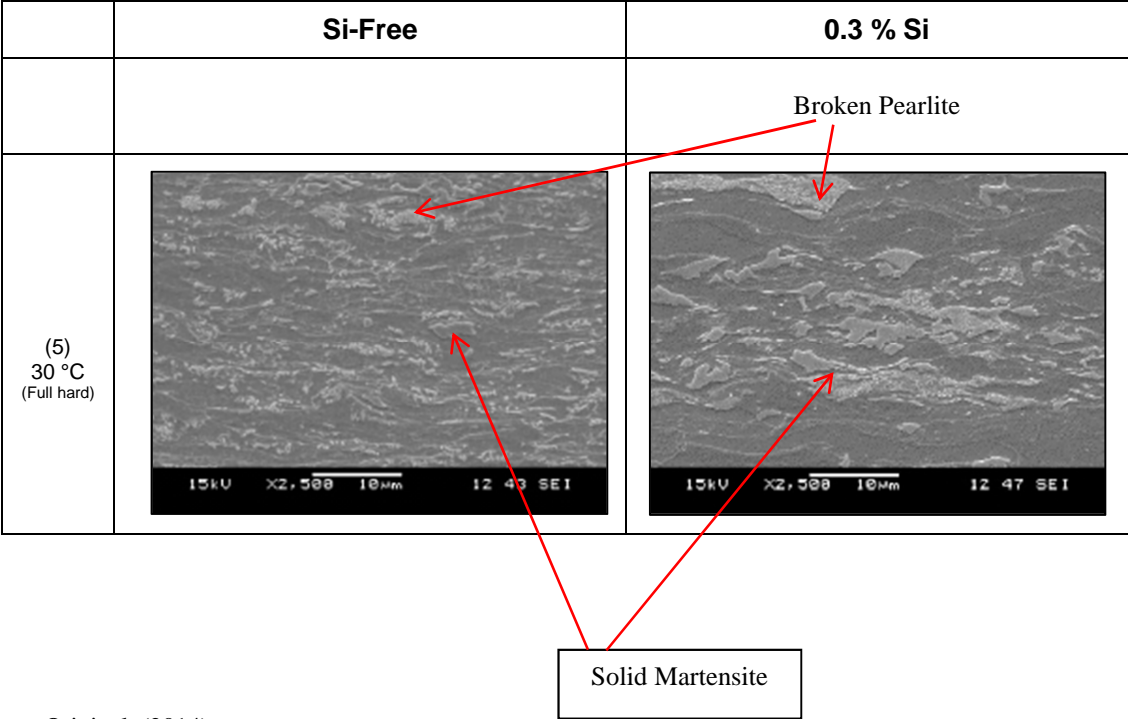
Source: Original, (2014).

5.1 EFFECT OF Cr IN STEEL AT "QUENCHING"

In this section the results addressed the effect of Cr and annealing (holding) temperatures on the microstructure of dual-phase steels after water quench.

Figure 5.4 displays a matrix with 32 microstructures that shows the effect of "Cr concentration" and "annealing temperature". The arrangement of microstructures in the matrix follows the precept of 4 columns ("a" up to "d") and 8 rows ("1" up to "8"). Columns a-d represents Cr concentrations.

Lines 1 to 8 show the microstructures of steel as functions of Cr concentrations and holding temperatures from 720 up to 860 ℃ with step of 20 ℃.

Considering the similarity in the behavior of microstructure of steels with 0.4 % Cr and 0.6 % Cr, the former was presented only in Figure 5.4 and suppressed thereafter for the sake of simplification. In case of need the 0.4 % Cr was depicted.

The methodology used for analyzing the microstructures was based on the investigation of the effect of Cr and temperature in the steels with the discussion focused on relevant differences.

The increase in Cr content from 0.0 to 0.6 % increased the amount of martensite as shown through the presence of island of refined martensite in the steels with 0.6 % Cr (Figure 5.4 - line 3).

Although carbides were mentioned along the text to explain some ideas, they were characterized and detailed in a specific section 5.1.1.1 at the end of this chapter (to avoid back and forth of idea) chemical composition is presented in Figures (5.19 – 5.21).

Figure 5.4 – Effect of chromium content and holding temperature on the microstructures (recrystallization, phase transformation and precipitates) of dual-phase steels – After quenching heat treatment.

	(a) 0 % Cr	(b) 0.2 % Cr	(c) 0.4 % Cr	(d) 0.6 % Cr
(1) 720 °C				
(2) 740 °C				
(3) 760 °C				
(4) 780 °C				
(5) 800 °C				
(6) 820 °C				
(7) 840 °C				
(8) 860 °C				
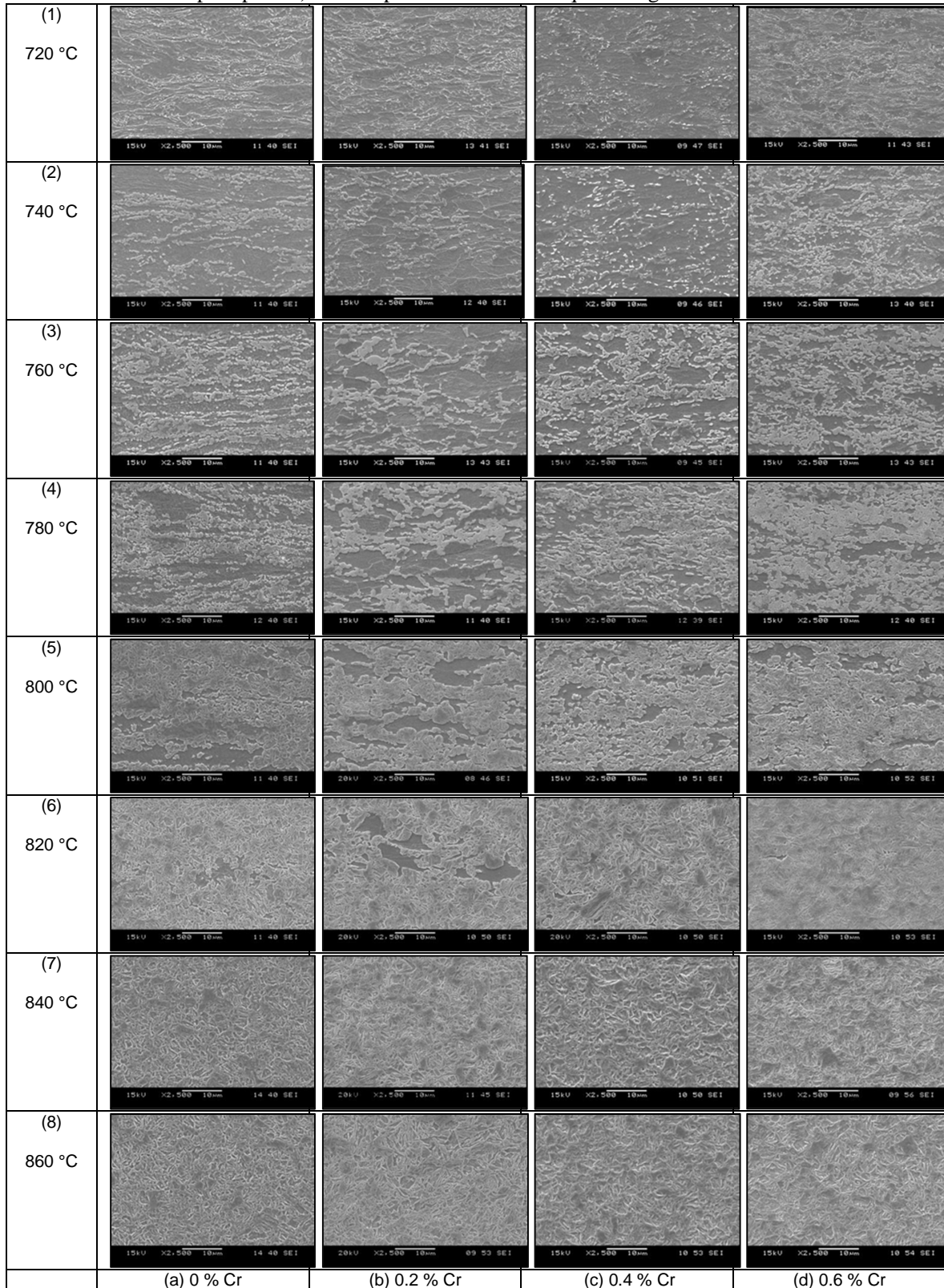
Source: Original, (2014).

The effects of Cr content were observed in the microstructure of steels through the phenomena of recrystallization, phase transformation and carbides precipitation.

At 720 ºC, coarse martensite, pearlite and less stable carbides (e.g. cementite) had already been dissolved (decomposed) almost completely and could not be seen as coarser as was observed in full-hard structures (see Figures 5.5 and 5.6). These dissolutions proceeded with the release of carbon atoms which diffuse to ferrite grain boundaries to enhance the formation of austenite and enrich its structure with carbon (BAIN, 1945). It is important to highlight that some carbides/precipitates still remained undissolved (Figure 5.5 c) indicating their higher stability, at this temperature, due to likely their specific chemical composition. It will be discussed later by comparing the effect of the Cr in the stability of carbides (section 5.1.1.1).

As shown in Figure 5.5 the ferrite recrystallization was accelerated with the additions of 0.2 and 0.6 % Cr in comparison with the microstructure of Cr-free steel. Even the additions of Cr have accelerated the ferrite recrystallization, differences were observed between 0.2 and 0.6 % Cr. The addition of 0.2 % Cr accelerated the recrystallization and allowed the growth of ferrite (coarse recrystallized ferrite grains were observed in Figure 5.5 b). This can be explained by chromium ability to reduce the activation energy barrier to nucleation and growth (BAR-OR & KIMMEL, 1968). It was attributed to the addition of Cr, the effect on jump frequency at the interface. Further addition of Cr (0.6 %) also accelerated the ferrite recrystallization (Figure 5.5 c), however, prevented the grain growth (Figures 5.5 and 5.9). It is likely due to the "side effect" of this element which, at high concentrations, forms carbides with the ability to pin the movement of recrystallized ferrite boundaries. This phenomenon is shown and explained later for annealing temperature of 740 ºC.

Figure 5.5 – Effect of chromium additions on carbides presence and stages of recrystallization of steel heat treated at 720 °C.
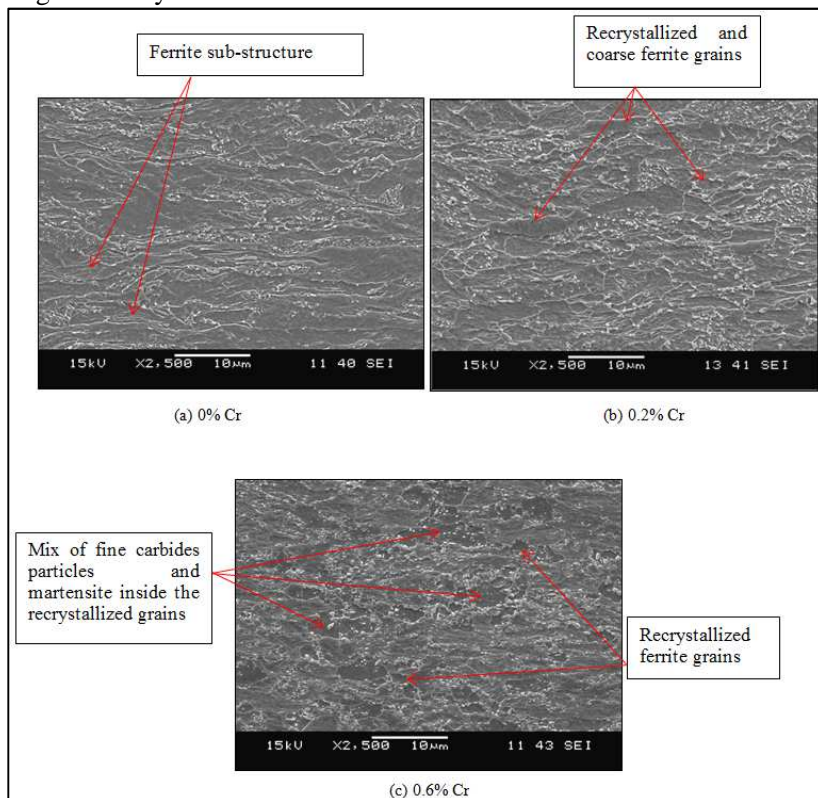
Source: Original, (2014).

The holding temperature 720 ºC was low enough to allow the coexistence of different stages of recrystallization (recrystallized; partially recrystallized and non-recrystallized/substructure) in the steel with 0.2 % Cr as shown in Figure 5.6. Recrystallized grains did not present carbides inside themselves; indicating the complete dissolution of unstable carbides during recrystallization. New martensite islands were present, predominantly at the grain boundaries (Figure 5.6), while phase transformation was slightly observed at these low temperature and moderate chromium concentration.

Figure 5.6 – Different stages of recrystallization (recrystallized/ partially recrystallized/non recrystallized substructure) and presence of martensite at grain boundary of steel with 0.2 % Cr annealed at 720 ℃ – SEM.
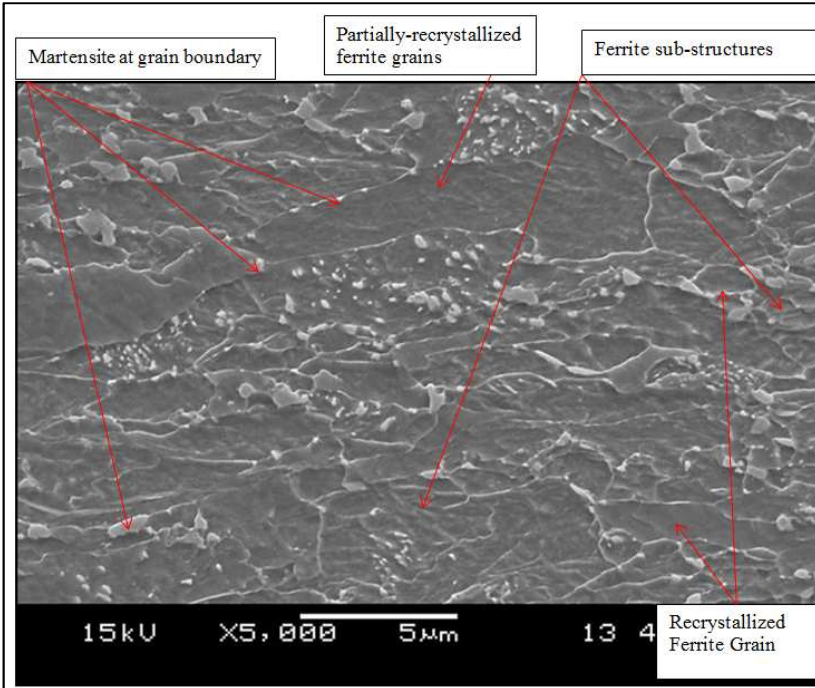
Source: Original, (2014).

Figure 5.7 displays the effect of Cr addition on the amount and stability of carbides that increased with the additions of Cr up to 0.6 %. The steels with additions of 0.6 % Cr have shown much more carbide particles distributed within the ferrite grains. It indicates that Cr acted on the formation (amount) and stabilization of carbides.

Figure 5.7 – Effect of the chromium additions on stability and amount of carbides/precipitates in the matrix, 720 °C.
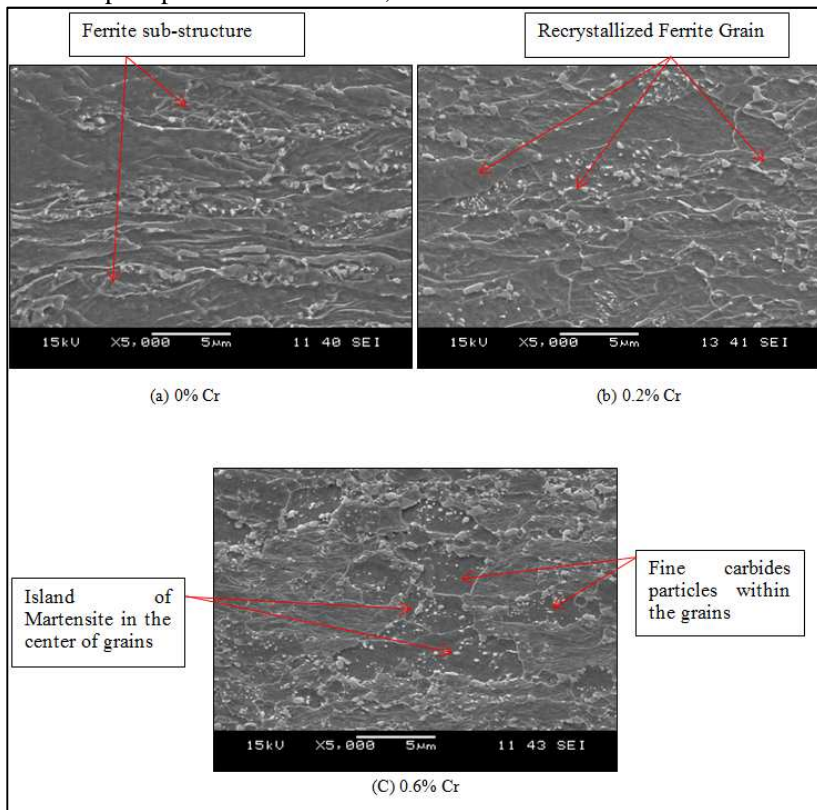
Source: Original, (2014).

On increasing the annealing temperature to 740 °C, it was observed fast changes in microstructures (phase transformation, recrystallization and carbides decomposition) as shown in Figure 5.8.

At this temperature (740 °C), no more dissolution of previous martensites were observed; however, the phenomena of phase transformation, recrystallization and carbides dissolution proceeded simultaneously. Phase transformations increased significantly with temperature for all Cr content as shown in Figure 5.8 (line 2) through the amount and size of martensite formed.

At this high annealing temperature, the amount of carbides particles inside ferrite decreased significantly. This suggests that the less

stable carbides (without Cr) were almost completely dissolved (Figure 5.8 a); whilst the more stable ones (with Cr additions) were only partially dissolved (Figure 5.8 c).

What should be pointed out is that martensite islands were found at different positions on ferrite grain according to the Cr concentration in steels. Figure (5.8 line 2) shows martensite predominantly at the boundaries of substructures (sub-grains) of 0 % Cr steels; - at the ferrite grain boundaries of 0.2 % Cr steels and; - randomly distributed (boundary and center of the ferrite grains) of 0.6 % Cr steels.

The amount and size of martensite observed on the microstructures of the 0 and 0.2 % Cr steels were only slightly different (Figure 5.8 "a" and "b") which should be explained by the difference in the mechanisms of phase transformation:

i) the steel with 0 % Cr showed microstructure with non-recrystallized sub-grain predominantly (Figures 5.8 "a" and 5.9 "a"). The boundaries of these sub-grains have stored enough strain energy to become more and favorable sites for austenite nucleation (OLIVEIRA et al., 2004). During the phase transformations, the austenite nucleated at the sub-grain boundaries and then transformed into island of martensite;

ii) on the other hand, since the steels with addition of 0.2 % Cr were almost full recrystallized then sub-grains were neglected; and austenite nucleation occurred preferentially at the surface of the recrystallized ferrite grain boundary (Figure 5.8 b).

Thus, the 0 % Cr steels exhibit nucleation of austenite in the "sub-grains boundaries" what could be misunderstood with the mechanism of nucleation in the "center of a grain".

Figure 5.8 - Effect of chromium additions and temperature on the martensite transformation and carbides occurrence of steels heated at 720 and 740 ºC and quenched.
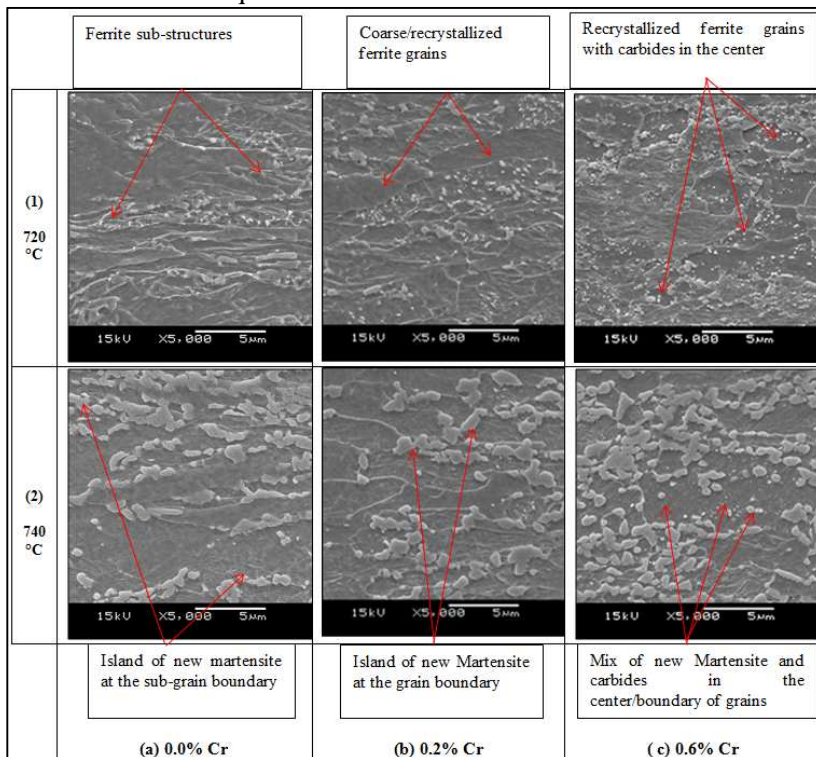
Source: Original, (2014).

Steels containing 0.2 % Cr showed the more advanced stage of recrystallization and growth of grains in comparison with microstructures of Cr-free steels (Figure 5.9).

Figure 5.9 displays the effect of Cr addition on the recrystallization and three stages of recrystallization predominantly:

a) regions of elongated non-recrystallized grains (substructure) with some fine recrystallized ones for steels with 0 % Cr (Figure 5.9 a);

(b) regions of coarse-recrystallized grains with few fine ones for steels with 0.2 % Cr. Grains showed equiaxed and coarse indicating the most advanced stage of recrystallization and growth (Figure 5.9 b);

(c) regions of recrystallized grains mixed in fine and coarse grains for steels with 0.6 % Cr. The fine and recrystallized

microstructure indicated that high Cr content in the steels have accelerated the recrystallization, nevertheless prevented the grain growth (Figure 5.9 c).

Figure 5.9 – Effect of Cr on the kinetic of recrystallization at 740 °C, prevailed: (a) low acceleration rate (non-recrystallized); (b) higher acceleration rate (recrystallized and grown) and (c) intermediate acceleration rate (recrystallized)- (EBSD).
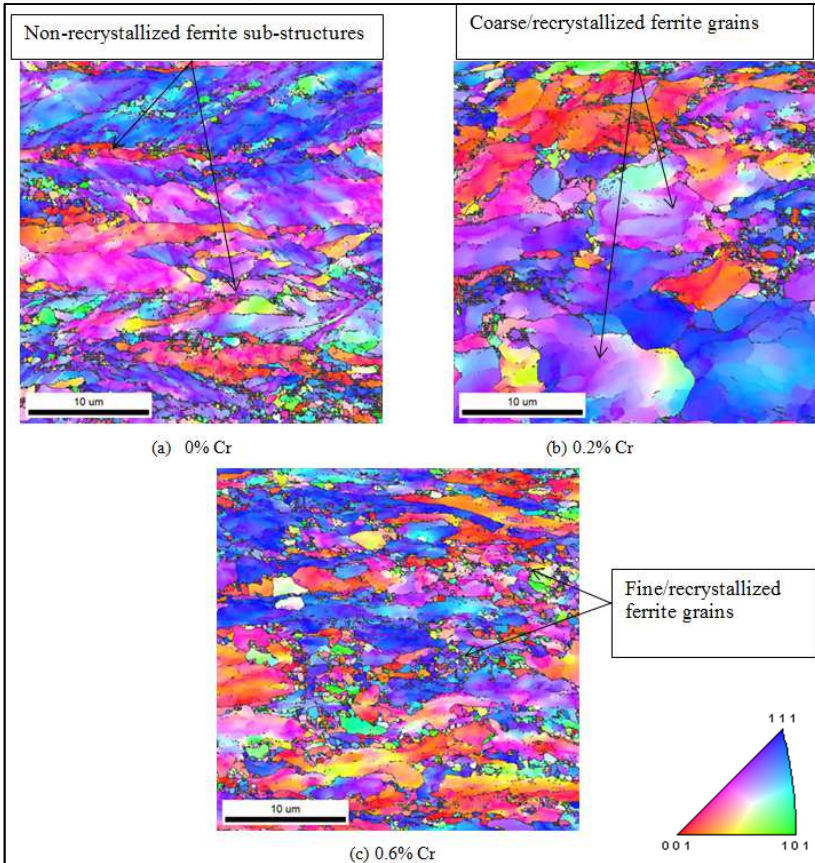
Source: Original, (2014).

To compare the kinetics of recrystallization of steels with different Cr content (0 to 0.6 % Cr) it was taken as reference the 0 % Cr steel. It was observed that the first additions of 0.2 % Cr in the steel

accelerated the recrystallization (nucleation and growth) with grains revealing recrystallized and coarse (Figure 5.9 b). As mentioned before, this acceleration is likely due to the reduction of the activation energy barrier for grain growth (Q_G) by the presence of Cr in the matrix. Reducing "Q_G" the grain growth rate (G) increased according to Avrami-Roosz' equation (CABALLERO et al., 2001).

$$G = f_G \exp(- Q_G/k\Delta T) \tag{8}$$

Where:
G is the growth rate
Q_G is the activation energy of grain growth
k is Boltzmann's constant
f_G is a function that describes the effect of the structure on growth rates
ΔT is the overheating (T-Ac$_1$)

Conversely, higher chromium concentration in steel (0.6 % Cr) has effectively refined the grains, in comparison to the concentration of 0.2 % Cr, even with the enhancement of recrystallization. This refinement is likely due to the pinning effect exerted by the small chromium carbides particles (HUMPHREYS & HATHERLY, 1994) and chromium in solid solution (interaction) (DOHERTY & MARTIN, 1962) acting as a barrier for the migration of the grain boundaries.

Pin effect was observed in this study, during the investigation of microstructure on field emission gun, through the alignment of small particles pinning the dislocations movement (Figure 5.10). The amount of chromium carbides particles increases with chromium content in the steels and pinning effect becomes more effectively. Many authors have mentioned the pinning effect exerted by small particles of carbides/precipitates on the movement of grain boundaries.

Sub-micrometer precipitates in the grain boundaries have strong effect on the retardation of movement of dislocations, e.g. cementite particles of average size below 250 nm caused a strong inhibition of grain boundary migration due to the pinning effect retarding the recrystallization and grains (HORNBOGEN et al., 1991; SONG et al., 2004).

Carbide-forming elements have shown dual effect on steels; as a carbide particle and as element in solid solution. The presence of moderate dispersion of carbides particles still undissolved after austenite formation produces a fine-grained austenite. Also, carbide-forming elements may at once influence austenite transformation characteristics

by being in part dissolved and contribute toughness through restriction of grain growth (BAIN, 1945; GAZDER et al., 2011).

Figure 5.10 – Small carbide particles aligned in the center of the grain and pinning the migration of dislocations (0.6 % Cr at 740 ºC).
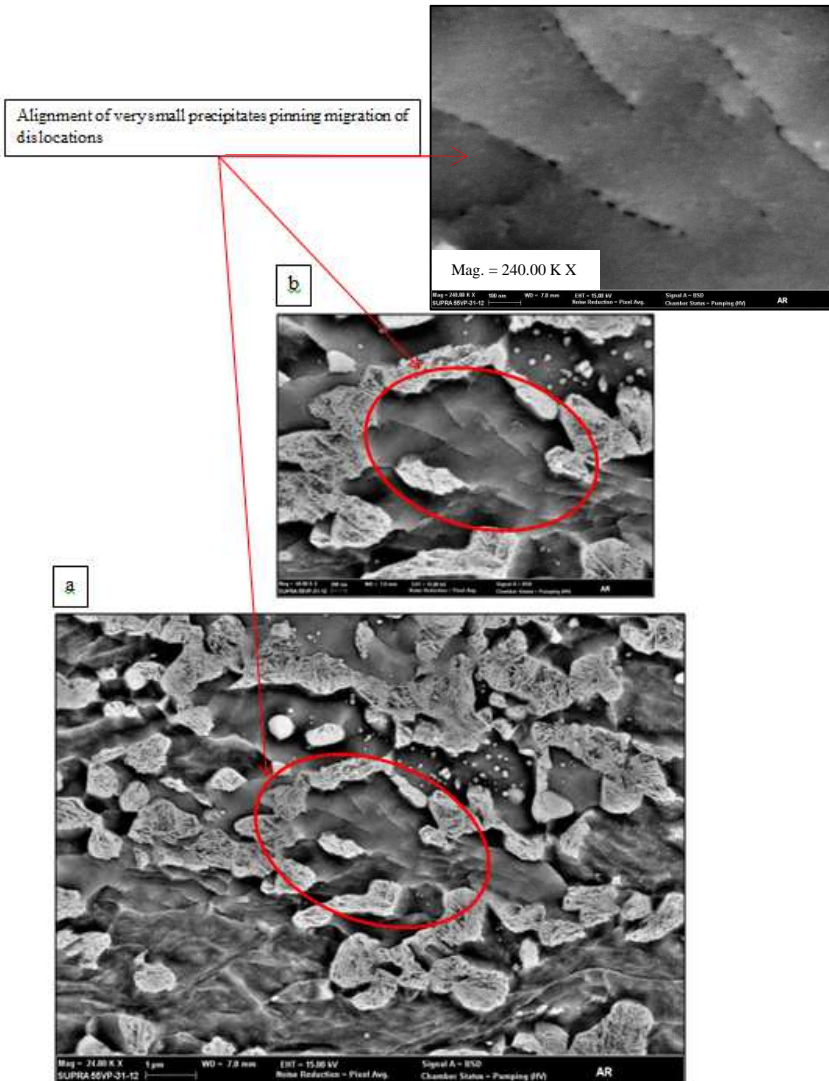
Source: Original, (2014).

Up to here the recrystallization phenomenon was more depicted than phase transformation (volume fraction of austenite /martensite) and carbide particles hereafter discussion will be inverted.

Figure 5.11 shows the percentage of martensite increasing with temperature and Cr content up to around 840 °C when the microstructures of steels became as full martensite.

From 720 ºC up to around 810 ºC, the austenitization is fastest for the steels with 0.6 % Cr and slowest for Cr-free steels. This confirmed the effect of Cr on the kinetic acceleration of martensite transformation.

Figure 5.11 – Effect of temperature and Cr content on kinetic of austenitization and percent of martensite after water quench.
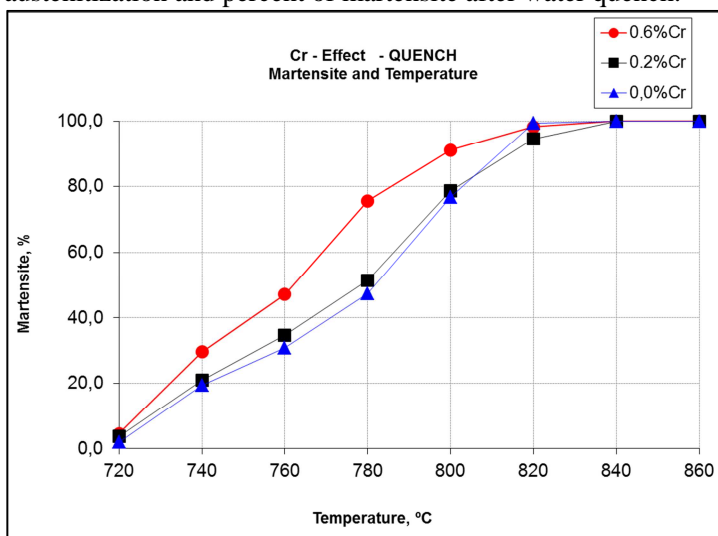
Source: Original, (2014).

Figures 5.4 and Figure 5.11 show the increase in the amount of (martensite) with the addition of Cr in steel. It is important to highlight that the mechanisms of austenite nucleation and growth differ with the amount of Cr in the steels, as following observations.

The "austenite grains" nucleate and grow, predominantly, at the ferrite sub-grains and grain boundaries of Cr-free steels (Figure 5.12); at the grain boundaries for steels with 0.2 % Cr (Figure 5.13) and at the both positions (grain boundaries and inside the ferrite grain) for steels with 0.6 % Cr (Figure 5.14).

Figure 5.12 shows microstructure of 0 % Cr steels with substructures all around and martensite growing in the boundaries.

Figure 5.12 – Martensite structure growing along the substructure boundaries (0 % Cr steel) - water quench.
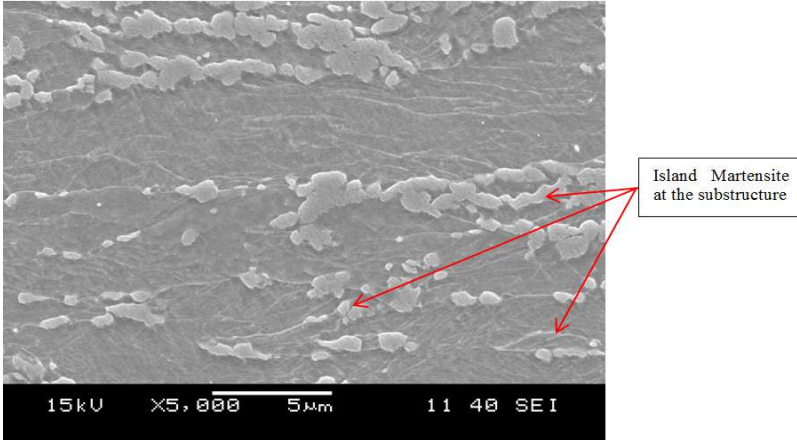
Source: Original, (2014).

Microstructure of steel containing 0.2 % Cr revealed clearly grain boundaries with martensite growing along them (Figure 5.13).

Figure 5.13 – Martensite structure growing along the grain boundaries (0.2 % Cr steel) - water quench.
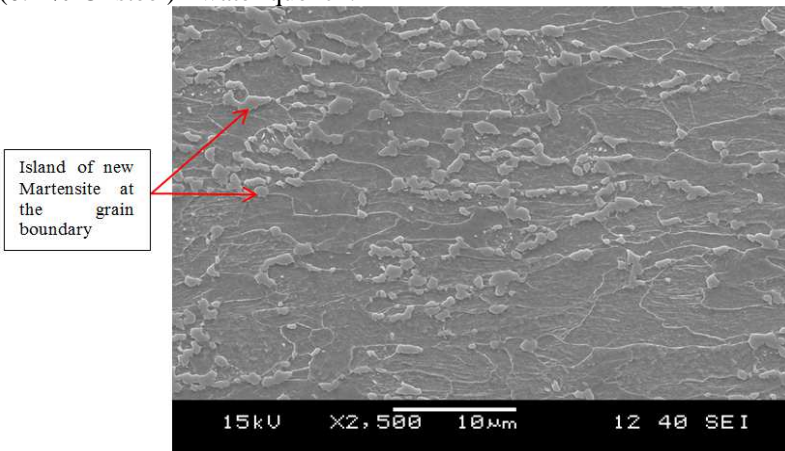
Source: Original, (2014).

Figure 5.14 shows the positions in ferrite grain, where austenite nucleated and grew, in the microstructure of the 0.6 % Cr steel. Martensitic structures were observed in the boundaries (Figure 5.14 – region a) and inside the ferrite grain (Figure 5.14 – region b). These observations suggest that the addition of Cr in the steels changed the balance of energy between grain boundary and the center of grain, favoring the nucleation rate ($\dot{N}$) and austenite growth (G) in this region (the center of the grains). Besides, the carbides without chromium decomposed faster than the ones with chromium additions as will be shown later (Figure 5.25). Thereby, carbon atoms released from less stable carbides diffuse to the grain boundaries favoring the nucleation and stability of austenite in these regions.

Figure 5.14 – Austenite nucleation and growth in the center of grains (outline) on the surface of precipitates of steel (0.6 % C at 740 ºC).
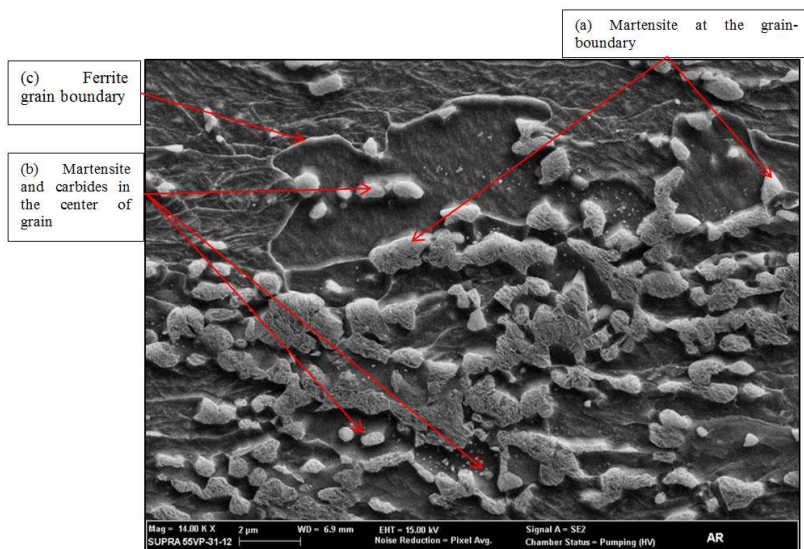
Source: Original, (2014).

Therefore, it indicates that Cr found in the steels should be in solid solution for low concentrations (since no Cr-carbide particles were found) and as chromium carbides for higher Cr concentrations (since those particles were found). This confirmed that addition of Cr in the steels favored the nucleation rate (N´) and growth of austenite (G), in the center of the grains. It can be endorsed by Porter et al. (2004) that

mentioned Cr as an element that can join the steels lattice and then lowering the activation barrier energy of nucleation and growth. Besides that chromium acted on forming and stabilizing carbides particles, which in turns became additional sites for nucleation and growth of austenite. This is coherent with Avrami's equation that describes the processes of nucleation and growth under isothermal condition.

$$V\gamma = 1 - exp\left(-\frac{\pi}{3}\dot{N}G^3t^4\right) \qquad (9)$$

Where V_γ is the austenite volume fraction, $\dot{N}$ is the nucleation rate, G the growth rate and t is the time.

$\dot{N} = f_N \exp(-Q_N/k\Delta T)$

$G = f_G \exp(-Q_G/k\Delta T)$

Where:

Q_N and Q_G are the activation energy of nucleation and growth, respectively.

K is Boltzmann's constant.

f_N and f_G are functions that describe the effect of the structure and the heating rate on the nucleation and growth rates, respectively (CABALLERO et al., 2001).

The additions of chromium in the steel affected the volume fraction of austenite (martensite) by two ways: through the increasing of nucleation rate ($\dot{N}$) and growth rate (G) of austenite: Increasing these rates the second term of Avrami's equation (9) reduces and the volume fraction of austenite (V_γ) increases.

The explanation for the increasing in the nucleation rate ($\dot{N}$) by chromium addition, is due to the effect of chromium, as carbide particles which act as additional sites for the nucleation of austenite in the center of ferrite grains (matrix). Considering that chromium carbide particles and ferrite matrix have different crystal structures their lattice planes are not common to both what creates a mismatch in the arrangement (incoherent interface between ferrite/chromium carbide particles). This incoherence increases the interphase energy in the center of the ferrite grains favoring the nucleation of austenite on the surface of carbide particles. Upon the dissolution of the chromium carbide particles, carbon atoms diffuse across the interface carbide/austenite with the carbon enrichment of austenite, thereby promoting its stability and growing. This carbon enrichment process enhances the hardenability of the austenite (GARCIA, et al., 2011).

The point of this affirmation is that excess of energy that promotes the nucleation of austenite in the center of the ferrite grains comes from the interface between ferrite matrix and the chromium carbides particles. This is based on the affirmation of Porter and Easterling (2004) that the insertion of a foreigner body in the parent structure of steel causes a distortion and discontinuity in the lattice at the vicinity. The discontinuity of lattice creates thereby, a separating boundary and strain at the neighborhood. Thus, particles create an incoherent interface with parent phases which in turns causes variation in energy of neighborhood structure.

Figure 5.15 confirmed the presence of these particles at the ferrite matrix.

Figure 5.15 – Transmission electron micrograph of (a) high resolution and (b) bright field showing particles inserted in the ferrite matrix.
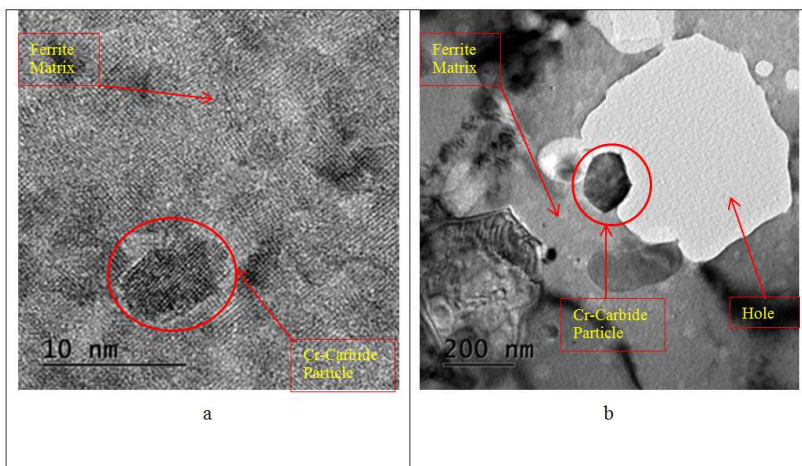
Source: Original, (2014).

Similarly to treatment at 740 ºC, the microstructure (phase transformation and recrystallization) of steels annealed at higher temperature (780 ºC) changed, but faster.

Figure 5.16 (a) shows the effect of chromium on (a) phase transformation (amount of martensite) and Figure 5.16 (b) recrystallization (refinement of austenite).

The high annealing temperature (780 ºC) resulted in the acceleration of recrystallization and faster carbides decomposition.

At 780 ºC all carbides have dissolved completely, except those containing chromium. The remaining Cr-rich carbides, decomposed slow and partially, thus reaching the adequate size (below 250 nm) to act as a barrier for the movement of dislocations (SONG et al., 2004). These particles sizes exert major pinning effect and prevent the further grain growth (ferrite grains refinement).

The increase in temperature caused different changes in the recrystallization as a function of Cr concentration (Figure 5.16 b):

i) in the Cr-free steel the recrystallization develops slowly with the presence of elongated non-recrystallized grains (mixing microstructure of recrystallized and non-recrystallized grains);

ii) the 0.2 % Cr steel shows the fastest recrystallization rate with coarse recrystallized grains (predominantly);

iii) in 0.6 % Cr steel the process of recrystallization was almost complete and showed, predominantly, refined grains. These refinements is likely due to the pining effect of fine carbides; which at 780 ºC reached the ideal size and acted as a barrier to the movement of dislocation.

Besides that, it was noted, that at high temperatures martensite structures appears like massive differently of solid martensite at lower temperatures. This is due to the lower concentration of carbon in austenite as the temperature increases.

Figure 5.16 – Effect of Cr content in (a) amount of martensite [(0 % Cr = 47.4 % α'); (0.2 % Cr = 51.5 % α'); (0.6 % Cr = 75.6 % α')] and (b) recrystallization, at 780 ºC.
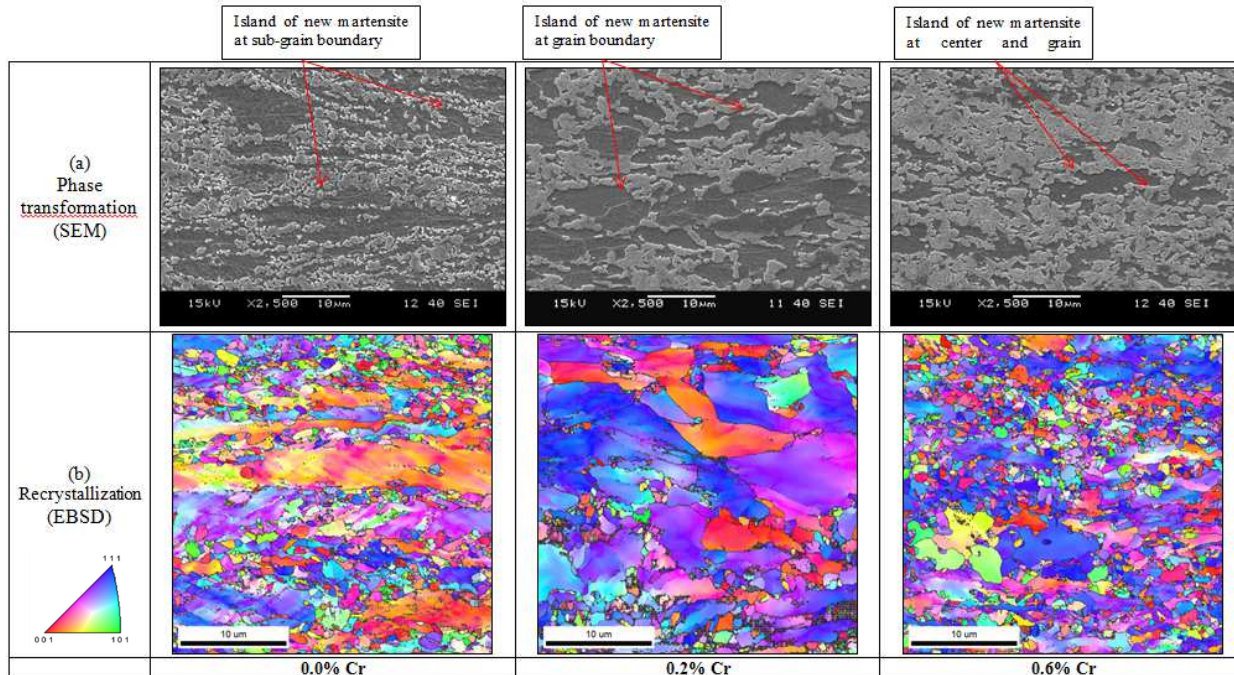
Further increases in temperature, from 800 to 860 °C the amount of martensite increases rapidly and region is almost 100 % with massive martensite.

5.1.1 Behavior of Chromium Carbides on the Nucleation and Growth of Austenite.

An intensive investigation on the role of carbides in the phase transformation and recrystallization of dual-phase steels was developed and discussed hereafter.

Figure 5.17 displays one representative grain of ferrite taken as an example to show in details the grain boundary, martensite and chromium carbides and their respective positions. This grain brings about the main idea of the proposed mechanism by which the refinement occurs.

The presence of many small island of martensite inside the grain confirms, in fact, the occurrence of nucleation and growth of austenite in this region.

The significant amount of martensite inside the grains was observed predominantly in steels with higher Cr content, which in turns showed more carbide particles (Figures 5.5c, 5.7c and 5.17).

Then a connection among higher Cr content, the presence of chromium carbides inside ferrite grains, nucleation of austenite inside ferrite grain, refinement of martensite and increase strengthening built up the idea of one mechanism to explain the phenomenon.

Microscopic investigations were carried on inside grains as shown in Figure 5.17. Particles found inside grains were analyzed and showed a strong relation between "the presence of carbides" and "nucleation and growth of austenite (martensite)" (Figure 5.18). Evidences of austenite (white body) nucleating on the surface of carbides (grey body) were shown in Figures 5.18 to 5.20. The presence of chromium in carbides was evidenced in Figures 5.19 to 5.21.

Figures 5.19 (point 1 - base 1) and Figure 5.20 confirmed the presence of Cr in carbides which became *site* for austenite nucleation.

The technique of carbon replica was used for extraction of carbides particles to be identified on STEM and aiming to support the hypothesis the presence and effect of Cr-carbide.

Figure 5.17 – Microstructure of a ferrite grain showing coarse martensite in the boundary; fine martensite nucleate and growing and fine chromium carbides in the center of grain for the 0.6 % Cr steel (740 ºC).
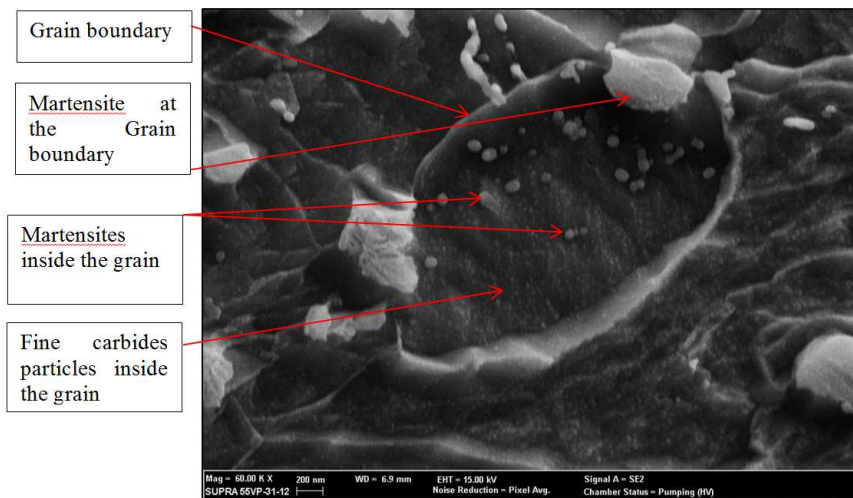
Source: Original, (2014).

Figure 5.18 - Microstructures of 0.6 % Cr steels showing the austenite nucleation and growth in situ (surface of chromium carbides).
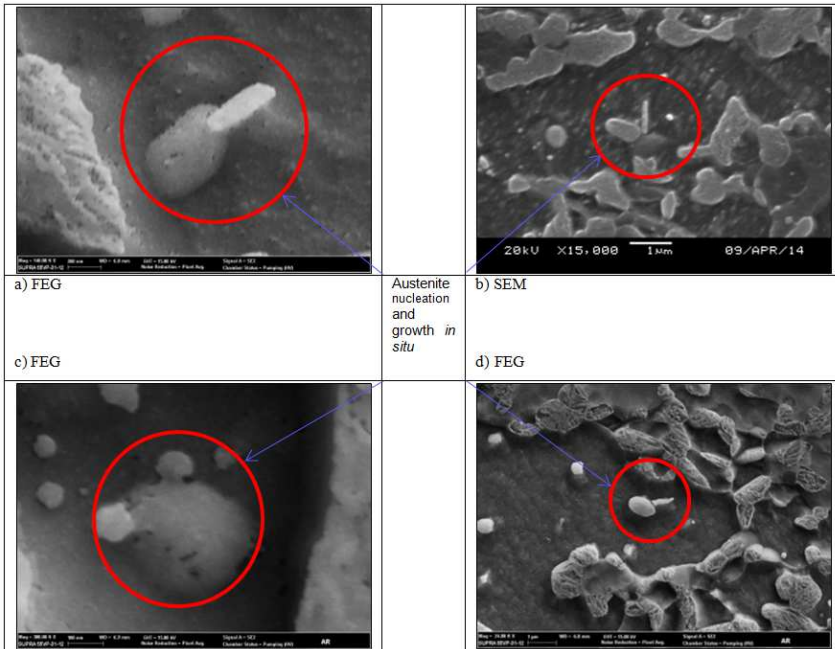
Source: Original, (2014).

It was observed the presence of chromium in the composition of carbide particles, where austenite nucleated and grew, as confirmed by EDS spectrogram (Figures 5.19 and 5.20 - point 1 - base).

More evidence of the presence of Cr and others elements in the carbides composition were observed by chemical analysis in STEM on carbon film, as shown in Figure 5.20.

Figure 5.19 – Austenite nucleation in situ (chromium carbide precipitate - pt1) and EDS spectrogram.

(a)   (b)
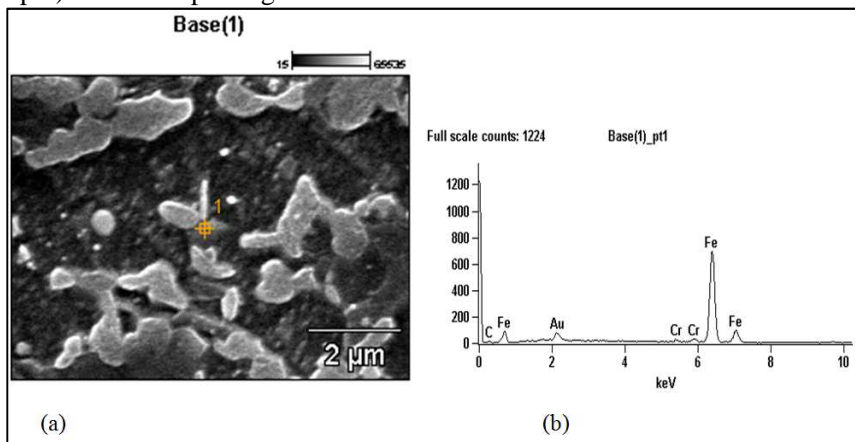
Source: Original, (2014).

Figure 5.20 – Chemical analysis of chromium carbides by STEM.

Element (wt%)	Mo	Cr	Mn	Fe (from matrix)
PPT1	0.00	5.13	8.53	86.34
PPT 2	0.00	5.34	8.32	86.33
PPT 3	0.00	7.40	13.26	79.33
PPT 4	3.00	7.88	11.30	77.82
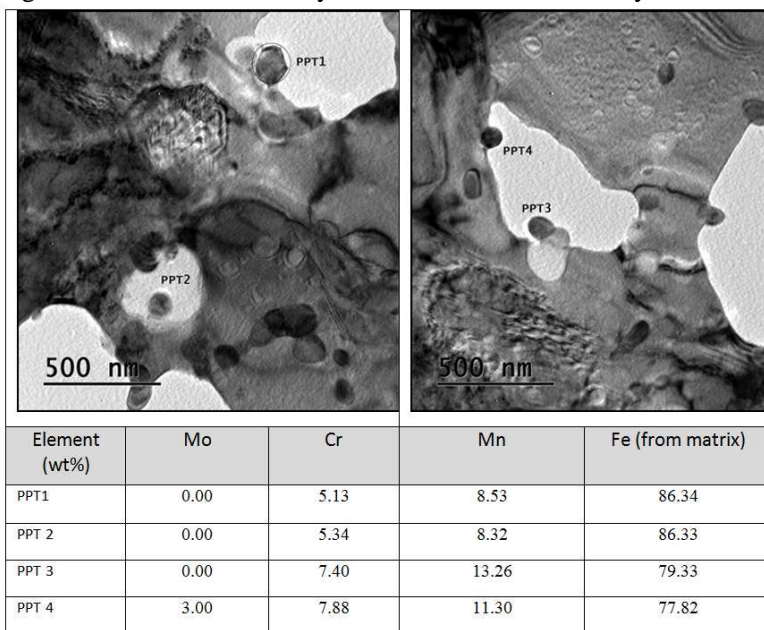
Source: Original, (2014).

Figure 5.21 shows these carbides (extracted from the steels with carbon film using the carbon replica technique) after etching in acid solution (appendix E).

It was observed, that the carbide particles were found, predominantly, within the areas that were initially occupied by the martensite island (grayish outlined area). This observation strengthens the association between the austenite grains and carbides particles (frequently in the presence of chromium).

Film of carbon replica investigated on TEM showed up two distinct areas on steels (0.6 % Cr) and carbides as follows (Figure 5.21).

    (a) the area that was occupied by the ferritic matrix or prior ferrite matrix area (clean area);

    (b) the area that was occupied by martensite island or boundary of prior martensite (greyish area);

    (c) the actual chromium-rich carbides particles extracted from the steel (black spots).

Figure 5.21 – Chromium carbides particles associated with martensite islands for steels of 0.6 % Cr at 740 ºC (transmission electron microscope).
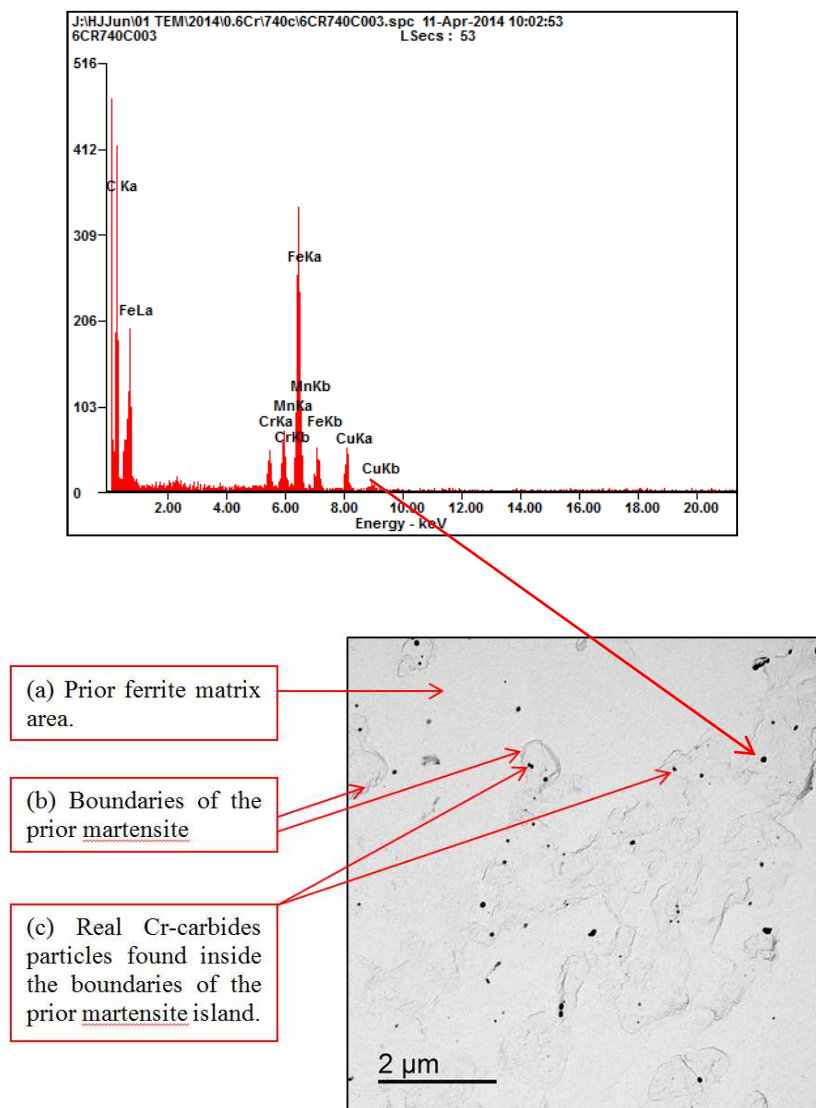
Source: Original, (2014).

5.1.1.1 Chromium Carbides Stability

Since the stability and presence of chromium carbides particles were often mentioned during the text, further study was developed to better understand the behavior of this species during heat treatment.

Many authors Krauss, (2010), Xie et al. (2005) and Xiao, et al., (2007) have mentioned the ability of chromium to stabilize precipitates. Based on the measurement of interatomic potential (cohesive energy) Xie et al. (2005) showed that stability of carbides decreases in the order Cr_7C_3, Mn_7C_3, Fe_7C_3 that is related to the increase in the atomic number of carbide-forming element. Accordingly, Cr is the element that has the smallest atomic number among the carbide-forming elements (Cr, Mo, Mn, Fe), thereby can form more stables carbides.

Simulation developed by using thermocalc software based on the chemical compositions of the steels of this study was developed to follow the occurrence of the most likeable precipitates.

Figure 5.22 shows the thermocalc equilibrium diagram with the formation of new phases (represented by new areas in following diagrams) due to the addition of chromium to steels. These new areas indicate the likelihood for the existence of new carbides (for instance carbides more complex than the M_3C).

The first simulation showed the effect of chromium (in the presence of manganese and molybdenum) on the eutectoid point and on the appearance of phase in the equilibrium diagram of steel. Additions of 0.6 % Cr shifted up and left the eutectoid point $E_{p\,=}$ (% C; T ℃) as shown in Figure 5.22. Thereby, Ep_1 (0.66 % C; 712 ℃) moved up and left to Ep_2 (0.57 %; 721 ℃). New fields have shown up (red shaded ellipse in Figure 5.22 (b) indicating the thermodynamic probability for the formation of more complex precipitates such as $M_{23}C_6$ and M_7C_3 as mentioned by KRAUSS (1995).

Figure 5.22 – Effect of Cr addition on dislocation of eutectoid point (Ep$_1$ → Ep$_2$).

a) 0%Cr

b) 0.6%Cr
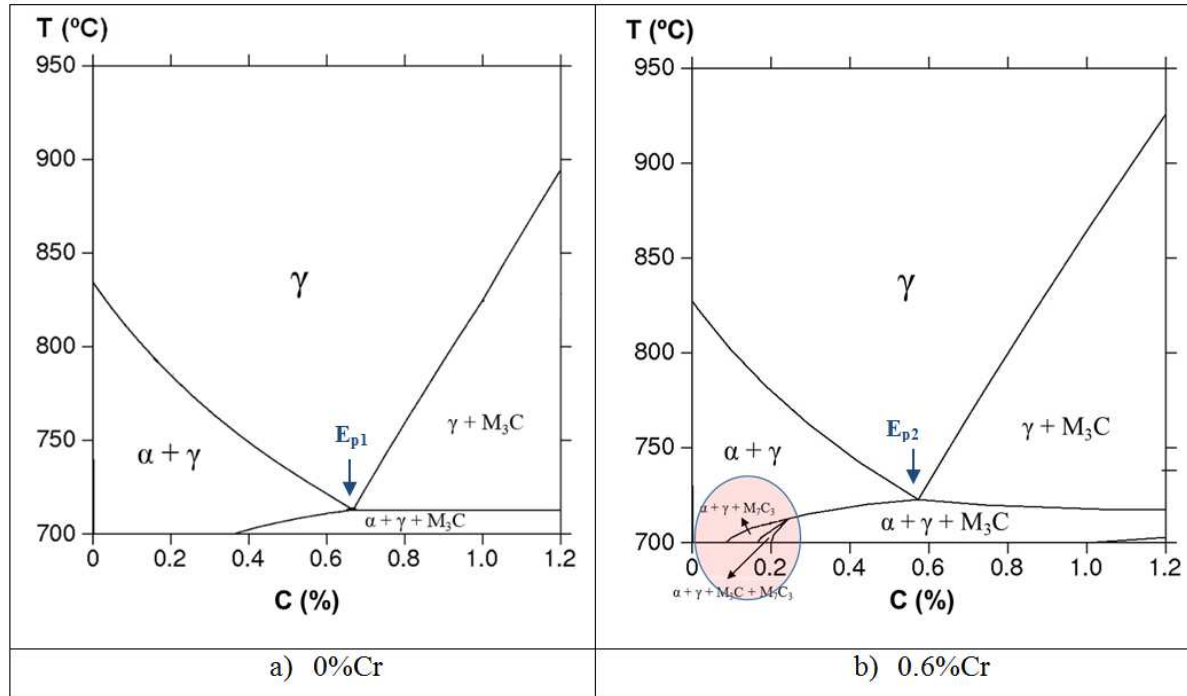
Source: Original, (2014).

Figure 5.23 displays the yellow shaded area that is higher magnification of M_7C_3 field shown in Figure 5.22. This shows that addition of 0.6 % Cr to steel may improve the stability of chromium-rich carbides even up to high temperatures as shown in Figure 5.23.

The maximum temperature for dissolution of M_7C_3 increased from 645 to around 710 ºC (enlargement of the field for the existence of M_7C_3).

Figure 5.23 – Effect of addition of 0.6 % Cr in the steel on the enlargement of the M_7C_3 field.

a) 0%Cr

b) 0.6% Cr
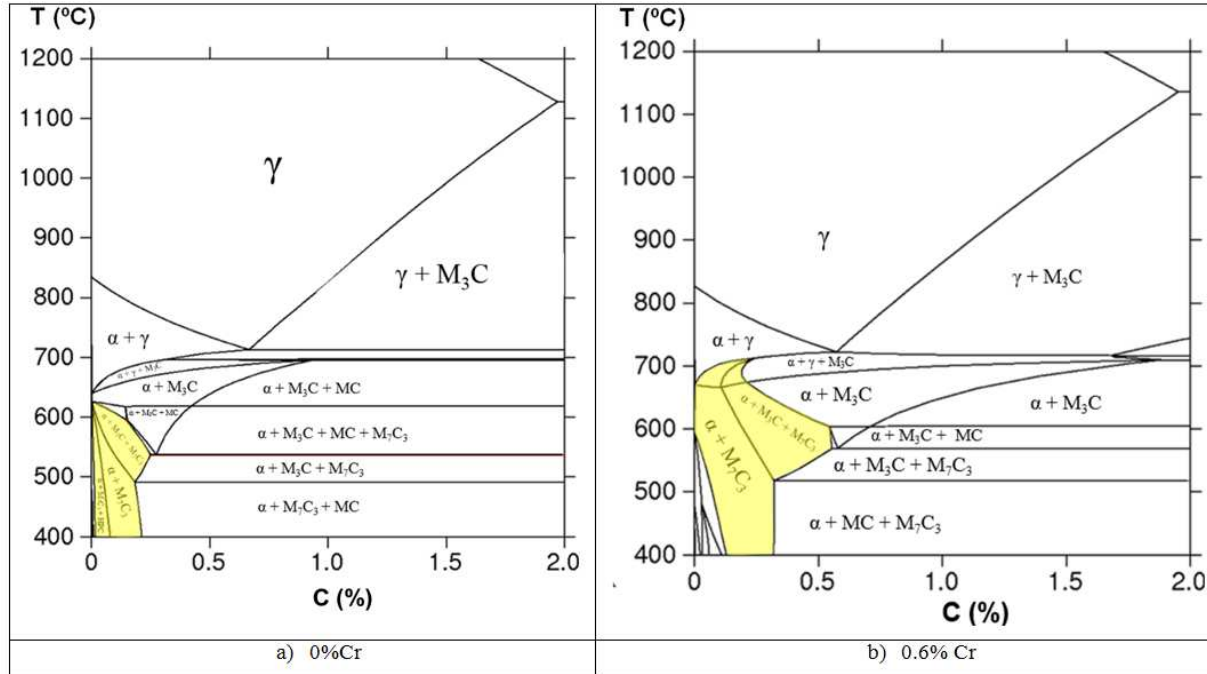
Source: Original, (2014).

Figure 5.24 – Effect of chromium addition on the field for $M_{23}C_6$ formation.

a) 0%Cr	b) 0.6% Cr
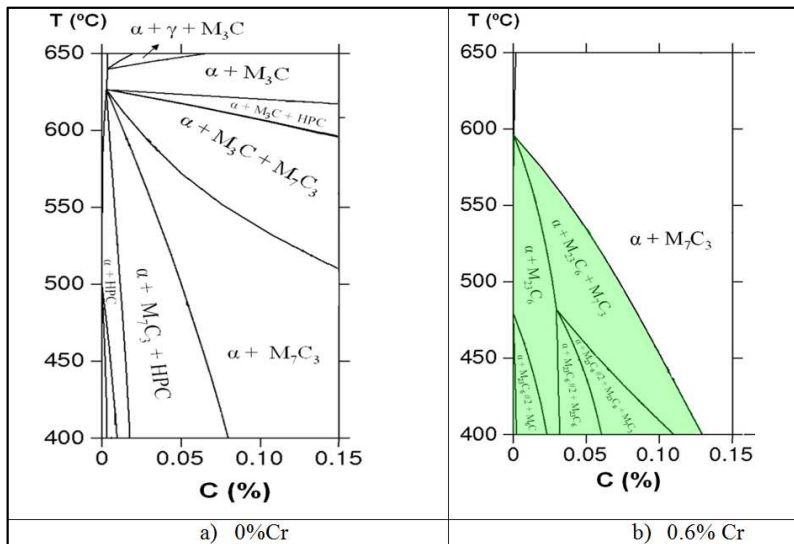
In Figure 5.24 the diagrams shows the thermodynamic possibility for the existence of carbides $M_{23}C_6$, M_7C_3 and M_3C (M: metals such as Cr, Mn, Fe, and Mo).

One important feature of these chromium-rich carbides is the higher stability (long-term existence) in comparison with the chromium-free carbides steels.

Hereafter, a brief discussion addresses the comparison in stabilities of Cr-free carbides versus Cr-added carbides.

Figure 5.25 displays the sequence of dissolution of chromium-free and chromium-added precipitates (carbides, nitrides).

In Figure 5.25 the chromium-free carbides appeared in the matrix at 720 °C as $(M)_x(C,N)_y$ (M: metal such as Fe, Ti, Nb, Mn or Mo); whereas in the chromium-added ones M can also be Cr (the x and y are integer numbers). Cementite composition in alloy steels could be represented by (FeM_3C) since the main structure is the cementite in the presence of alloying elements M (PORTER & EASTERLING, 2004). On investigating changes in precipitates features (shape and size) with temperature (from 720 to 780 °C), it was observed that the addition of Cr (chromium-rich steels) slowed the kinetic of carbides dissolution, as mentioned by Fonstein et al. 2015.

Figure 5.25 b showed, at 740 ºC, that the Cr-rich carbides particles decomposed partially, whereas the Cr-free ones have already complete decomposed (Figure 5.25 e). At this temperature, the remaining carbides were the result of the decomposition of the coarse agglomerates carbides observed at 720 ºC (Figure 5.25 a). The coarse carbides remained were the sables (M) (C, N) where M can be (Ti, Nb, Cr, Mo, Mn).

At 780 ºC, even after dissolution of the initial carbides, the Cr-rich still remained (high stability), nevertheless as a bunch of very small particles. These very tiny particles (15~ 50 nm size) were extracted on carbon replica film and identified chemically and lattice parameters by STEM.

Transmission electron microscopy investigation allowed to pointed out:

i) the majority of precipitates was found inside the "shadow" areas outlined in Figure 5.25 (red arrows). It suggested that these areas were outlined from regions previously occupied by martensitic structures.

Figure 5.26 shows the tiny particles extracted on carbon film and their respective chemical analysis (STEM). It confirmed the presence of Cr and Mn in carbides (ppt 2, 3 and 4) and TiN (ppt 1). The atomic d-spaces of these carbides are shown in appendix E.

The dissolution of chromium carbides come through the diffusion of carbon atoms that join to the austenite structure, enhancing its hardenability.

Figure 5.15 – Effect of chromium content on the kinetic of carbides dissolution at different temperatures.
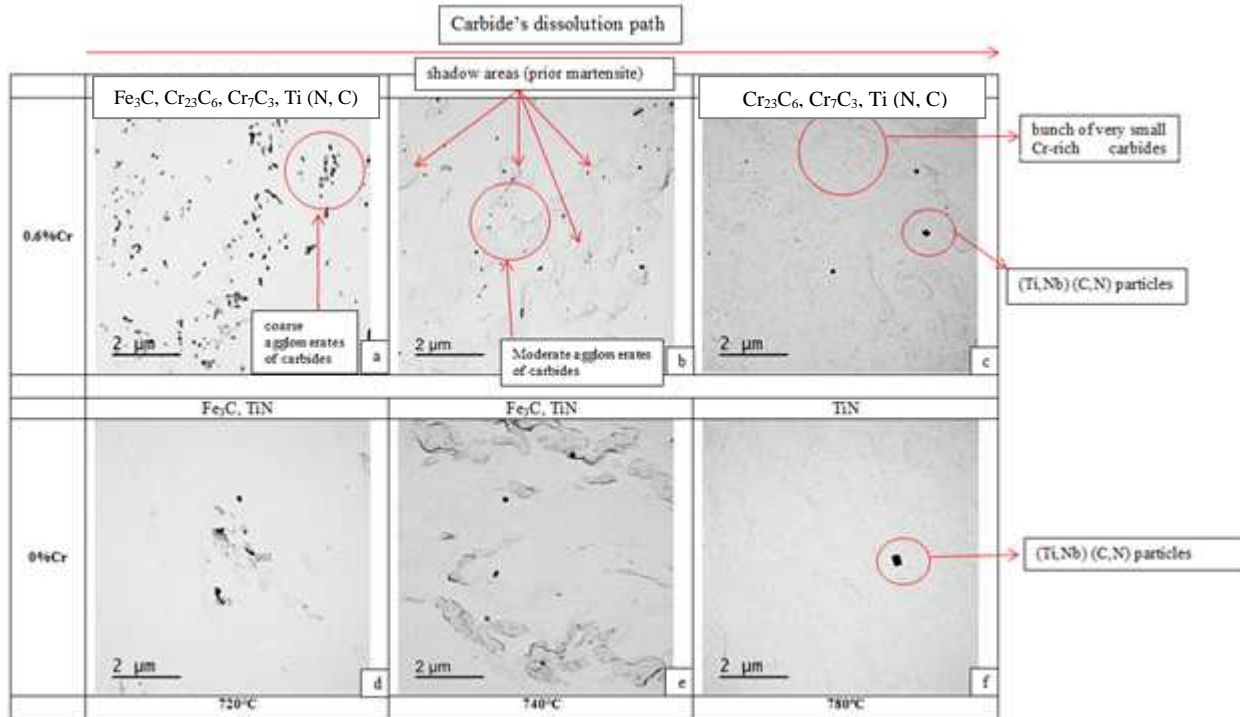
Source: Original, (2014).

Figure 5.26 - Chemical analysis of the remaining nano-particles after at 780 ºC for 60 s - STEM.
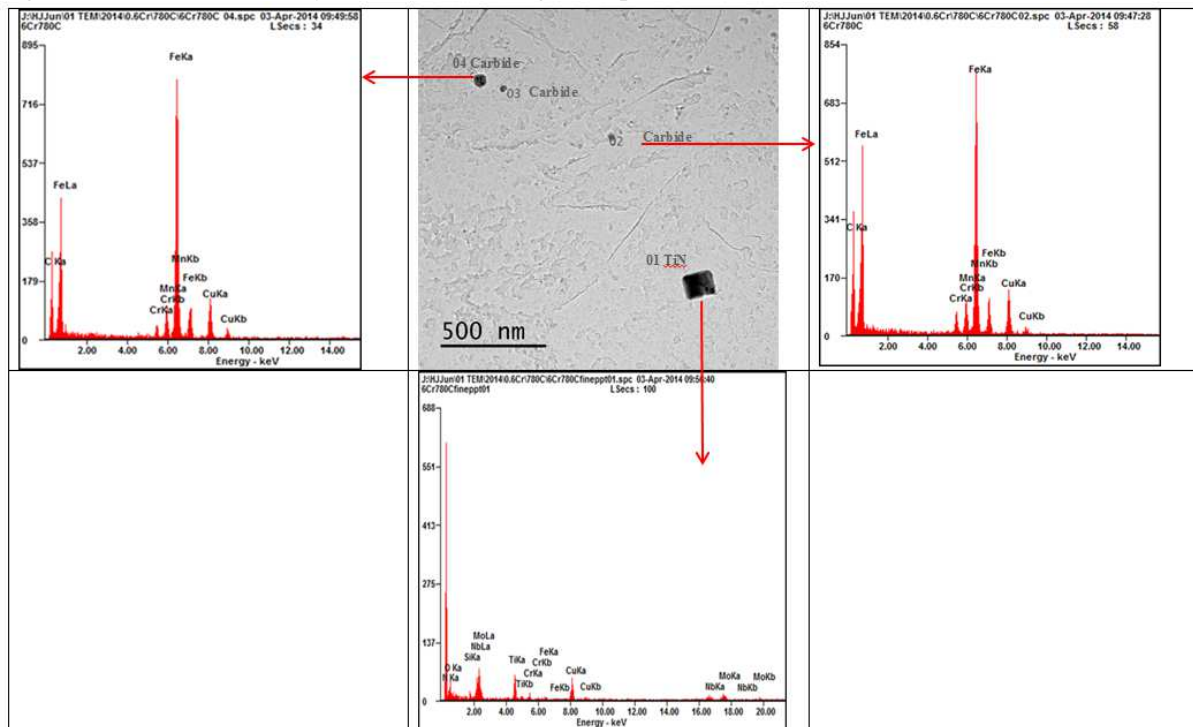
Source: Original, (2014).

These analyzes showed many different precipitates (carbides and nitrides) in the steels used in this study. During heat treatment these carbides performed by different ways, which in turns affected the thermodynamics and kinetics of reactions. As an example, the increase in temperature resulted in completely dissolution of Fe_3C; partial dissolution of both $M_{23}C_6$ and M_7C_3. It indicates that Fe_3C was the less stable carbide; however the $M_{23}C_6$ and M_7C_3 showed intermediate stability in steel with low to moderate Cr concentration and high stability in steel with high Cr concentration.

5.1.2 Modeling the Mechanism of Nucleation and Growth of Austenite in the Steel

Based on these previous observations a schematic model (Figure 5.27) was proposed to explain an additional mechanism that contributes to the refinement of austenite when Cr is added and, consequently, to their strengthening.

According to Porter and Easterling (2004), additions of Cr to the steel up to the solubility limit result in the solid solution and above it forms chromium carbides.

In solid solution Cr promotes stress/strain in the lattice lowering the activation energy barrier for further nucleation and growth of ferrite/austenite.

As chromium carbides, these particles act by two ways; first by sharing their surfaces for the nucleation of austenite grains (lowering surface energy) and later, during the particles dissolution, as a source of carbon, thereby enhancing the austenite hardenability.

Accordingly, since by transmission and electron microscopy investigation, the chromium carbide particles were found, predominantly, inside the grains; thus their presence affected the austenite nucleation process (inside of the grain).

Besides the presence of carbides within the grain, it was also observed the association of the pair martensite/chromium carbides; which suggested the favorability for the occurrence of this synergic pair.

As mentioned by Porter and Easterling (2004), carbides/precipitates are non-equilibrium defects with a solid surface formed, which can act as an available nucleation sites; and consequently supply their own surface for the heterogeneous nucleation of austenite.

During the reactions of decomposition of carbides particles, the energy that was generated contributed to lowering the total surface free

energy required for austenite surface formation (lowering the activation energy barrier).

Austenite nucleation rate $\dot{N}$ is proportional to the number of affordable sites for nucleating austenite (REED-HILL, 1982). The more is the number of chromium carbides the more is the number of sites for the nucleation of austenite.

Thus, increasing chromium concentration in steel, resulted in the increase of the number of chromium carbide particles, which in turn generated more sites for nucleation of austenite (increased the rate of nucleation), consequently, promoted the refinement of grains.

During the decomposition process of chromium carbides the carbon atoms diffuses through a common interface carbide/austenite enriching the austenite in carbon, thus increasing its hardenability.

These two roles of the carbides during heating and holding result in the formation of much more nuclei of austenite.

The austenite that nucleate, within the grain have to grow in all directions, thus also to the grain boundaries. During the movement of growing, the surface of one grain reaches the surface of other austenite grains which move from the boundaries into the center of ferrite. These collisions between grains, growing in the opposite directions, restrain their further growth and, consequently, preventing them from coarsening. This characterizes the growth impediment by the spatial restriction.

The final result is the refinement of grains of austenite in the microstructure of steels. Since chromium carbides dissolve slowly, they can supply their surface and carbon for austenite nucleation and formation any longer.

The compilation of all these steps is the basis for the proposed model of the mechanism at which the microstructures of steels with and without chromium develop to achieve the final grain size (Figure 5.25).

Microstructure changes observed in steels containing 0 % Cr, 0.2 % Cr and 0.6 % Cr were compared at different holding temperature.

Text boxes on the left side (Figure 5.27) explain the changes in microstructure of 0 %   Cr and the ones on the right side explain changes of steels with 0.2 and 0.6 % Cr.

Temperatures were displayed on the left side (30 ℃ to 860 ℃). Temperature 30 ℃ means that steel is on the full-hard condition (i.e. just after cold rolling). Temperatures from 720 ℃ to 860 ℃ mean that the steels were heat treated at this holding temperature. Above 800 ℃ microstructures were similar.

Figure 5.27 – Schematic model proposed for explaining the mechanism of nucleation and phase transformation of austenite with Cr content.

Source: Original, (2014).

In summary, chromium refines dual-phase microstructure through the mechanism of "generation of much more austenite nuclei with high hardenability, which in turns transform into fine martensite due to grain growth restraint. This refinement is clearly observed in Figure 5.28.

Figure 5.28 – Microstructure refinement of low-alloy dual-phase steel due to Cr addition, annealed at 740 ºC, quench.
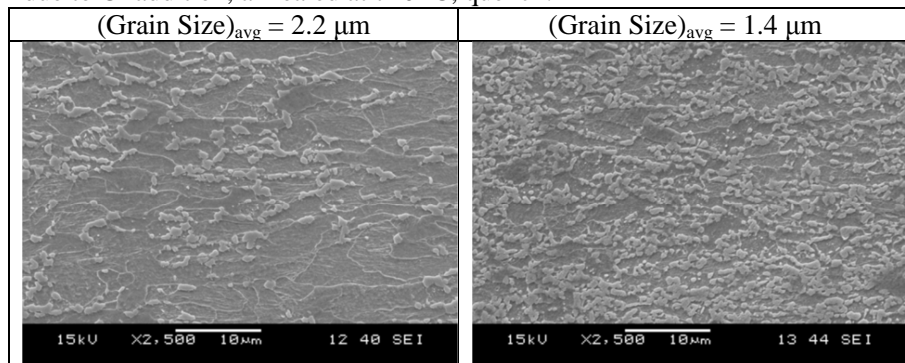
(Grain Size)$_{avg}$ = 2.2 µm	(Grain Size)$_{avg}$ = 1.4 µm
(a) 0.2 % Cr	(b) 0.6 % Cr

Source: Original, (2014).

5.1.3 Dilatometry Experiment

Dilatometry technique was used to better understand the effect of chromium on phase transformation phenomena. Samples were cooled from inter-critical (α + γ) region to room temperature to obtain continuous cooling transformation diagrams (CCT).

CCT diagrams showed in Figures 5.29 (a and b) and microstructures in Figures 5.28 (a and b) showed significant changes during transformation due to the addition of Cr in steels:

The addition of 0.6 % Cr moves the ferrite formation field to a slightly lower temperature to the right side to a slower cooling rate (from ~40 to ~20 ºC/s) which indicates that the addition of chromium suppressed ferrite transformation.

The volume fraction of ferrite is slightly higher in Cr-free steel which could be related to both factors:

i) the higher volume of initial ferrite (20 % in Cr-free and 10 % in Cr-added steel) and;

    ii) the effect of chromium on preventing the austenite structure from transforming to ferrite (enhancement of the hardenability).

Bainitic transformation region is moved to a lower temperature too. The volume fraction of bainite is higher in Cr-added steel which results in a higher martensite start temperature for 0.6 % Cr steel. It is likely due to rejection of carbon during bainite transformation, which enriches the austenite and enhances their hardenability.

Figure 5.29 – Effect of chromium addition on CCT diagram of 0.1 % C DP steels cooled from 800 ºC after 60 s holding (from inter-critical temperature); (a) Cr-free steel and (b) 0.6 % Cr steel.
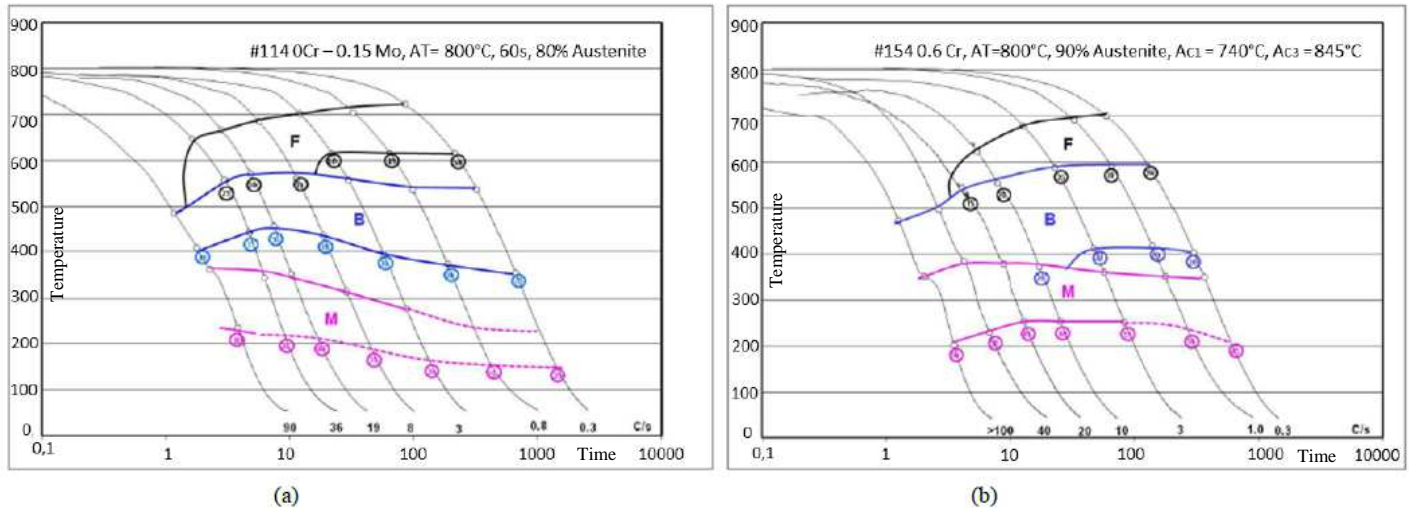
Source: Original, (2014).

Figure 5.30 shows, through the microstructure of steels, that the additions of 0.6 % of Cr delayed the formation of ferrite for all cooling rates.

Figure 5.30 - Effect of Cr addition on the microstructures of steels quenched from $(\alpha + \gamma)$ region at different cooling rates.

Cooling Rate (°C/s)	0% Cr	0,6% Cr
0,3		
8		
100		
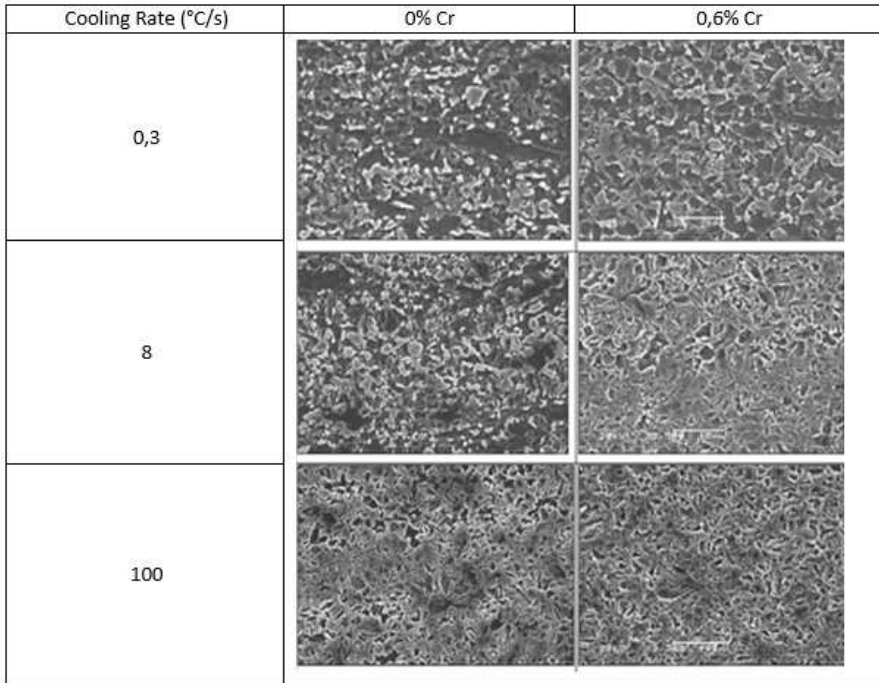
Source: Original, (2014).

5.2 EFFECT OF Cr IN STEEL AT "AIR COOLING"

5.2.1 Microstructure

Figure 5.31 shows the effect of Cr and annealing temperature on microstructure of dual-phase steels after air cooling.

Figure 5.31 – Effect of Cr and temperature on the microstructures (recrystallization, phase transf. and precipitates) of DP after air cooling.

| | (a) 0 % Cr | (b) 0.2 % Cr | (c) 0.4 % Cr | (d) 0.6 % Cr |
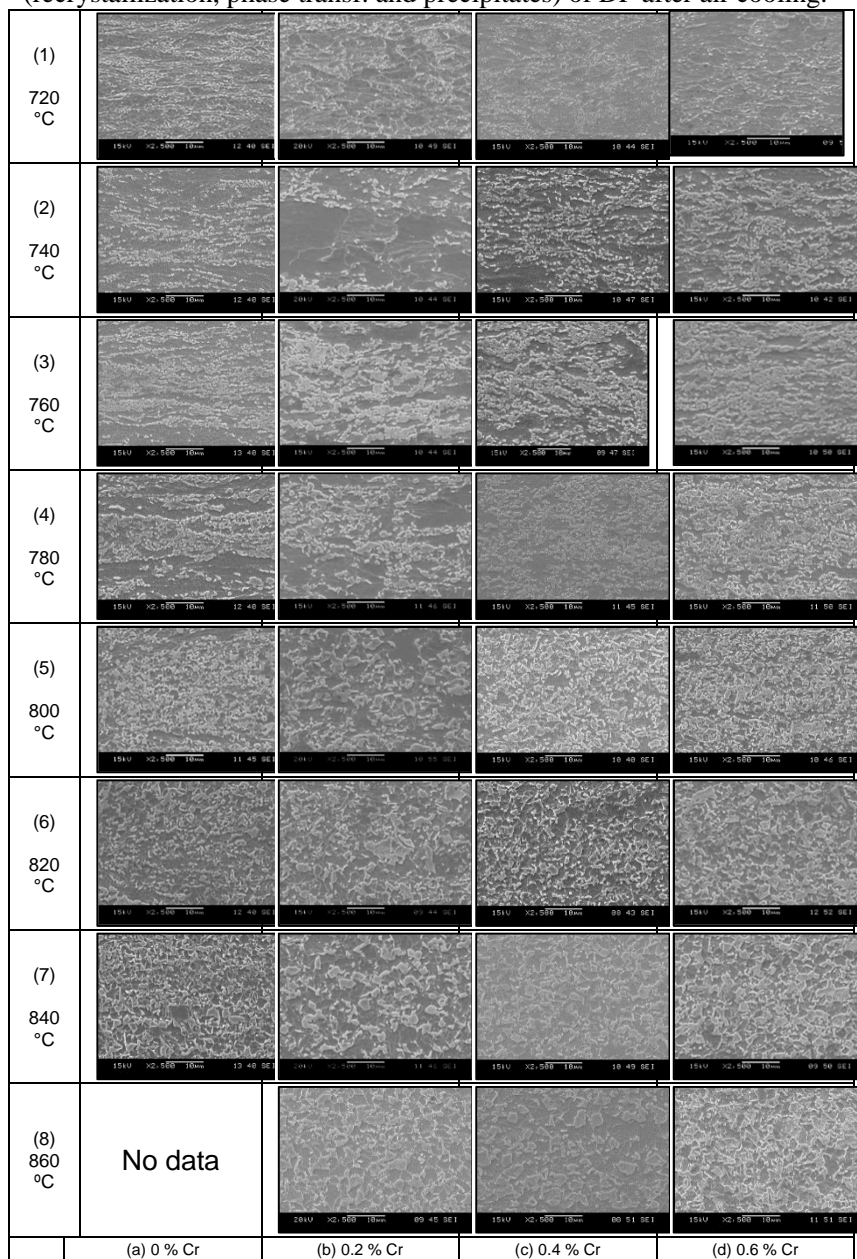
Source: Original, (2014).

5.2.2 Martensite Quantification – Air Cooling

Figure 5.32 shows the effect of Cr and annealing temperature on the amount of martensite that increased with Cr concentration in steels for all temperatures. Martensite increased with temperature up to around 760 ºC and then decreased for temperatures above it. The maximum amount of martensite was reached at around 760 ºC because up to this the amount of austenite increased, with temperature, and its carbon content was enough to keep hardenability. Above 760 ºC more austenite were produced, thus with less carbon concentration (low hardenability) and fraction transforms into others constituents than martensite (e.g. bainite, ferrite). Since air cooling proceeded much slower than quench it allowed the transformation reactions come through the formation fields of ferrite and bainite.

Figure 5.32 – Effect of chromium content and holding temperature on the amount of martensite.
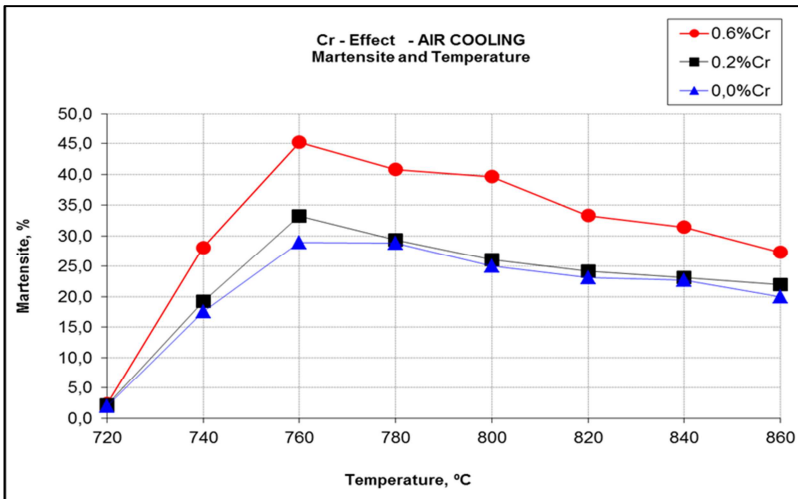
Source: Original, (2014).

Figures 5.33 (a and b) display the effects of Cr concentrations (0 % Cr and 0.6 % Cr), temperatures, and cooling media (quench and air cooling) on the amount of martensite (%). The observed difference in amount of martensite is due to the effect of cooling media air (blue triangle) or quench (green dot).

On water quenching, the amount of martensite increased continuously with temperature up to reach 100 %, at around 820 ºC, for

both steels with and without Cr addition (Figure 5.33 a and b). Differently, the steels cooled in air resulted in the increase of martensite up to a maximum amount at 760 ºC (the maximum amount of martensite is around 30 % for Cr-free steel and 45 % for 0.6 % Cr steel). Afterwards, the volume of martensite decreased slowly with temperature. These differences between the amount of martensite obtained by water quenching and air cooling were due to a fraction of austenite that transformed into ferrite and other constituents such as bainite.

Figure 5.33 – Effect of cooling media (air and water quench) on the volume of martensite for (a) Cr-free and (b) 0.6 % Cr steel.
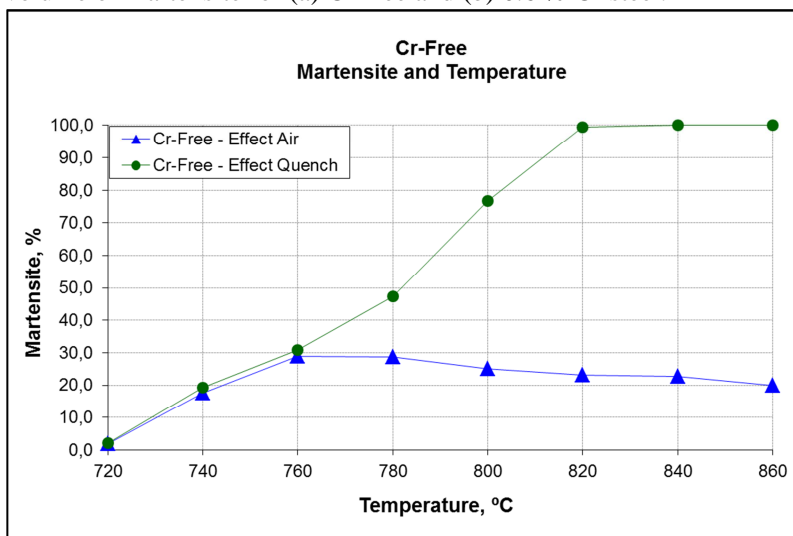
(a) Cr-Free
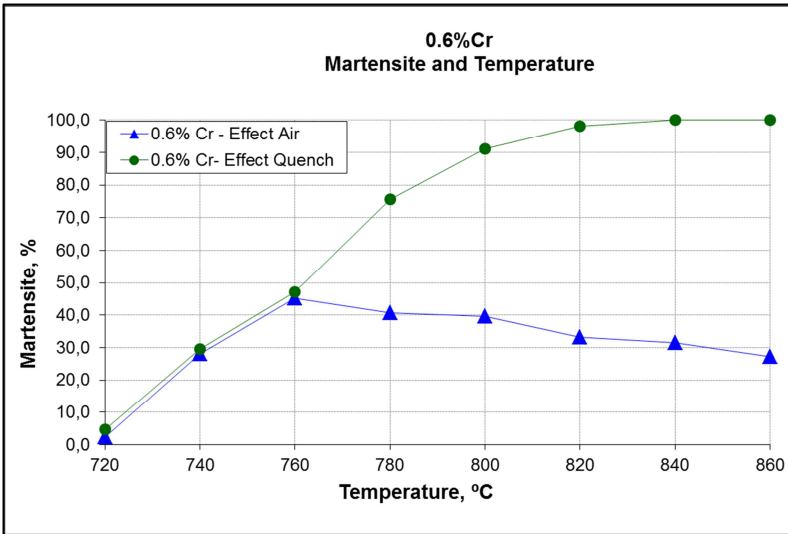
(b) 0,6 % Cr

Source: Original, (2014).

5.2.3 Microstructure Evolution with Cr and Temperature

Figures (5.34 to 5.39) display details of some microstructures of Figure 5.31 in larger magnification (5000X).

Cr-free steels showed non-recrystallized regions with some island of martensite from 720 up to 780 ºC. Above 800 ºC recrystallized ferrite appeared significantly. On the other hand, steels with additions of 0.2 % and 0.6 % Cr have already shown the recrystallized microstructures since 720 ºC.

The microstructure of 0.2 % Cr steel (Figure 5.34 b) is coarser than Cr-free (Figure 5.34 a) and 0.6 % Cr steels (Figure 5.34 c). The coarsening of 0.2 % Cr is due to the effect of Cr as accelerator of recrystallization that grows without restraint. Despite the occurrence of the effect of ferrite recrystallization acceleration due to the addition of 0.6 % Cr to the steel, its growth was restrained by particles due to the drag force against the movement of grain boundaries (GB), therefore the microstructure became refined. On the other side, Cr-free steels showed microstructure refined but non-recrystallized (substructure). The non-recrystallization was due to the absence of Cr effect and the refinement of martensite was due to the nucleation of austenite on ferrite

substructures (nucleation and growing of austenite before ferrite recrystallization). This phenomenon will be shown later.

Figure 5.34 – Effect of Cr on the microstructures (recrystallization and phase transformation) of dual-phase steels held at 720 ºC (air cooling).
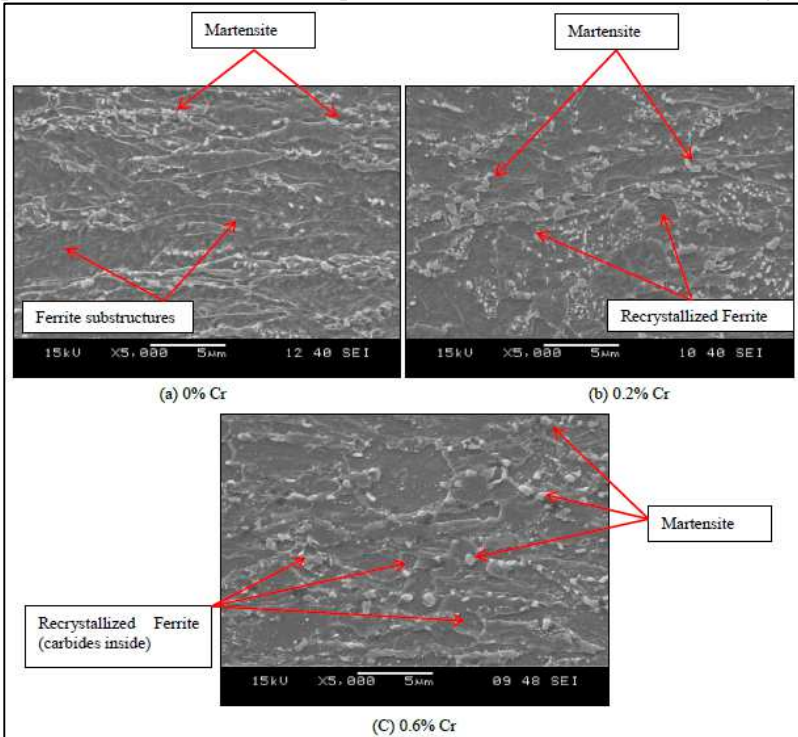
Source: Original, (2014).

Figure 5.35 – Effect of Cr on the microstructures (recrystallization and phase transformation) of dual-phase steels held at 740 ºC (air cooling).
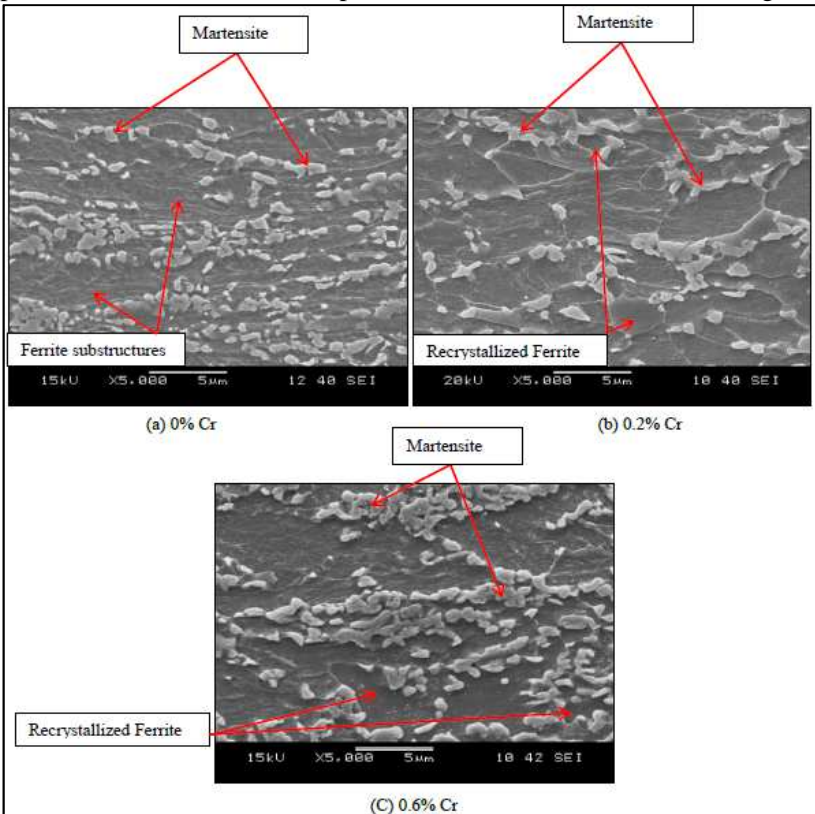
Source: Original, (2014).

Figure 5.36 – Effect of Cr on the microstructures (recrystallization and phase transformation) of dual-phase steels held at 760 ºC (air cooling).
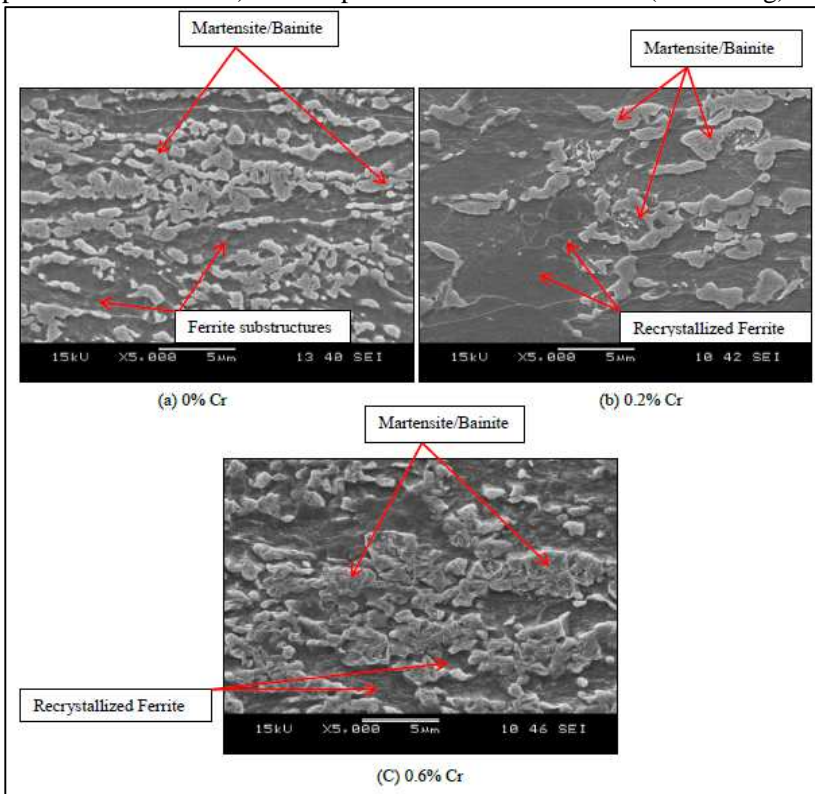
Source: Original, (2014).

Figure 5.37 – Effect of Cr on the microstructures (recrystallization and phase transformation) of dual-phase steels held at 780 ℃ (air cooling).
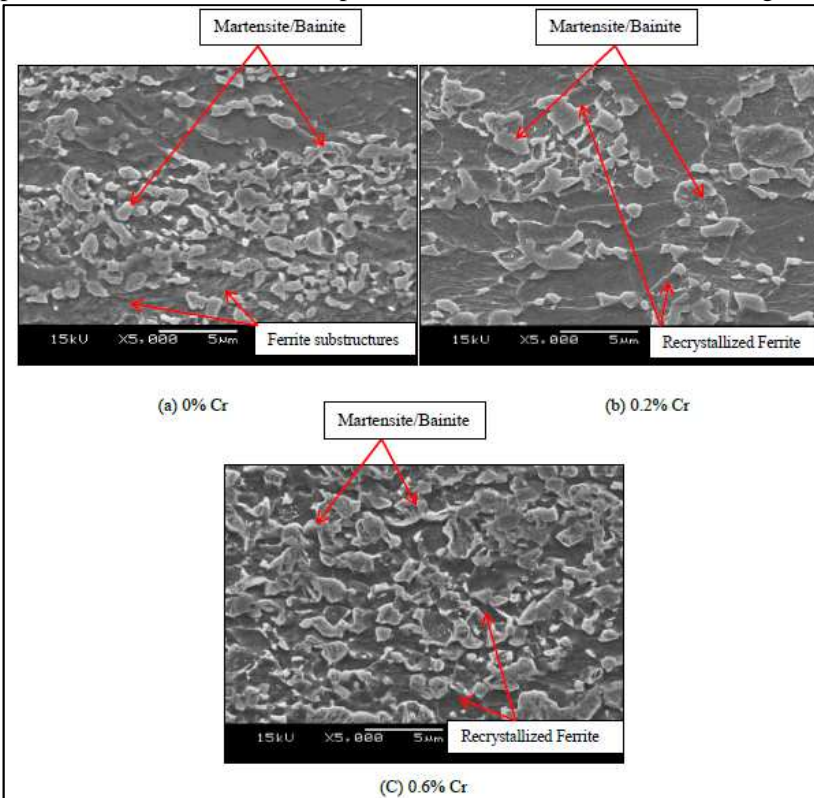
Source: Original, (2014).

Figure 5.38 – Effect of Cr on the microstructures (recrystallization and phase transformation) of dual-phase steels held at 800 ºC (air cooling).
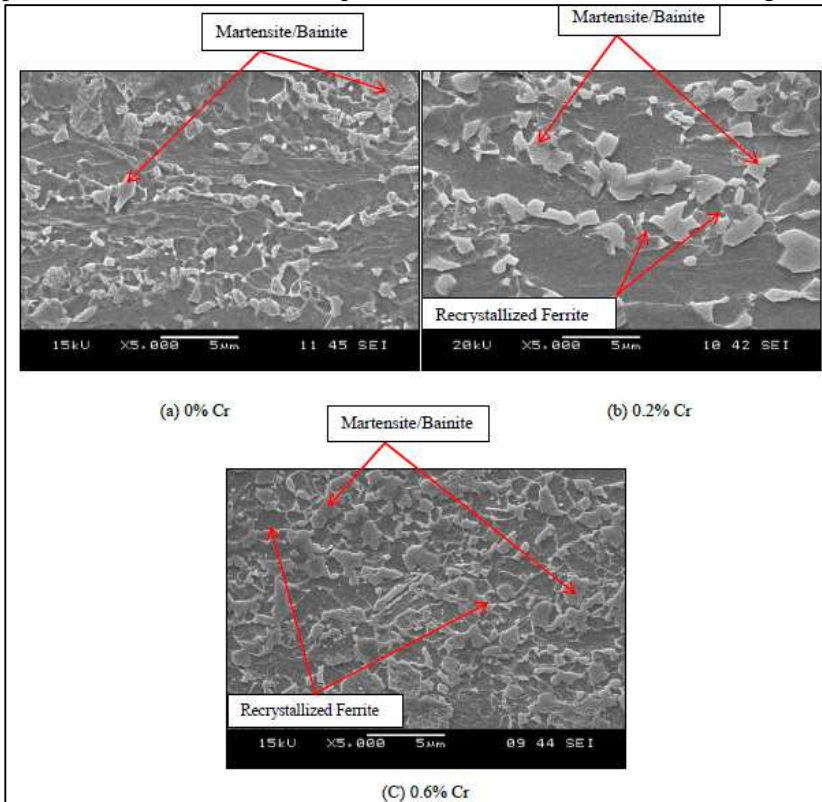
Source: Original, (2014).

Figure 5.39– Effect of Cr on the microstructures (recrystallization and phase transformation) of dual-phase steels held at 840 ºC (air cooling).
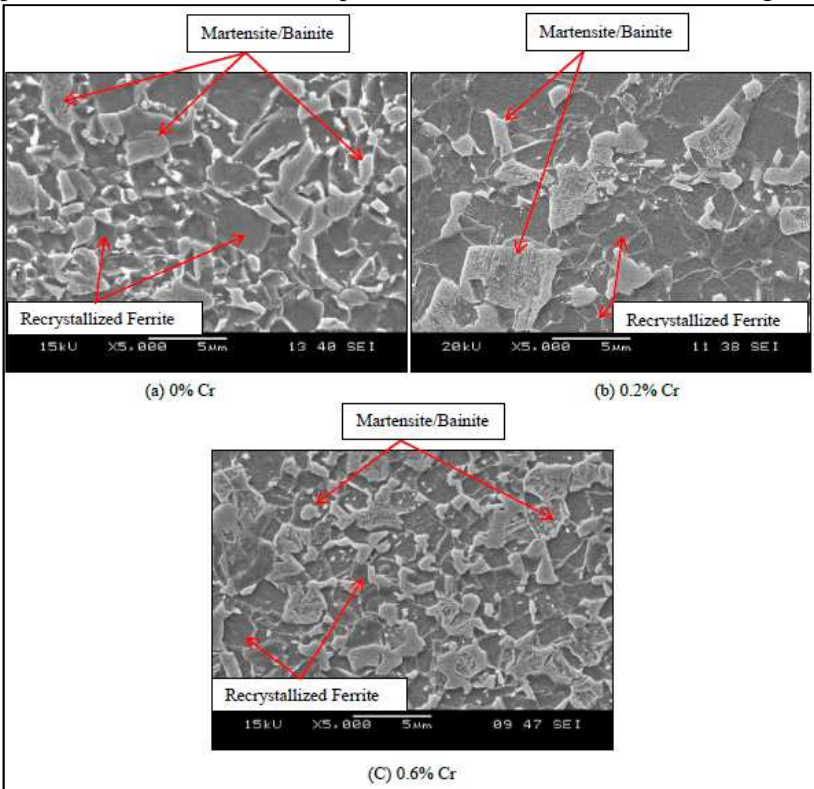
Source: Original, (2014).

5.2.4 - Mechanical Properties

Figure 5.40 (a) shows that tensile strength increased with temperature up to around 760 ºC, afterwards, above this temperature, strength decreased. At 760 ºC the strength of 0.6 % Cr steel is around 140 MPa higher than the 0 % Cr one. This is likely due to the combined effects of higher volume fraction of refined martensite and chromium in solid solution. The refinement is due to the effect of Cr-carbides on creation of additional sites for nucleation of austenite, as discussed before.

The tensile strength of Cr-free steels kept always below the Cr-added steels for all holding temperatures (from 720 to 860 °C). The tensile strength of the steel with 0.6 % Cr started at around 930 MPa and

reached the maximum value around 1180 MPa; while the tensile strength of Cr-free steel started at 890 MPa and reached the maximum value at 1040 MPa.

Figure 5.40 (b) shows that the yield strength of 0 % Cr steel was lower than Cr-added steels for all annealing temperatures (exception at 720 ºC). At lowest temperature (720 ºC) yield strength was higher due to the presence of non-recrystallized hard ferrite and carbide phases (Figure 5.34 a).

Yield strength decreased continuously with temperature up to 820 ºC when increased slightly. The yield strength of 0.6 % Cr steels decreased slower than the 0.2 % and Cr-free steels due to the low decomposition rate of chromium carbides.

The decreasing or increasing tendency of yield strength was due to the domination of recrystallization or phase transformation, respectively. When both processes overlap the resultant profile can be a balance or the overcoming of the predominant.

Elongation shown strong relation with level of recrystallization of steels. The less recuptallized Cr-free steel showed the lowest elongation level up to 820 °C. The 0.6 % Cr steel with recrystallized but refined grains showed intermediate elongation; and the 0.2 % Cr steel with coarser and recrystallized grains showed the highest level of elongation.

.

Figure 5.40 – Effect of chromium content and holding temperature on the mechanical properties of dual-phase steels (air cooling).
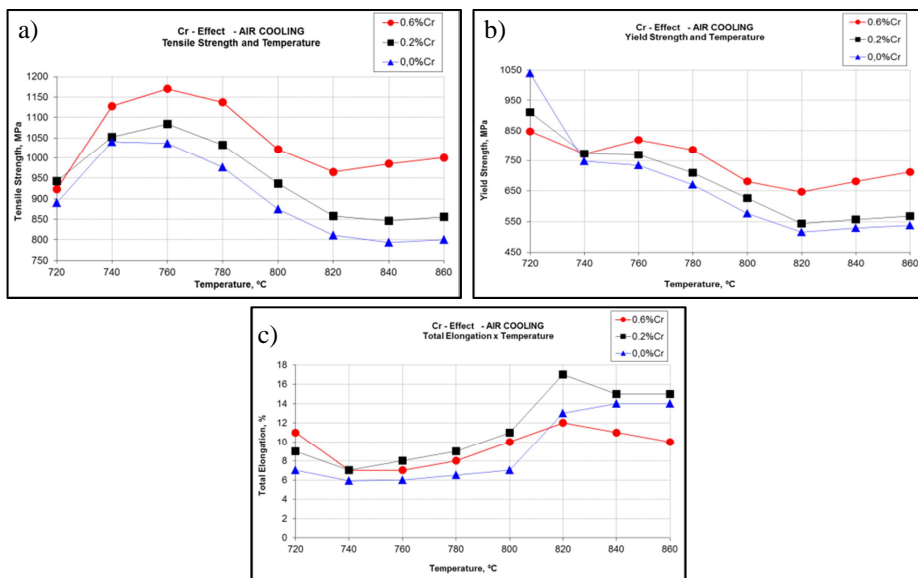
Summary of Cr effect:

Chromium showed the effect on acceleration of ferrite recrystallization, on refinement of grain size, on enhancement of austenite nucleation rate and on strengthening the steels. Besides, Cr forms and stabilizes carbides that act on the determining the final microstructures of steels.

The acceleration of ferrite recrystallization is due to the ability of chromium for reducing the activation energy barrier for nucleation and growth.

The grain refinement is due to the effect of Cr as chromium carbides formed within ferrite grains and supply their surfaces for additional sites for austenite nucleation. This higher nucleation rate has increased the density of austenite; which in turns restrained the growth of neighbor grains.

The strengthening of steels was increased by chromium additions due to the higher amount of austenite with refined grains.

The additions of chromium in the steels promoted the production of more stable and complex carbides than the regular

cementite. These carbides affected significantly the mechanisms of recrystallization and phase transformation and resulted in more refined martensite (final microstructure) and consequently the mechanical properties of steels.

CCT diagrams showed that the addition of 0.6 % Cr moves the ferrite formation field to a slightly lower temperature to the right side to a slower cooling rate (from ~40 to ~20 the ºC/s). This indicates that addition of chromium has suppressed partially ferrite transformation, in spite of accelerated its recrystallization.

The addition of 0.6 % Cr delayed the formation of ferrite for all cooling rates, increased Ms and decreased slightly the Bs.

Higher Ms means lower carbon in austenite and that Cr additions at this concentration did not enhance hardenability; however the higher volume fraction of martensite was likely due to the more higher austenite nucleation rate favored by chromium carbides.

Cr moved bainitic transformation region to lower temperature and the volume fraction of bainite was higher in Cr-added steel which results in a higher martensite start temperature for 0.6 % Cr steel.

Cr increased mechanical properties UTS and YS systematically; nevertheless elongation behavior was slightly different. The highest elongation occurred for 0.2 % Cr, the intermediate for 0.6 % Cr and the lowest ones for Cr-free steel. This sequence in elongation matches with the ferrite recrystallization level.

5.3 EFFECT OF Mo IN STEEL AFTER "QUENCHING"

Figure 5.41 shows the microstructures of steels without Mo and with additions of 0.15 and 0.45 % Mo. The additions of Mo resulted in coarser microstructure of full hard, but refined microstructures of steels after heat treatment and reduced the amount of constituents: martensite and bainite.

Samples heat treated at different annealing temperatures (720-860 ºC) and followed by quenching resulted in a final microstructure consisted, predominantly, in ferrite and martensite; but at some conditions a few portion of bainite.

Figure 5.41 - Effect of molybdenum and holding temperature on the microstructures (recrystallization, phase transformation) of dual-phase steels after water quench.

	0% Mo	0.15% Mo	0.45% Mo
1 (720° C)			
2 (740° C)			
3 (760° C)			
4 (780° C)			
5 (800° C)			
6 (820° C)			
7 (860° C)			
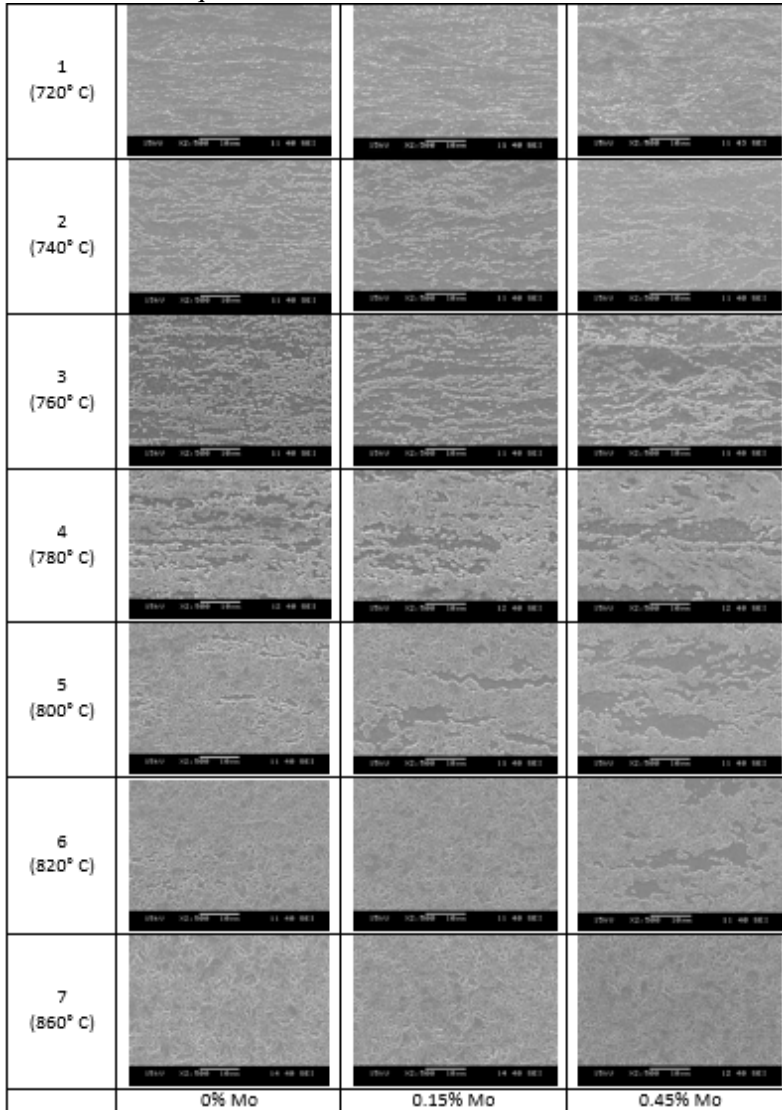
Figure 5.41 supported by Figure 5.42 shows that the amount of martensite increased with temperature and addition of 0.15 % Mo,

nevertheless decreased with further additions (0.45 % Mo). According to Fonstein (2015) and Togazhi (1976) Mo decreases significantly the mobility of ferrite-austenite interface thus retarding the formation and growth of austenite and expands the area on non-recrystallized austenite (SUN & YONG, 2010). However, additions of 0.15 % Mo in the steel increased the amount of martensite suggesting that small additions do not affect significantly the mobility of ferrite-austenite interface.

Figure 5.42 – Effect of Mo and annealing temperatures on the amount of martensite + bainite in dual-phase steels (quench).
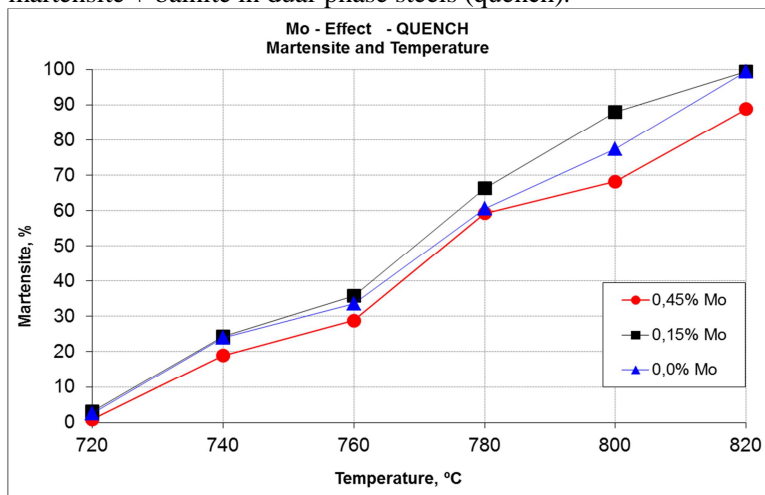
Source: Original, (2014).

Figure 5.43 displays details of full hard microstructures with different Mo content (0, 0.15 and 0.45 %). Increasing Mo content from 0 to 0.45 % the amount of constituents (MA) also increased and became coarser as shown in Figures 5.43 (b-c) in comparison with Figure 5.43 a.

Figure 5.43 – Effect of Mo additions on full hard microstructures of dual-phase steels.
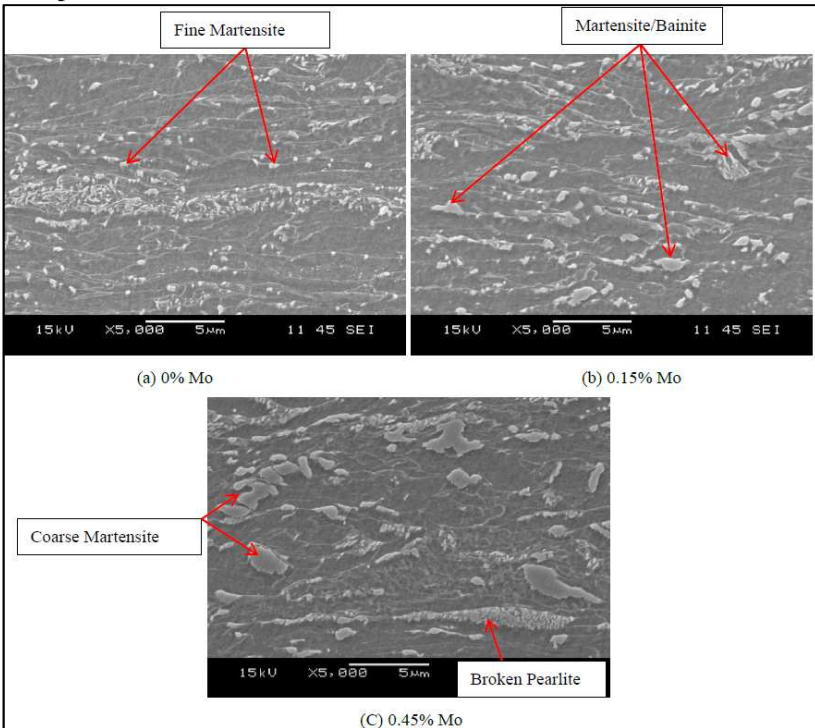
Source: Original, (2014).

Conversely, microstructure of steels with Mo additions and heat treated showed refined microstructures.

Figure 5.44 displays the effect of Mo on retarding the ferrite recrystallization and the phase transformation after heat treating full hard steels samples at 720 ºC and quenching.

Figure 5.44 – Effect of Mo content on the microstructures of dual-phase steels annealed at 720 ºC – 60 s and quench.

(a) 0% Mo

(b) 0.15% Mo

(C) 0.45% Mo
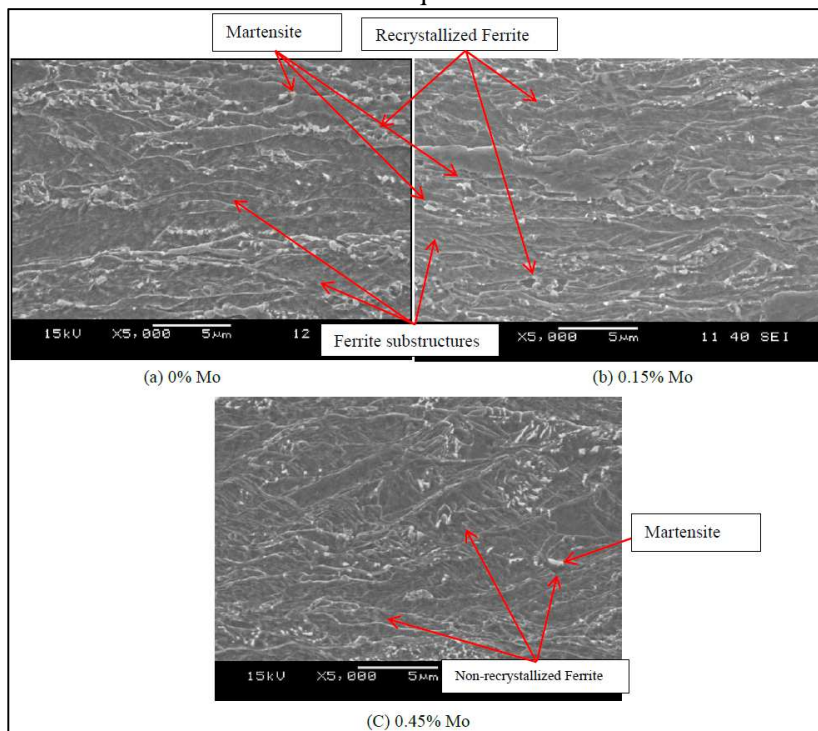
Source: Original, (2014).

Figure 5.45 shows that phase transformation increased significantly with temperature (740 ºC), but was retarded with the addition of Mo as well as the ferrite recrystallization.

The effect of Mo is likely due to its ability to delay the formation and recrystallization of austenite and to expand the area of non-recrystallization (SUN & YONG, 2010).

Figures from 5.45 to 5.49 show the effect of Mo on retarding the phase transformation and ferrite recrystallization of samples heat treated at temperatures from 740 to 860 ºC. It was also observed that phase transformation prevailed over the recrystallization for Mo-added steels.

Figure 5.45 – Effect of Mo content on the microstructures of dual-phase steels held at 740 ℃ – 60 s and quench.

(a) 0% Mo

(b) 0.15% Mo

(C) 0.45% Mo
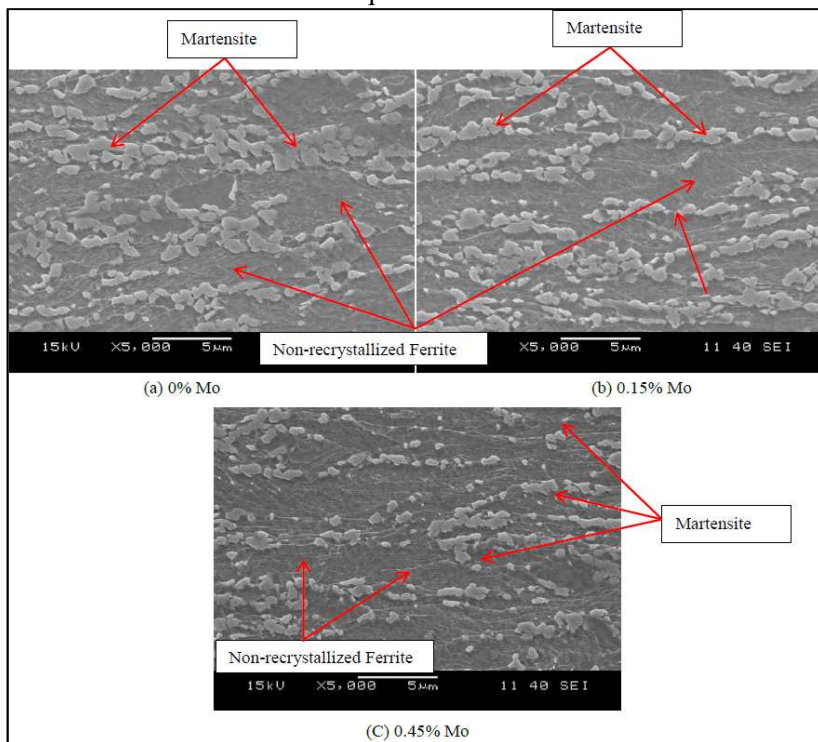
Source: Original, (2014).

Table 5.1 displays the effect of Mo on the refinement of austenite and consequently on MA products (martensite + bainite). It can be explained by the effect of this element in decrease the mobility of γ/α interface, and form carbides that reduces C diffusion.

Table 5.1- Effect of Mo on the MA (martensite + bainite) grain size (coarsening).

MA size (μm) – 740 ℃ (Quench)			
Mo Content (%)	Mínimo	Máximo	Média
0	1,06	3,66	1,73
0.15	1,07	3,24	1,64
0.45	0,62	2,85	1,48

Figure 5.46 – Effect of Mo content on the microstructures of dual-phase steels held at 760 ºC– 60 s, quench.
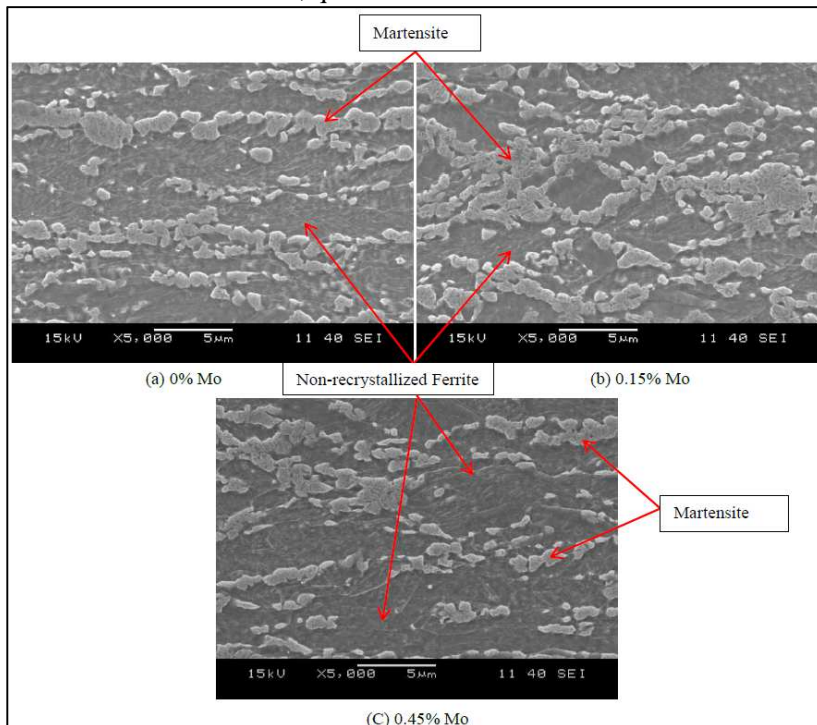
Source: Original, (2014).

Figure 5.47 – Effect of Mo content on the microstructures of dual-phase steels held at 780 ºC– 60 s (quench).
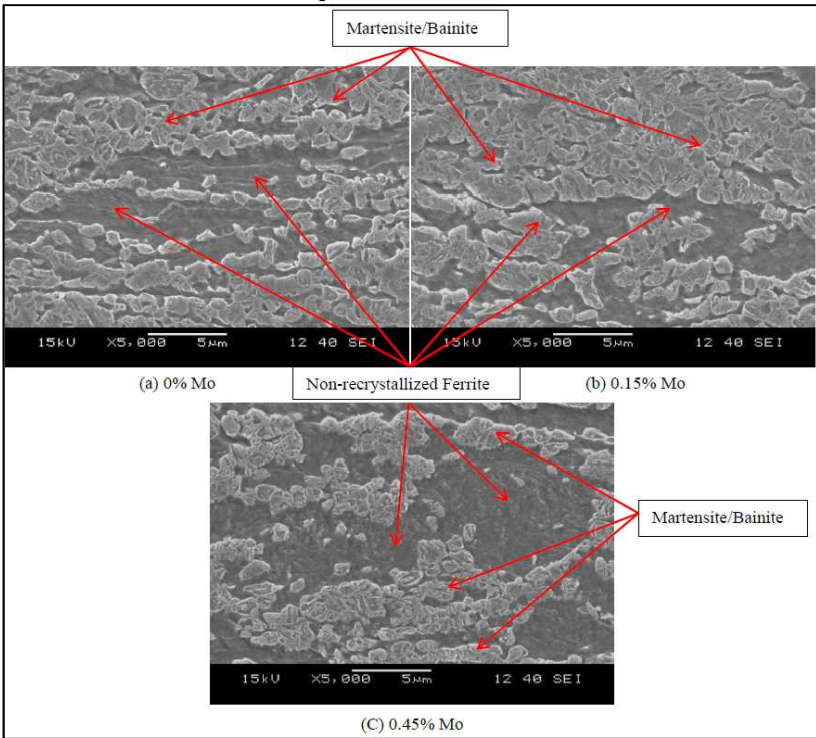
Figure 5.48 – Effect of Mo content on the microstructures of dual-phase steels held at 820 ºC – 60 s (quench).
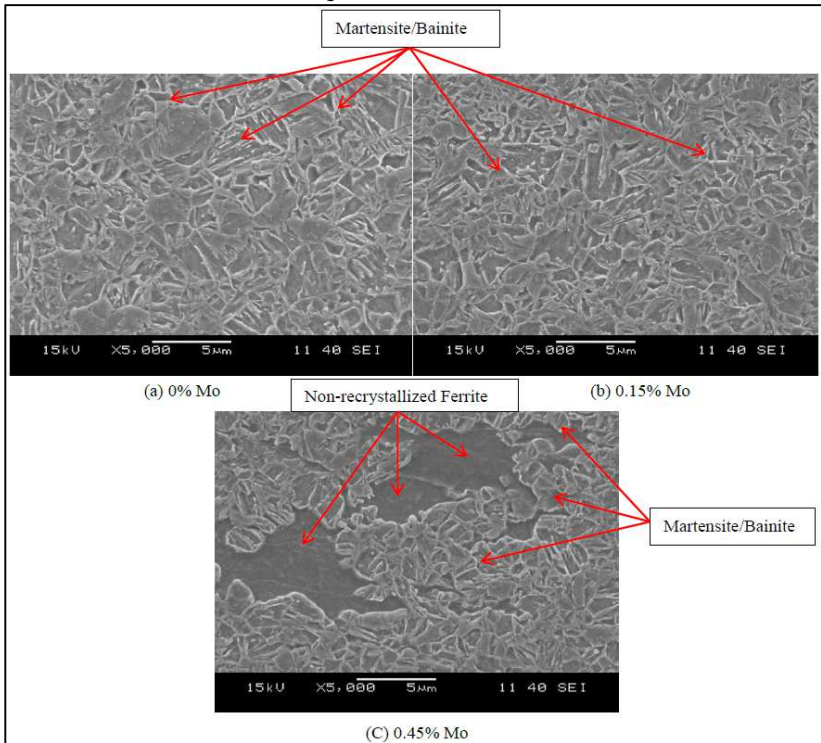
Source: Original, (2014).

Figure 5.49 – Effect of Mo content on the microstructures of dual-phase steels held at 860 ºC – 60 s (quench).
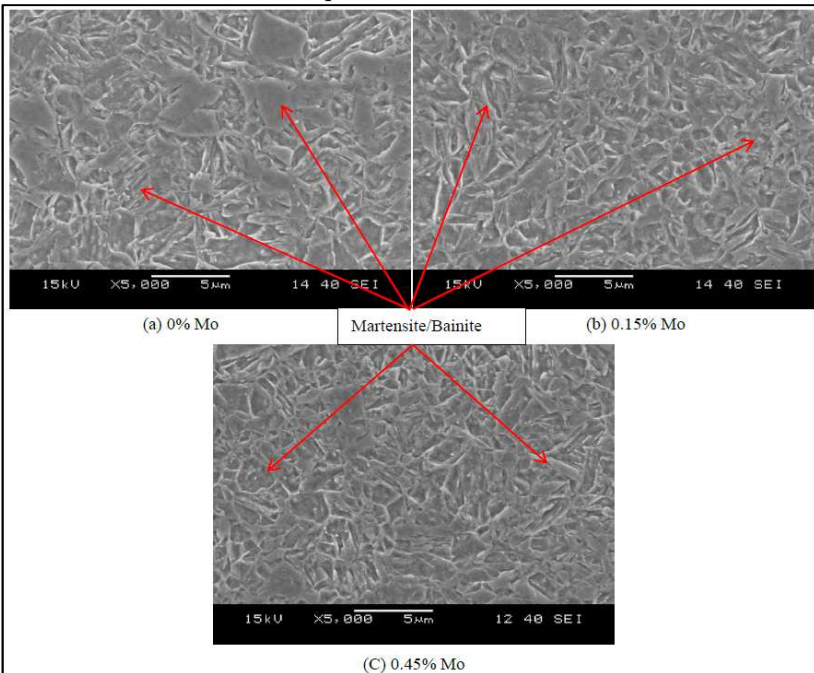
Source: Original, (2014).

Quench treatment allowed to observe that the addition of 0.15 % Mo in dual-phase steels accelerated austenite phase transformation (increasing the volume fraction of austenite) and retarded the ferrite recrystallization; however higher additions (0.45 % Mo) have retarded both the phase transformations (decreasing the volume fraction of austenite) and ferrite recrystallization besides the refinement of MA constituents. Considering that Mo decreases the mobility of ferrite/austenite interface and expands the area of non-recrystallization of ferrite, concentrations up to 0.15 % did not retard significantly the mobility but higher concentrations did it.

5.4 EFFECT OF Mo IN STEEL AFTER "AIR COOLING"

Discussions were developed mainly on the basis in the microstructures of steel obtained by SEM and shown in Figure 5.50 and detailed on Figures from 5.53 to 5.57.

Figures 5.51 and 5.52 show the amount of MA (Martensite + bainite) in all steels together aiming to show the tendencies of microstructures with Mo additions.

Figures 5.52 (a and b) show the effect of cooling media on the amount of martensite for steels with 0.45 % Mo and Mo-free steels.

The amount of MA (Martensite + bainite) increased with Mo additions and temperature up the critical temperatures (Tc) according to the Mo content, and then decreased slowly, as shown in Figures 5.52 a. Critical temperatures were reached around 760 ºC for Mo-free steel; and 780 ºC for Mo-added steels.

170

Figure 5.50 - Effect of Mo content and holding temperature on the microstructures of DP steels (air cooling).

(1) 720°C			
(2) 740°C			
(3) 760°C			
(4) 780°C			
(5) 800°C			
(6) 820°C			
(7) 860°C			
	0%Mo	0.15%Mo	0.45%Mo
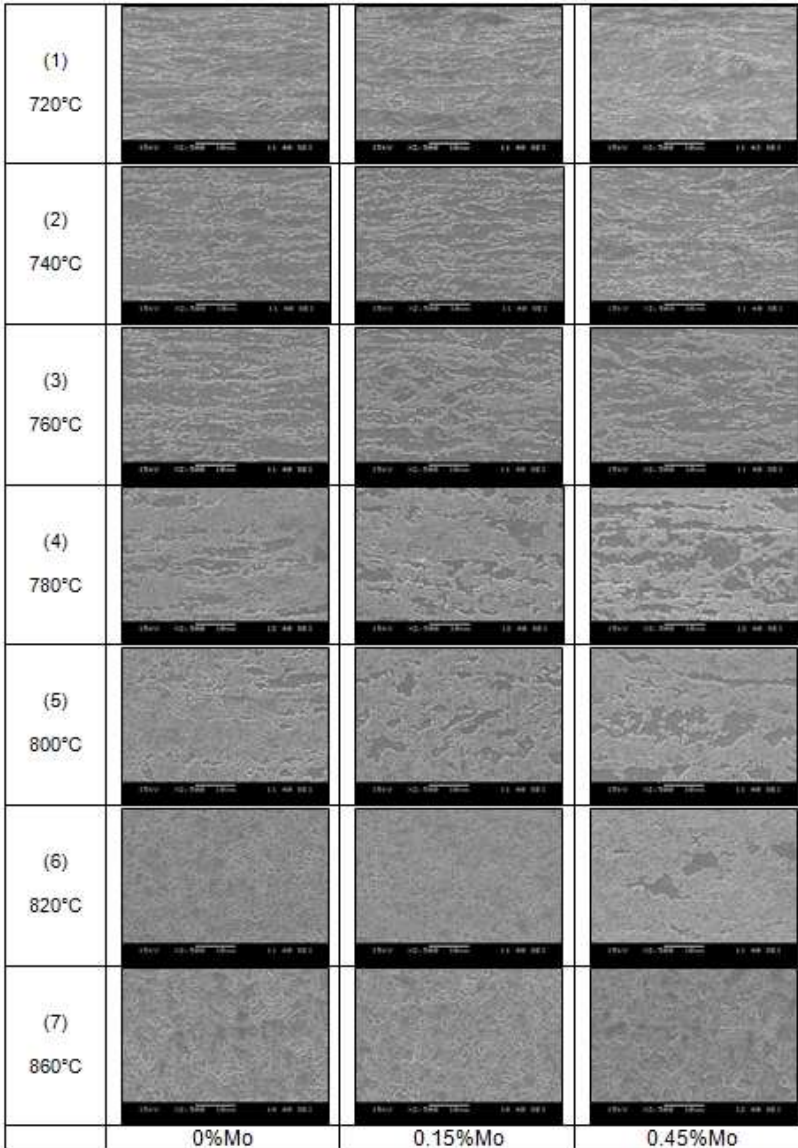
Source: Original, (2014).

Figure 5.51 shows the effect of Mo additions (0.15 % and 0.45 %) in the steels on amount of martensite, in comparison with Mo-free one, at cooling in air, from intercritical temperature.

It was observed that addition of 0.15 % Mo increased the amount of martensite at whole range of temperatures.

As described in section 5.3 (quench), at low Mo concentration (0.15 %) the effect on inhibition of movement of austenite-ferrite interface was not significant on heating (allows austenite formation in inter-critical region); besides, Mo increased austenite hardenability at cooling (enhances austenite stability). The combination of both positive effects resulted in more martensite in the final microstructure of Mo-added steel when comparing with Mo-free one.

Addition of 0.45 % Mo reduced the amount of martensite at annealing temperatures between 720 and 760 ºC; but increased at temperatures above to around 760 ºC.

At high Mo concentration (0.45 %) its global effect on microstructure was also function of annealing temperature, since it determines the amount of carbon in austenite. At low annealing temperatures (up to around 760 ºC), the amount of austenite formed in intercritical region was so small that Mo effect (on hardenability) at cooling was not enough to result more martensite than Mo-Free steel. At higher annealing temperatures (above 760 ºC), it was formed more austenite and the Mo effect (on hardenability) was enough to stabilize ones; while in Mo-Free steel (above 760 ºC) carbon-poor austenite transformed to non-martensitic structures and resulted in less martensite.

This indicates that Mo showed different effects that depended on its concentration in steels and temperature of annealing treatment. It suggests that the effect of Mo on hardenability of austenite became significant, on cooling, when austenite was poor in carbon.

The amount of martensite found in the microstructure at the critical temperature 780 ºC were around 38 %, 35 % and 27 % for Mo concentration in steel of 0.15 %, 0.45 % and Mo-free steel, respectively (Figure 5.51).

Figure 5.51 - Effect of molybdenum content and annealing temperature on amount of martensite (air cooling).
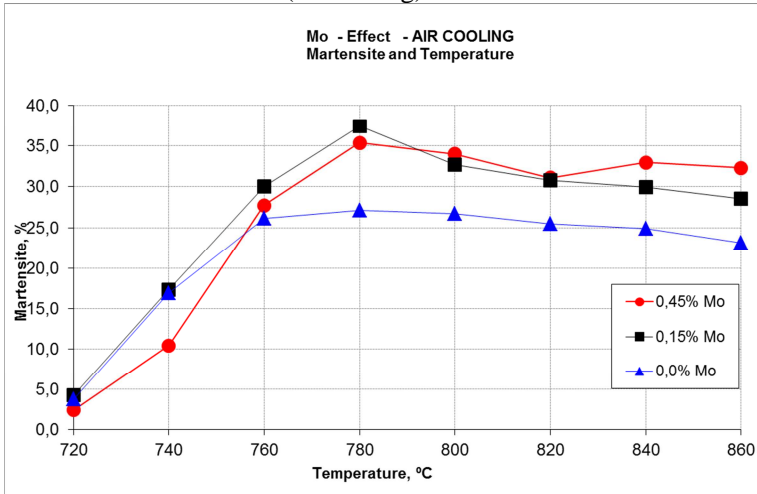
Source: Original, (2014).

Figure 5.52 shows the effect of cooling media on amount of martensite. Area between curves of cooling at quench (green) and at air (blue) estimates the amount of austenite transformed to non-martensitic structures during air cooling; however molybdenum inhibited, in some extension, this reaction. Up to 760 °C, the austenite was C-enriched then the high hardenability allowed the cooling in air to be similar to water quench in term of delaying the non-martensitic reactions. Above, 760 °C, the austenite was low-carbon and the effect of Mo on delaying non-martensitic reactions was significant.

Figure 5.52 - Effect of quench (green) and air cooling (blue) on amount of martensite in (a) Mo-free and (b) 0.45 % - Mo steels.
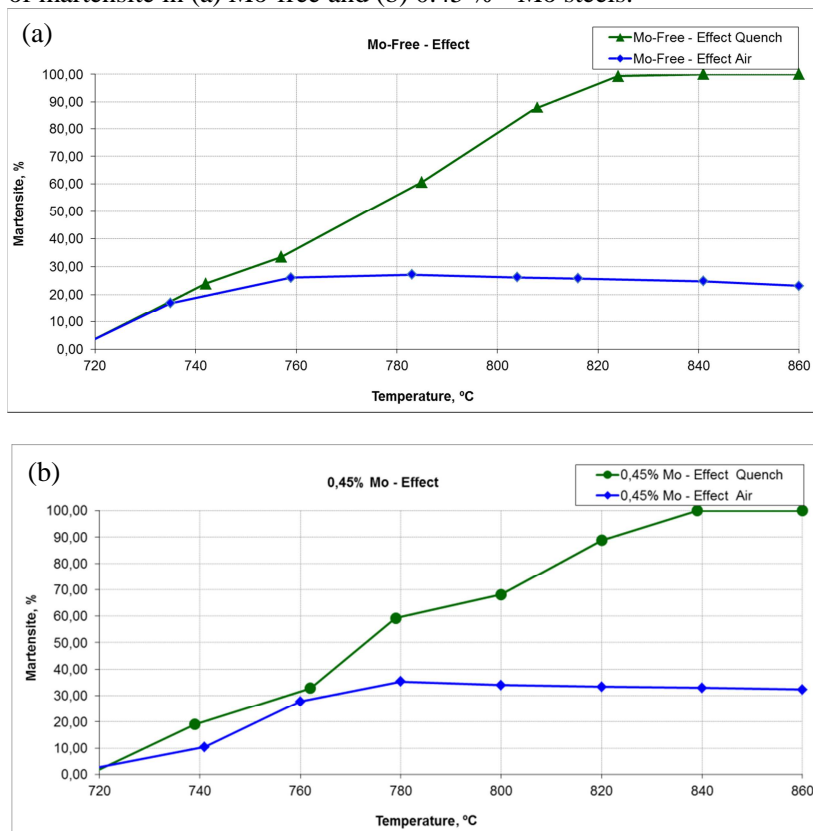
Figures from 5.53 to 5.57 show the effect of Mo on retarding the phase transformation and ferrite recrystallization of samples heat treated at temperatures from 720 to 840 ºC. Phase transformation prevailed over the recrystallization for Mo-added steels.

Figure 5.53 – Effect of Mo content on microstructures of dual-phase steels held at 720 ℃ (air cooling).

(a) 0% Mo Martensite (MA) (b) 0.15% Mo

(C) 0.45% Mo
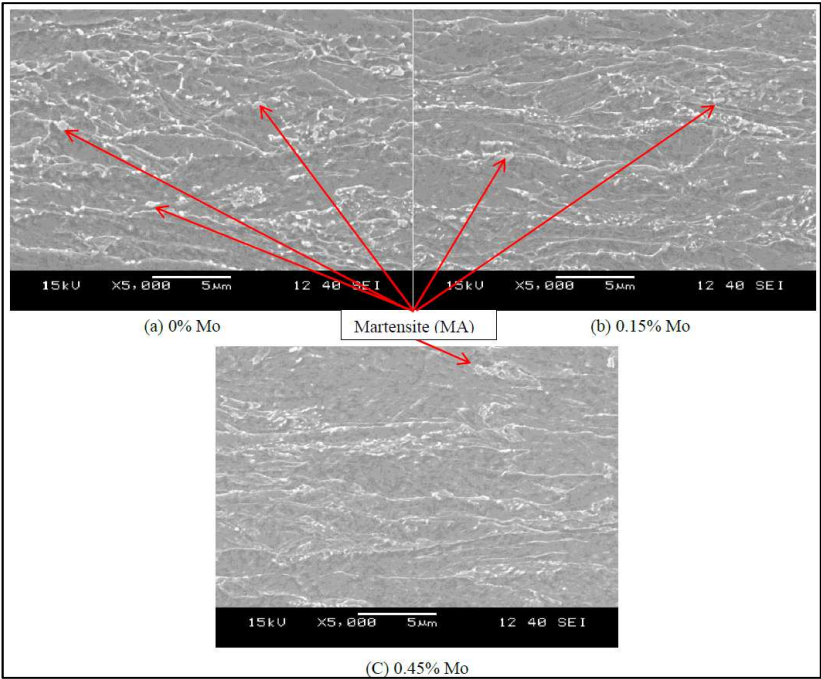
Source: Original, (2014).

Figure 5.54 – Effect of Mo content on microstructures of dual-phase steels held at 740 ºC (air cooling).

(a) 0% Mo

(b) 0.15% Mo

(C) 0.45% Mo
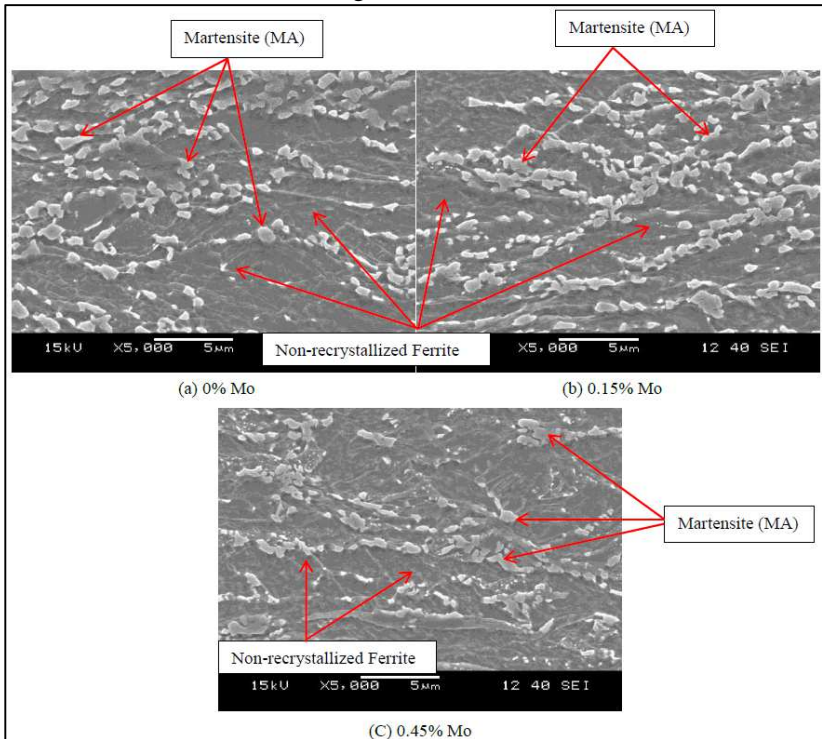
Source: Original, (2014).

Figure 5.55 – Effect of Mo content on microstructures of dual-phase steels held at 760 ℃ (air cooling).
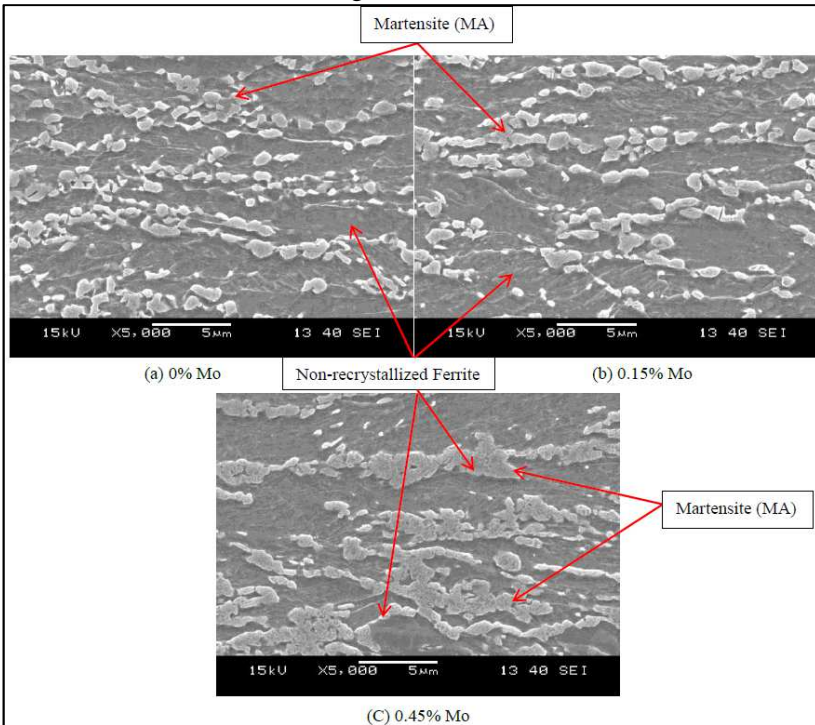
Source: Original, (2014).

Figure 5.56 – Effect of Mo content on microstructures of dual-phase steels held at 780 ℃ (air cooling).
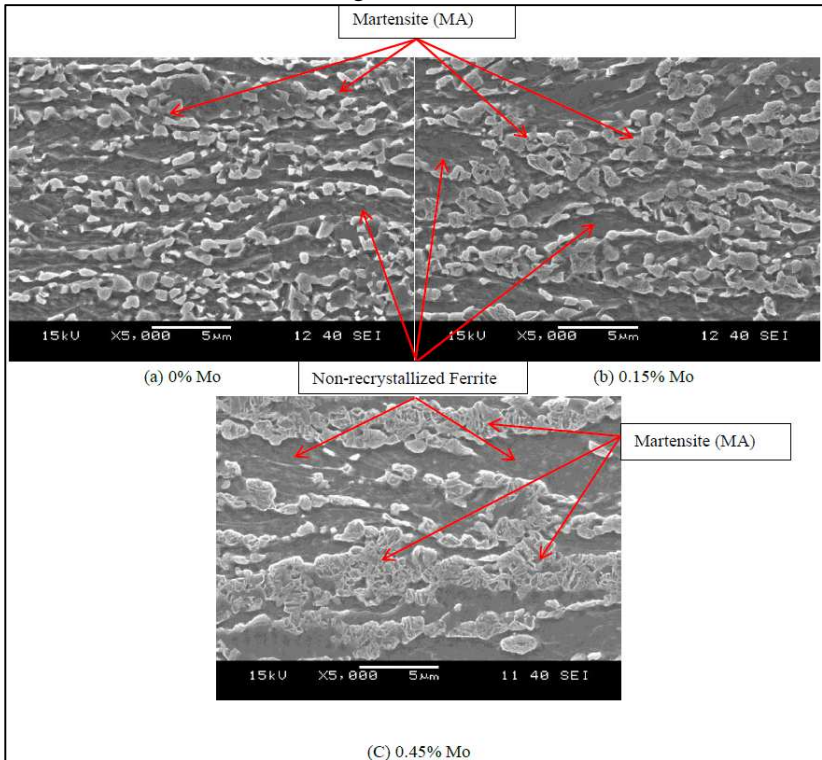
Source: Original, (2014).

Figure 5.57 – Effect of Mo content on microstructures (recrystallization, phase transformation) of dual-phase steels held at 840 ℃ (air cooling).

(a) 0% Mo

Martensite (MA)

(b) 0.15% Mo

(C) 0.45% Mo
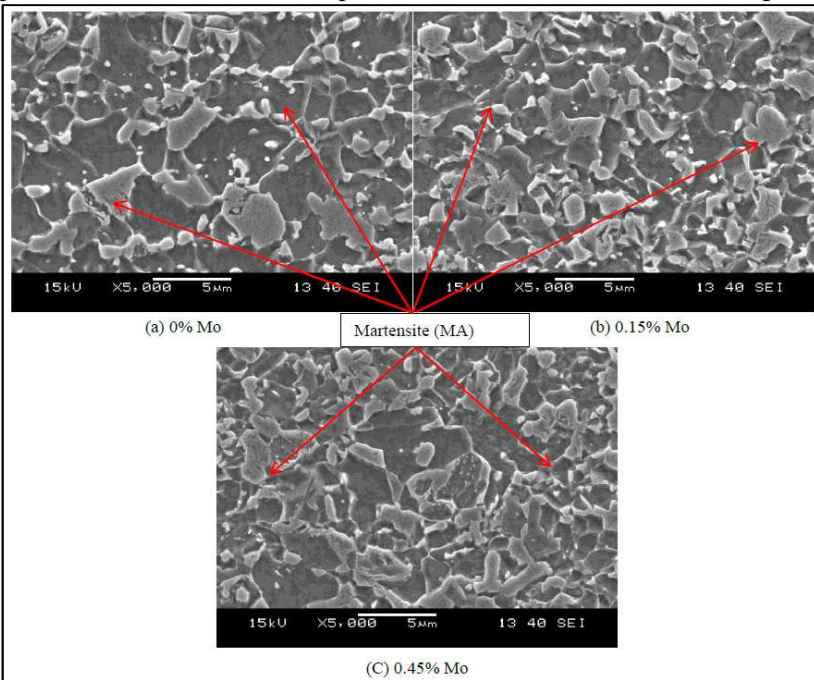
Source: Original, (2014).

5.4.1 Mechanical Properties (Mo-steel)

Figure 5.58 shows the effects of Mo content and annealing temperature on (a) tensile (TS), (b) yield (YS) strengths and (c) elongation (EL) of steels after air cooling.

Molybdenum increased tensile strength at all annealing temperatures.

The tensile strength of the steels with three Mo contents reached the range of 840~980 MPa at 720 ℃ afterwards, when temperature increased up to around 760 ℃, more austenite has nucleated and transformed to martensite; which in turn increased strengths. However, at temperatures above 760 ℃ more austenite has formed with less C content (less hardenability) resulting in less martensite and, consequently, TS decreased.

Molybdenum increased yield strength at all annealing temperatures (except at 720 ℃).

Yield strengths reached the range of 940~1163 MPa at 720 ºC, then decreased continuously to (442~734 MPa) up to around 820 ºC and kept rather constant.

Elongation of Mo-free steels kept predominantly above the Mo-added steels. This shows that, the level of ferrite recrystallization has strong relation with recrystallization.

Figure 5.58 – Effect of Mo content and holding temperature on mechanical properties of dual-phase steels (air cooling).
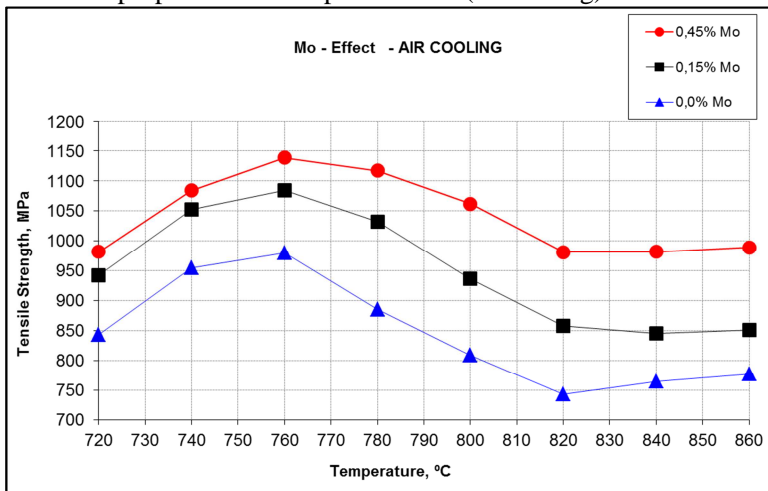
(a) Tensile Strength
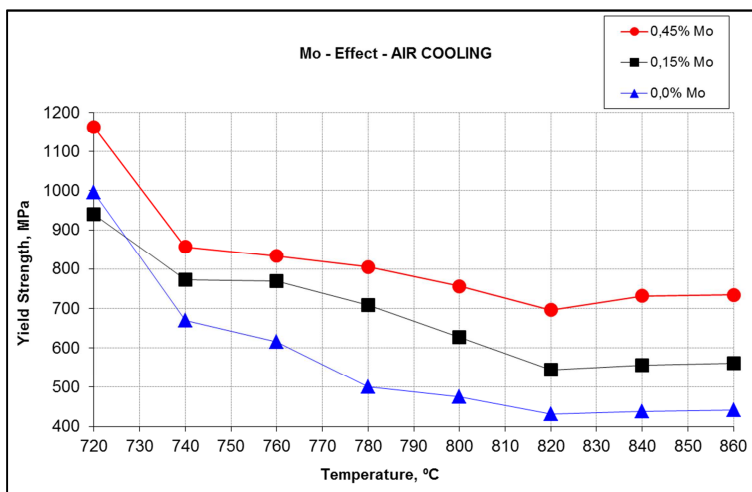
(b) Yield Strength
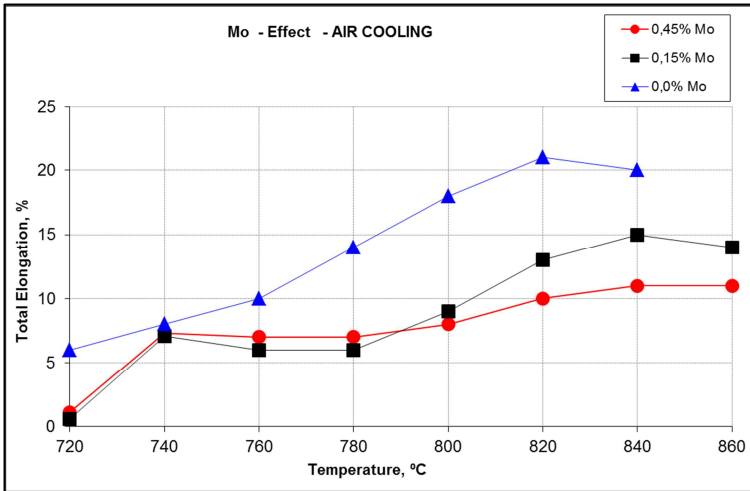
(c) Total Elongation

Source: Original, (2014).

5.4.2 Dilatometry

The analysis of dilatometry aimed to investigate the effect of molybdenum on microstructures of steels and their kinetics of transformation. Experiments were carried out by heating the steels at the α/γ-region, holding isothermally and quench at different cooling rates.

The analysis of CCT diagrams associated to the microstructures (via SEM) brought about information concerning to the dynamic transformations in the structure as shown in Figures 5.59 and 5.60.

Figure 5.59 shows the complete CCT diagram for the low-carbon dual-phase steels (a) without and (b) with Mo additions.

Additions of 0.45 % of Mo moved the ferrite formation region to the right side to slower cooling rates from 90 to 1.0 °C/s; the volume fraction of ferrite was higher in Mo-free steel after the same cooling rate from two-phase region.

Lower volume of bainite was formed in Mo-added steels and martensite start temperature (M_s) was higher, especially after slow cooling rates (<10 °C/s).

Separation of bainitic and martensitic constituents after high cooling rates (>10 °C/s) was difficult using visual microstructure evaluation.

Figure 5.59 – Effect of Mo additions (a) 0 % Mo and (b) 0.45 % Mo on CCT diagrams of 0.1 % C DP steels cooled from two-phase region (800 ºC) after 60 s holding.
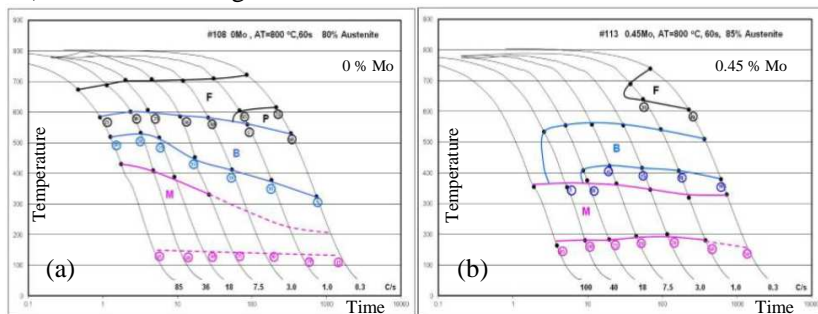
Source: Original, (2014).

Figure 5.60 shows the effect of addition of 0.45 % Mo on suppressing ferrite formation thus promoting more volume fraction of martensite and refining the microstructure especially after low cooling rates.

Figure 5.60 – Effect of Mo addition on microstructures of steels cooled from two-phase region at 800 ºC.
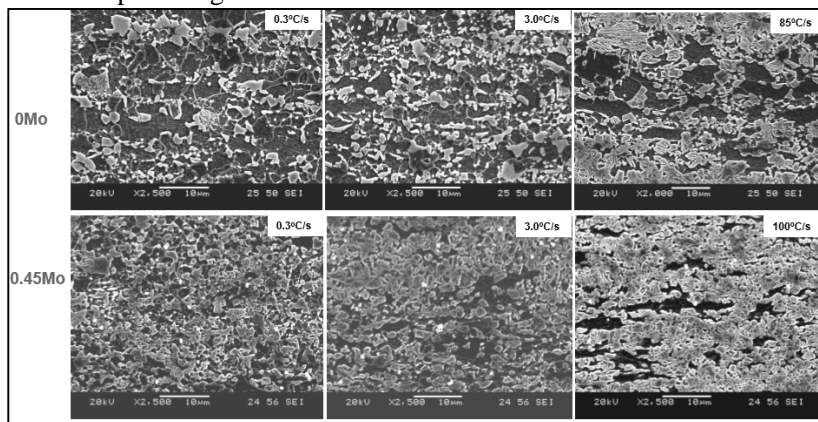
Source: Original, (2014).

Summary of Mo effect:

Molybdenum showed the effect on suppressing bainite and ferrite formation besides retarding the ferrite recrystallization; refining

of microstructure; on enhancement of austenite hardenability and strengthening of the steels.

Ferrite recrystallization was retarded due to slower self-diffusion of iron in the presence of Mo with consequent expansion of area of non-recrystallized ferrite.

Grain refinement was due to the effect of Mo on decreasing the mobility of ferrite-austenite interface. In this study this effect was observed only for Mo additions higher than 0.15 %.

The amount of martensite increased with temperature and addition of 0.15 % Mo, nevertheless decreased with further Mo additions (0.45 %) on quench (Figure 5.42). Fonstein (2015) and Togazhi (1976) showed that Mo decreases significantly the mobility of ferrite-austenite interface and retards the formation and growth of austenite (SUN & YONG, 2010). This suggests that small additions of Mo to steels do not affect significantly this mobility.

Mo acted on inhibition of austenite formation at heating, but increased the hardenability of austenite formed in the $\alpha+\gamma$ region. At cooling the austenite formed was avoided to transform to non-martensitic structures (ferrite/pearlite/bainite).

At air cooling, the effect of Mo on martensite transformation depends on the amount of carbon in austenite upon annealing. Whether annealing proceeded at low temperatures, austenite was enriched in C (high hardenability) thus the effect of Mo on hardenability was not evident. However at higher temperatures, C content was low and the effect of Mo became significant on enhancing austenite hardenability).

Mo showed different effects that depended on its concentration in steels and temperature of annealing treatment. It suggests that the effect of Mo on hardenability of austenite became significant, on cooling, when austenite was poor in carbon.

The amount of martensite found in microstructure at critical temperature 780 ºC were around 38 %, 35 % and 27 % for Mo concentration in steel of 0.15 %, 0.45 % and Mo-free steel.

In fact, Mo has the strongest effect on stability of low-carbon austenite formed on $\alpha+\gamma$ region and favors the austenite-to-martensite transformation at the lowest cooling rate.

The strengthening of steels was increased by the molybdenum additions due to the higher amount of refined austenite.

5.5 EFFECT OF Si IN STEEL AFTER "QUENCHING"

This section addressed the effect of Si and annealing temperatures on microstructure of dual-phase steels after water quench.

Treatment comprised in heating the steels up to the annealing temperatures keeping them isothermally for 60 seconds before quenching in water. The steels' compositions differ according to the addition of 0.3 % Si or not (0 % Si).

Figure 5.61 displays 12 microstructures changing with "Si concentrations" and "annealing temperatures" (720 – 840 ℃).

Besides, Si-added steel exhibited more refined cold-rolled microstructure with higher volume of carbon containing colonies. It is well known that smaller grains have a larger area and thus greater surface energy. Therefore, the higher surface energy associated with the grain boundaries of Si-added steels generate a higher thermodynamic potential for ferrite recrystallization which agrees with Drumond et al. (2012).

184

Figure 5.61 - Effect of silicon content and holding temperature on microstructures (recrystallization and phase transformation) of DP steels (water quench).

	0%Si	0.3%Si
(1) 720 °C		
(2) 740 °C		
(3) 760 °C		
(4) 780 °C		
(5) 820 °C		
(6) 840 °C		
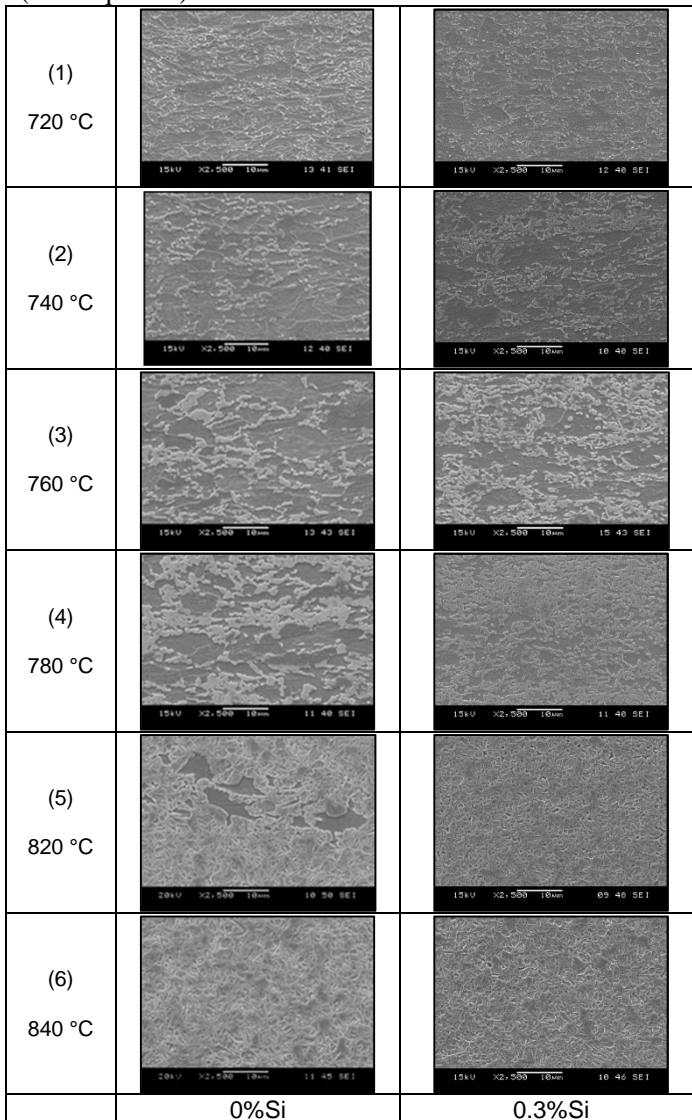
Source: Original, (2014).

The phenomena of ferrite recrystallization and austenitization were analyzed through the microstructures of final product resulted from

heat treatment of cold rolled samples followed by water quenching. A representative set of microstructures of steels annealed at temperatures 720 to 760 °C is shown in Figure 5.62 where the arrows indicate the non-recrystallized ferrite grains.

Silicon accelerated ferrite recrystallization inasmuch as microstructure was almost completed at 760 ºC in Si-added steel, whereas only partially recrystallized in Si-free steel at same temperature. The effect of acceleration on ferrite recrystallization in Si-added steel was already related to the initial microstructure (CABALLERO et al., 2001; MOHANTY et al., 2011).

Earlier publications Wu et al. (2003) and Speich et al. (1981) mentioned the formation of austenite nuclei firstly at ferrite-cementite interfaces in the carbon containing colonies, such as pearlite, bainite or martensite, and later at the recrystallized ferrite grain boundaries.

Figure 5.62 - Microstructures of Si-free and Si-added steels after annealing between 720 and 760 ºC followed by water quenching (SEM, 2 % Nital).
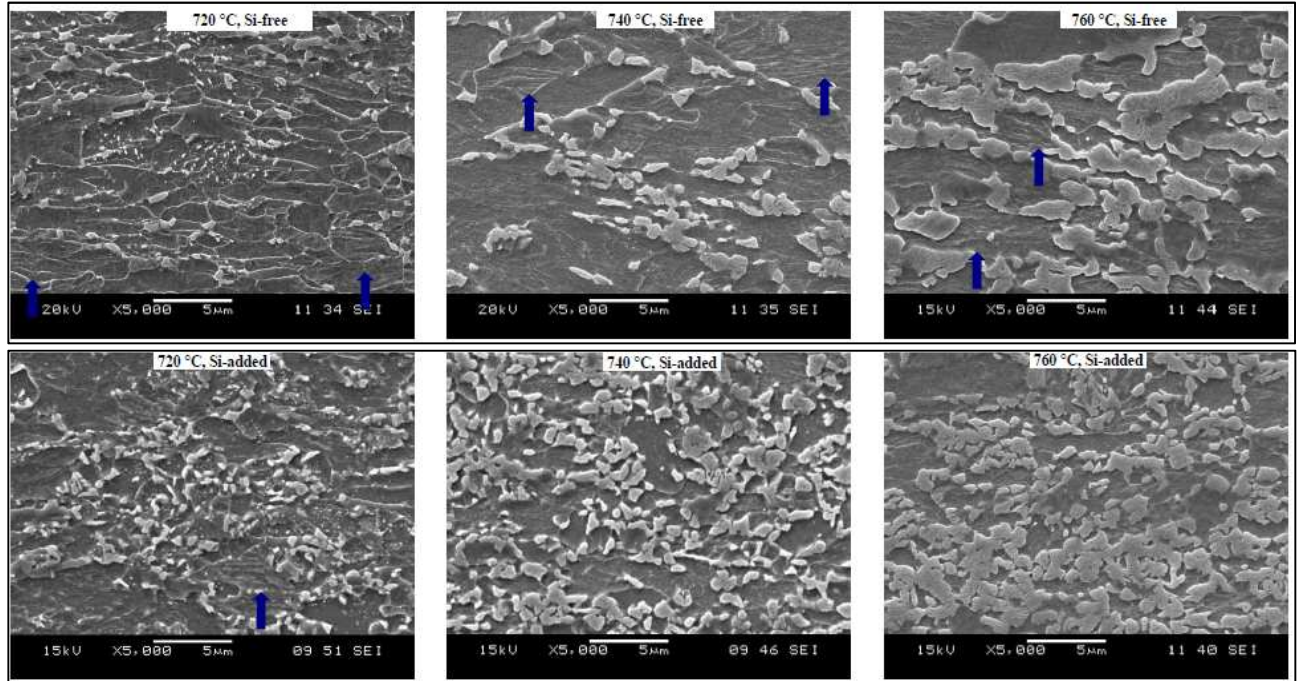
Source: Drumond et al. (2012).

It is worth to note the simultaneous occurrence of the ferrite recrystallization and austenite formation after quenching from two-phase region (Figure 5.63). This exerted significant effect on kinetics of austenite formation since it occurs through the process of nucleation and growth that was controlled by carbon diffusion in solid state.

Figure 5.63 - Microstructure of Si-free steel after annealing at 760 ºC followed by water quenching (SEM, 2 % Nital).
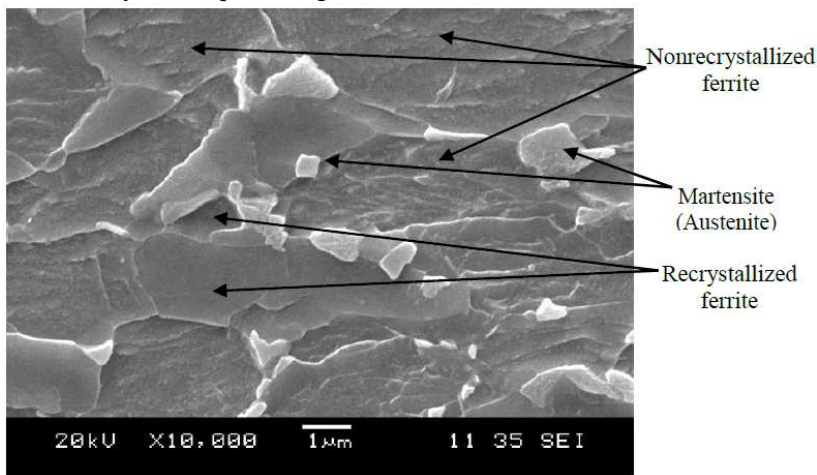
Source: Original, (2014).

The difference in the extent of recrystallization affected the process of austenitization. Austenite formation took place in the structure containing a partially recrystallized ferrite in the Si-free steel; whereas in the Si-added steel, the austenite started to form in the structure where the recrystallization of ferrite was almost completed.

The simultaneous occurrence of two processes, the ferrite recrystallization and austenite nucleation, exerted significant effect on the kinetics of austenite formation. Austenite formed through the processes of nucleation and growth that were controlled by carbon diffusion in solid state, Drumond et al. (2012).

In Si-free steel, the presence of a large amount of non-recrystallized ferrite grains led to a small volume of austenite nuclei that grew up along the rolling direction (region enriched in carbon). Therefore, the formation of a smaller amount of coarse elongated islands of austenite became more probable in the Si-free steel.

Conversely, in the Si-added steel, the recrystallization process started earlier and when the austenite formation began, most ferrite grains had already been recrystallized. This has favored the formation of multiple austenite nuclei. The formation of austenite mostly occurred through the nucleation process which resulted in a more uniform distribution of smaller islands of martensite within the matrix of refined ferrite grains.

This explanation was confirmed by the microstructures shown in Figure 5.62 especially at 760 ºC. The fine martensite islands obtained in the Si-added steel were more evenly distributed in comparison to those formed in the Si-free steel, where the coarse martensite islands were aligned along with the rolling direction.

Figure 5.64 shows that amount of martensite (austenite) increasing with the annealing temperature. The Si-added steel exhibited around 10 % higher amount of martensite at the same annealing temperature than the Si-free steel. At temperatures close to the full austenitization (~ 820 °C), the effect of Si addition on amount of formed austenite was not relevant due to the large amount of austenite, which makes the diffusion distance for carbon, much shorter.

The growth of austenite through the increase density of austenite nuclei in the Si-steel resulted in a higher volume fraction of austenite in the inter-critical temperature range facilitated by an earlier completion of recrystallization and higher carbon diffusion along the refined grain boundaries of ferrite.

Figure 5.64 - Effect of Si on amount of martensite at different annealing temperature, after water quenching.
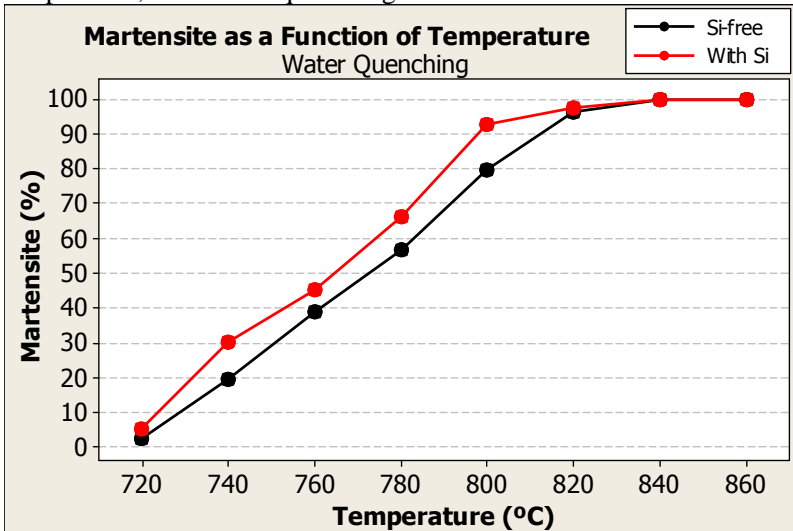
Source: Original, (2014).

5.6 EFFECT OF Si IN STEEL AFTER "AIR COOLING"

Figure 5.65 displays the effect of Si and annealing temperatures on the microstructure of dual-phase steels after air cooling.

Figure 5.65 - Effect of 0.3 % Si and annealing temperature on microstructures of low-alloy dual-phase steels.
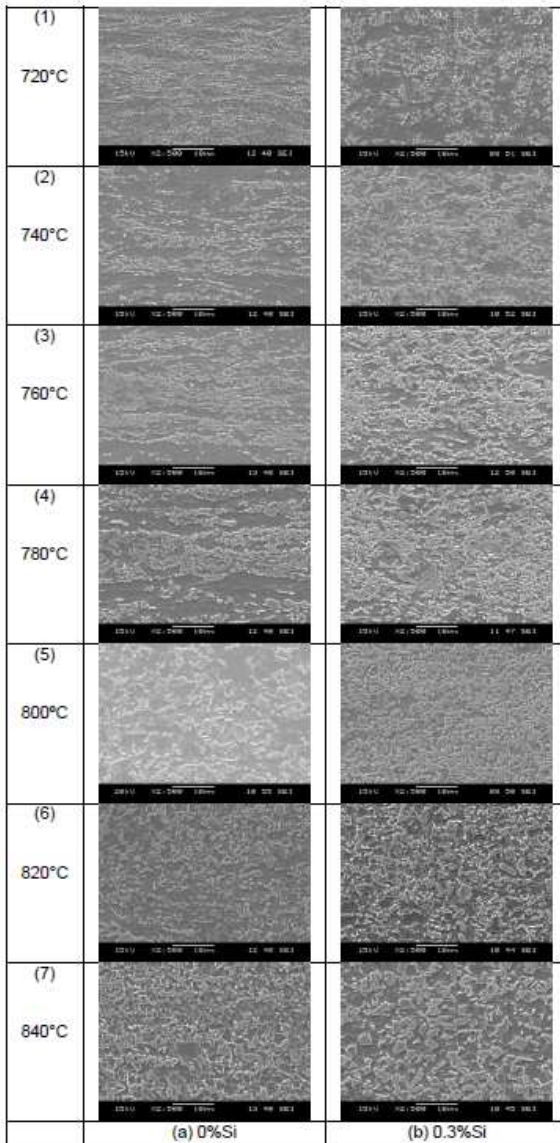
Source: Original, (2014).

Figure 5.66 displays that the amount of martensite increases with annealing temperature up to around 760 ºC, then decreases slightly. The Si-added steel exhibited around 50 % higher amount of martensite at the same annealing temperature than the Si-free steel. Differently of the quenching shown before, on air cooling at temperatures above ~ 820 °C, the effect of Silicon on amount of formed austenite still kept relevant due to the ability of Si to refine and enhance the hardenability of austenite.

Figure 5.66 - Effect of silicon on amount of martensite at different annealing temperature, after air cooling.
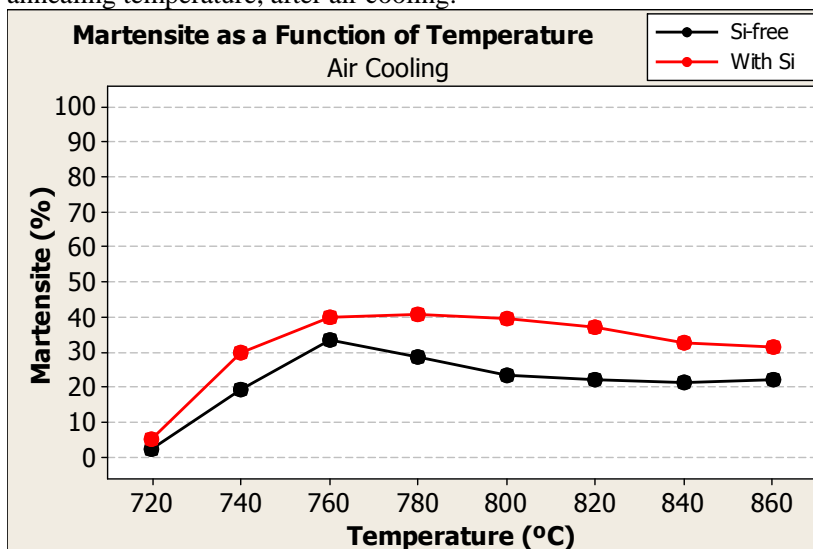
Source: Original, (2014).

Addition of 0.3 % Si to the steels favored the formation of larger volume of martensite (Figure 5.65) with much fined microstructure at all annealing temperatures and the kinetic of ferrite recrystallization. It is likely due to the previous process of austenitization.

The increase in the volume fraction of austenite resulted in the reduction of its hardenability due to the lower average carbon content. Nevertheless, it is necessary to take into account the morphology and homogeneity of the formed austenite. As mentioned before, the formation of austenite in the Si-added steel took place through the nucleation process followed by limited growth resulting in a refined

microstructure with small islands of austenite of uniform carbon distribution. In the case of the Si-free steel, the growth of austenite occurs through austenite nuclei growth in the ferrite resulting in the formation of coarse islands of non-homogeneous austenite. During slow cooling, the portions of austenite with a lower carbon content transforms to ferrite and/or bainite instead of martensite (DRUMOND et al., 2012).

The difference in the homogeneity of the martensite in both steels may be observed in Figure 5.67 that represents a set of microstructures of samples annealed at temperature ranging from 740 to 820 °C followed by air cooling.

Figure 5.67 – Refinement and recrystallization of microstructures due to the addition of 0.3 % Si to the low carbon steels, after annealing between 740 and 820 ºC and cooling on air (SEM / 2 % Nital).
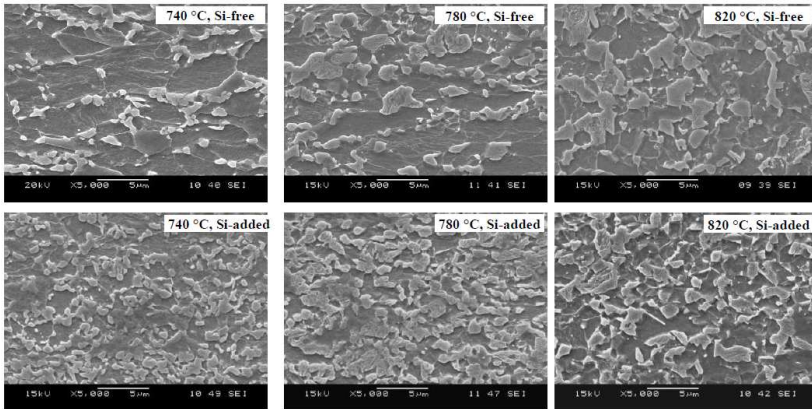
Source: Original, (2014).

Figure 5.68 shows that Si-free steel resulted in higher volume of bainite in comparison to the Si-added steel after slow cooling from annealing temperatures above 800 °C. As explained earlier, the non-homogeneous austenite of lower hardenability present in the Si-free steel induced the formation of a larger fraction of bainite instead of martensite.

Figure 5.68 - Effect of Si on the volume of bainite, as a function of annealing temperature, after air cooling.
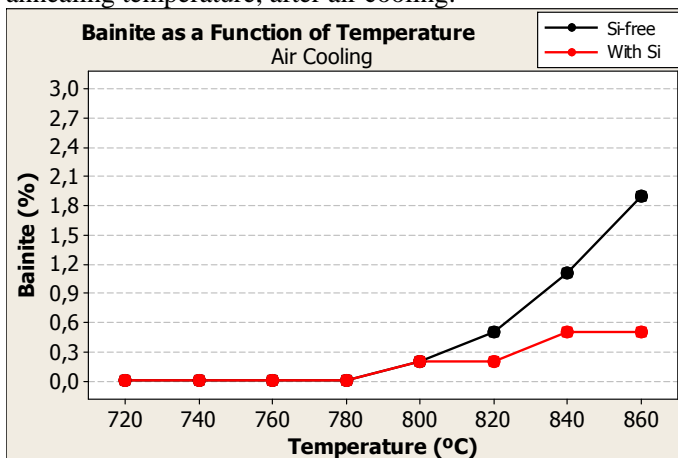
Source: Original, (2014).

Figure 5.69 shows the morphology of Si-free steel annealed at 860 ºC and cooled on air detailing the coexistence of bainite, ferrite and martensite structures.

Figure 5.69 - Microstructure of Si-free steel after annealing at 860º C and cooling on air, (SEM / 2 % Nital).
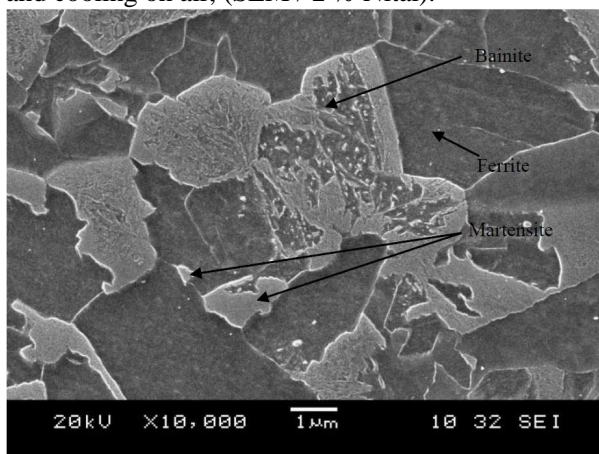
Source: Original, (2014).

Figure 5.70 shows that at 720 ℃ the yield strength of Si-free steel (~930 MPa) was around 190 MPa higher than the Si-added steel (~740 MPa), due to the presence of non-recrystallized ferrite grains; afterwards it decreased with the recrystallization evolution and curves have crossed up at 760-770 ℃ when yield strength of Si-added became higher. The tensile strength increased with holding temperature up to 760 °C for both steels. Similar level of UTS for both steels at temperatures below 760 °C, regardless the higher volume of martensite in the Si-added steel, was due to the enhanced contribution of a higher volume of non-recrystallized ferrite grains in the Si-free steel. At temperatures above 760 °C the addition of Si favored higher levels of UTS and YS due to a higher volume of martensite. The curves of total elongation (TE) followed the opposite sense of YS and TS. At temperatures below 760 ℃ TE of Si-free steels were lower than Si-added ones; above 760 ℃ TE of Si-free became higher (Figure 5.71).

The higher level of UTS in the Si-added steel can be partially attributed to the Si strengthening of ferrite that contributed to around 30 MPa, according to Pickering (1977), and should reside in potential differences in microstructural constituents and their properties. As well known, the final microstructure after cooling reflects not only the type and amount of austenite formed during heating and isothermal holding but also the hardenability of austenite, which strongly depends on both, carbon content and homogeneity of its composition.

Figure 5.70- Effect of Si addition on mechanical properties of the steel at different annealing temperatures, air cooling.
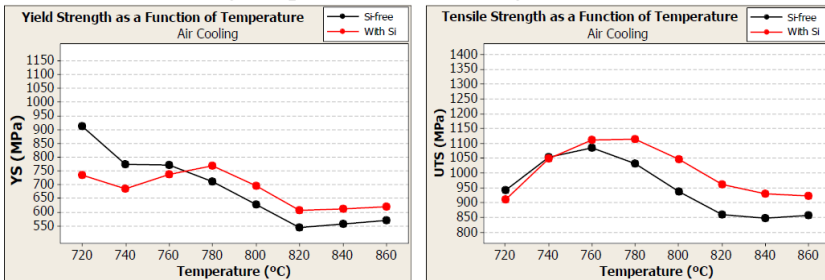
Source: Original, (2014).

Figure 5.71- Effect of Si addition on total elongation of the steel at different annealing temperatures, air cooling.
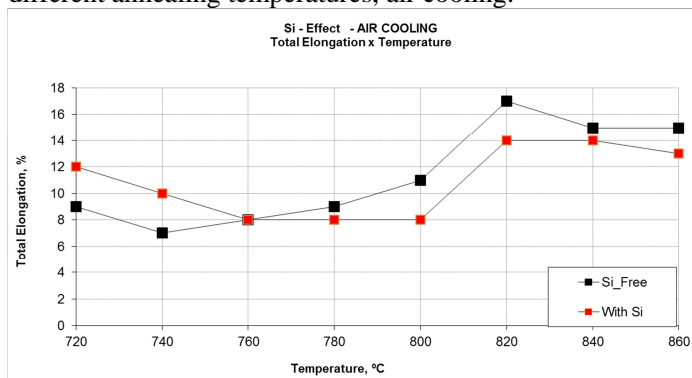
Source: Original, (2014).

Summary of Si effect

Si addition increases the strength of dual-phase steels after annealing and slow cooling because of the formation of a high volume of homogeneous austenite of high hardenability, leading to a high volume of martensite in the final structure.

Addition of Si accelerated the ferrite recrystallization during heating in the inter-critical temperature range and was attributed to the effect of more refined initial cold-rolled structure in the Si-added steel.

While the processes of recrystallization and austenitization proceeded simultaneously in the Si-free steel, ferrite recrystallization started earlier, in Si-added steel, and thus the austenite formation occurred preferably through the nucleation process, which leads to a uniform distribution of small islands of martensite within the refined ferrite matrix.

6 SUMMARY

Additions of Cr, Mo and Si to low carbon steels affected significantly the microstructures and mechanical properties of the final product. The variation in the content of each element showed relevant changes in the microstructures and final properties.

Figure 6.1 displays a summary of effects of each element on the martensite in steels after water quench which reflects the kinetic of austenitization. The base steel (blue line) is used as reference of changes comparison due to the addition of a specific element.

Cr and Si accelerated austenite transformation while Mo retarded one.

Cr accelerated the rate of austenite transformation due to its ability for promoting additional sites of nucleation within the ferrite grain on the surface of chromium carbides; and Si accelerated because it favors the ferrite recrystallization occurs earlier, and when the austenite formation begins, most ferrite grains are already recrystallized. This facilitates the formation of multiple austenite nuclei.

Mo retarded the austenite transformation due to its effect on decreasing the mobility of ferrite-austenite interface thus retarding the formation and growth of austenite.

Figure 6.1 – Effect of addition of Cr, Mo and Si on amount of martensite after water quench.
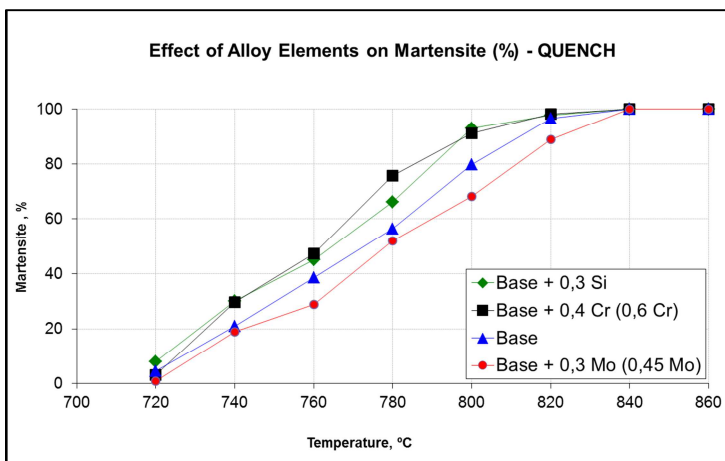
Source: Original, (2014).

Figure 6.2 displays the effect of addition of each element on the amount of martensite after air cooling, in comparison with base steel.

Additions of Cr and Si increased the amount of martensite at all annealing temperatures. Additions of 0.45 % Mo to the base steel resulted in less martensite at low temperatures, and more martensite at high temperature due to the effect of Mo on hardenability of austenite.

Figure 6.2 – Effect of addition of Cr, Mo and Si on amount of martensite after air cooling.
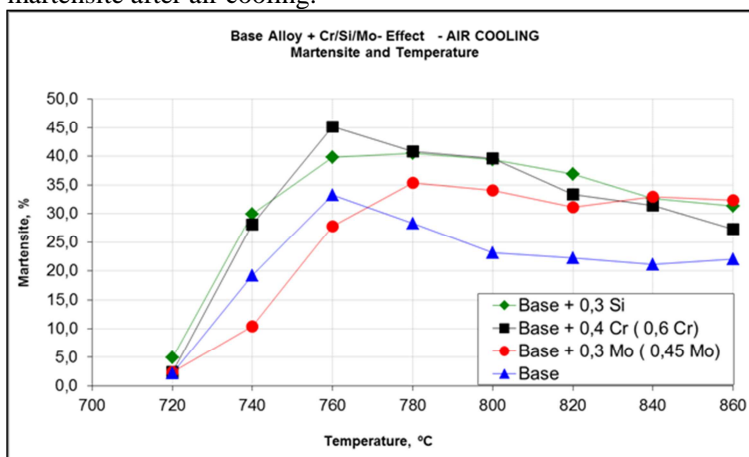
Source: Original, (2014).

Figure 6.3 displays the effect of each element on strengthening the steels.

In general Cr, Si and Mo increased the strength of steels.

Figure 6.3 – Effect of addition of Cr, Mo and Si on the strengthening of steels (air cooling).
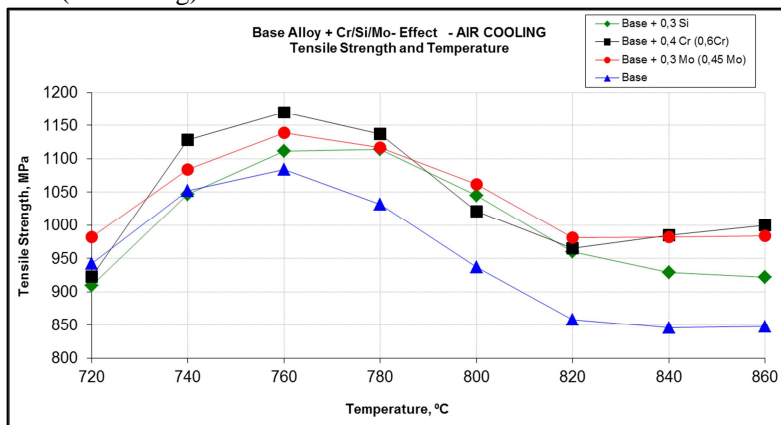
Source: Original, (2014).

Considering the observed effects of elements in the base steel on the final microstructure and properties, it is suggested that the best design balance would have in its composition (0.6 % Cr + 0.3 % Si + 0.15 % Mo). Cr and Si aimed to generate more refined and uniformly distributed austenite and Mo to suppress the transformation of this austenite to non-martensitic structures at cooling (hardenability).

The higher amount of martensite was obtained with annealing temperature between 760-780 ºC that produced high amount of austenite with enhanced hardenability.

The present study has agreed with literature concerning to the nucleation occurrence at grain boundaries of regular ferrite; nevertheless the novelties in the study is that additions of Cr in the steels changed the thermodynamic potential in the center of ferrite grains favoring the nucleation of austenite also in these regions (within the grains and on the surface of chromium-carbides). The presence of extra and refined austenite in the center of ferrite grains affected the final microstructure and increased the strength of steels.

It should point out that the steels used in this study showed different carbides precipitates which played important role in determining the final microstructures and properties. During heat treatment carbides reacted by different ways, which in turns affected the thermodynamics and kinetics of reactions. As an example, the increase in temperature resulted in dissolution of Fe_3C and partial dissolution of

both $M_{23}C_6$ and M_7C_3. It confirmed that Fe_3C is the less stable carbide while $M_{23}C_6$ and M_7C_3 in the presence of Cr at "low to moderate" concentration (~0.2 %) showed intermediate stability and at higher Cr concentration (~0.6 %) showed to be more stable carbides.

These differences in stability of carbides determined their presence or not inside the ferrite grains during heat treatment; which in turns affected recrystallization and phase transformation.

These observations have supported the building of a model to explain the effect of these carbides particles on austenite formation.

Mo showed strong effect on the stabilization of austenite, formed at inter-critical region, which transformed to martensite at cooling.

Concerning to Mo effect on the dual-phase steels its addition up to 0.45% caused the retarding on austenitization and recrystallization reactions, consequently less volume fraction of austenite was observed at heating and martensite at quenching.

However, Mo has increased the hardenability of formed austenite at heating (avoiding the austenite transformation to ferrite/pearlite during cooling). At low annealing temperatures lower amount of austenite was formed then the effect of Mo was not so evident; nevertheless, at high annealing temperatures higher amount of austenite was formed and Mo effect as austenite stabilizer was more efficient on producing more martensite and strengthening the steels.

Addition of Si accelerated the ferrite recrystallization during heating in the inter-critical temperature range and was attributed to the effect of more refined initial austenite structure in the Si-added steel.

The process of recrystallization and austenitization proceeded simultaneously on the Si-free steel. Since ferrite recrystallization started earlier in Si-added, steel the austenite formation occurred preferably through the nucleation process, which leads to a uniform distribution of small islands of martensite within the refined ferrite matrix.

Si addition increased the strength of dual-phase steels after slow cooling due to the formation of a high volume of homogeneous austenite of high hardenability leading to a high volume of martensite in the final structure.

After air cooling, the Si-added steel showed less ferrite and bainite than the Si-free (heated at temperatures above 800 ºC), which is also related to the higher hardenability of austenite formed in Si-added steel.

After air cooling, the Si-added steel showed higher mechanical properties than the Si-free steel. On average, there was an increase of 50 MPa (YS) and 100 MPa (UTS) with addition of silicon.

Addition of 0.3 % silicon proved beneficial to meet the mechanical properties, especially with respect to the tensile strength.

CONCLUSION

Additions of Cr, Mo and Si to low carbon steels affected significantly the microstructure (refinement, recrystallization and volume fraction of phases) and consequently increased mechanical properties.

Chromium, molybdenum and silicon have refined the microstructure of heat treated steel, however by different ways. Chromium through the nucleation of additional austenite on the carbides surface which restrained growth; molybdenum through the decreasing of mobility of ferrite/austenite interface and silicon through the effect of more refined initial cold rolled structure and acceleration of ferrite recrystallization.

Chromium and silicon accelerated ferrite recrystallization, whereas molybdenum retarded. Silicon accelerated recrystallization of ferrite through its effect on initial microstructure.

Chromium and silicon accelerated the austenite transformation for all concentrations, whereas molybdenum accelerated austenite transformation only at 0.15 % but retarded austenite transformation at low temperatures and higher concentrations (e.g. 0.45 %).

Chromium and silicon enhanced hardenability of austenite at all concentrations and inter-critical annealing temperature; whereas Mo effect on hardenability became more significant at high temperatures (above 760 ºC) at lower carbon content in austenite.

The presence of carbides $M_{23}C_6$ and M_7C_3 inside the ferrite grain on heating has modified the condition of the center of the grain favoring the nucleation of additional austenite sites; which in turns resulted in more and finer austenite (martensite) and consequently higher strength steels.

The addition of Cr, Mo and Si effectively increased the strengths of low carbon steel; therefore, a more judicious balance of these elements can improve the properties of steels.

Contrary to what was seen in the literature, the alloying elements such as Cr, Mo and Si did not act as ferrite stabilizers.

SUGGESTION FOR NEXT STUDIES

- Effect of Mo concentration on microstructure and mechanical properties (focus in Mo content between 0 and 0.30 % to understand the transition).
- Effect of chromium carbides on austenite nucleation
- Effect of Si on microstructure of hot rolled steel

REFERENCES

BAIN, E. C. **Functions of the alloying elements in steel**. Illinois, U.S.A.: American Society for Metals. (Vol. 4, pp. 133, 104-109). 1945.

BLECK, W., FREHN, A., & OHLERT, J. **Niobium in dual Phase and TRIP Steels.** (A. U.-D. Metallurgy, Ed.). (pp. 10 - 31). (2002).

BUCHER, J. H., & HAMBURG, E. G. (n.d.). **Structure-Property Relationships for VAN-QN Dual-Phase Steels, Formable HSLA and Dual-Phase Steels.** pp. 142-150.

CABALLERO, F. G., CAPDEVILA, C., & GARCÍA, C. **Modelling of Kinetics of Austenite Formation in Steels with Different Initial Microstructures** (Vol. 41). Madrid, Spain: ISIJ International. (2001).

CALLISTER, W. D. **Material Science Engineering - An Introduction.** Salt Lake City. (2006).

CHO, K., REDKIN, K. V., HUA, M., GARCIA, C. I., & DEARDO, A. J. **Recent Development of Nb-Containing DP 590, DP 780 and DP 980 Steels for Production on Continuous Galvanizing Lines.** Advanced Steels, pp. 177 - 185. (2011).

COHEN, M., & WAYMAN, C. M. **Metallurgical Treatises**, 445. (1981).

DAVIES, G. R., & MAGEE, C. L. **Physical metallurgy of automotive high strength steels**. In R. A. KOT, & J. W. MORRIS, Structure and Properties of Dual - Phase Steels (pp. 1-157). New Orleans, La, USA: The Metallurgical Society of AIME. (1979).

DAVIES, R. G. **Influence of Martensite Composition and Content on the Properties of dual Phase Steels.** American Society for Metal and the Metallurgical Society Metallurgical Transactions A, 9A, 671- 679. (1978, May).

DOHERTY, R. D., & MARTIN, J. W. T**he Effect of a Dispersed Second Phase on the Recrystallization of Aluminium-Copper Alloys.** Journal of the Institute of Metals, 91, 332-338. (1962, Mar).

DRUMOND, J., GIRINA, O., DA SILVA FILHO, J. F., FONSTEIN, N., & SILVA DE OLIVEIRA, C. A. **Effect of Silicon Content on the Microstructure and Mechanical Properties of Dual-Phase Steels.** Metallography, Microstructure and Analysis, 1(2). (2012, September 21).

ENOMOTO, M., AARONSON, H. I. On the Critical Nucleus Composition of Ferrite in an Fe-C-Mn Alloy. Metallurgical Transactions A. Vol. 17 A. pp. 1381 - 1384). (August, 1986).

FONSHTEIN, N. M., & EFIMOVA, T. M. **Study of the effect of "new" ferrite on the properties of dual phase steels.** Metallurgist, 50, 481-489. (2006, September).

FONSTEIN, N. M. **Advanced High Strength Sheet Steels. Physical Metallurgy, Design, Processing and Properties.** Switzerland: Springer International Publishing. (2015).

FONSTEIN, N., & GIRINA, O. **Effect of C, Mn and Al on Structure and Mechanical Properties of Dual-Phase and TRIP Steels.** Mittal Steel. USA- Research & Development. Chicago, p. 20. (2005).

FUJITA, N. **Development of Ultra-High Strength Steel Sheets with Tensile Strength of 980MPa.** Proceedings JSAE Annual Congress, v. 114-06, p. 9-12. (2006).

GARCIA, C. I. **Transformation Strengthening of MA Steels In Iron and Steel Society** (Ed.), International Conference "Microalloying '95", (pp. 365-373). Pittsburgh. (1995).

GARCIA, C. I., CHO, K., REDKIN, K., DEARDO, A. J., TAN, S., SOMANI, M., et al. **Influence of Criical Carbide Dissolution Temperature during Intercritical Annealing on Hardenability of Austenite and Mechanical Properties of**

DP 980 Steels. ISIJ International , Vol. 51), pp. 969-974. (2011).

GAZDER, A. A., ARAIZA-SÁNCHEZ, M., JONAS, J. J., & PERELOMA, V. E. **Evolution of Recrystallization Texture in a 0.78 wt% Cr Extra-low-carbon Steel After Warm and Cold Rolling.** Acta Materialia, 4847-4864. (2011, May 9).

GIRINA, O. **Influence of Al Additions on Austenite Decomposition in Continuously Annealed Dual-Phase Steels** (p. 12). ISPAT INLAND INC. Chicago. (2005).

GIRINA, O. A., & FONSTEIN, N. M. **Influence of Al Additions on Austenite Decomposition in Continuously Annealed Dual-Phase Steels.** Materials Science & Technology (p. 952-963 ed.). (2005).

GIRINA, O., FONSTEIN, N., & BHATTACHARYA, D. **Effect of Nb on the phase transformation and mechanical properties of advanced high strength dual-phase steels.** East Chicago, Indiana 46312 USA: Arcelor Mittal, Global R & D. (pp. 1 - 7). (2007).

GREEN, M. L., ESPINAL, L., TRAVERSA, E., & AMIS, E. **Materials form sustainable development.** MRSBulletin, 37, pp. 303-308. (2012, April).

HAN, F., HWANG, B., SUH , D. W., WANG, Z., LEE, D., & KIM, S.-J. **Effect of Molybdenum and Chromium on Hardenability of Low-Carbon Boron-Added Steels.** METALS AND MATERIALS InternationaL, Vol. 14, No. 6, pp. 667-672. (2008, December 18).

HAN, Q.-h., KANG, Y.-l., LU, C., & GAO, L.-f. **Microstructure and Properties of Mo Microalloyed cold Rolled DP1000 Steel.** JOURNAL OF IRON AND STEEL RESEARCH, INTERNATIONAL, pp. 52-58. (2011).

HAYAMI, I. A. **Family of High Strength, Cold Rolled Steels.** Microalloying 75. (pp. 78-87). London: [s.n.]. (1975).

HAYASHIDA, T. O. **"Development and Applications of Continuous Annealed Low Carbon Al Killed BH Steel Sheets"** (Oct ed., Vols. pp.135-139.). in: proceedings of the symposium on high strength steels for automotive, baltimore, iron and steel society. (1994).

HIRONAKA, S. **Effect of Si on Mechanical Property of Galvannealed Dual Phase Steel.** (S. Trans Tech Publications, Ed.) Materials Science Forum , Vols. 638-642, pp. 3260-3265. (2010).

HIRONAKA, S., HOSOMI, K., TANAKA, H., & MATSUMOTO, T. **Nisshin Steel Tech.** pp. 27. (2006).

HIRONAKA, S., TANAKA, H., & MATSUMOTO, T. **Effect of Si on Mechanical Property of Galvannealed Dual Phase Steel.** (S. Trans Tech Publications, Ed.) Materials Science Forum, Vols. 638-642, pp. 3260-3265. (2010, Jan 12).

HONEYCOMBE, R. W. **Ferrite.** Metal Science. pp. 201 - 214. (1980).

HONEYCOMBE, R. W. **Steels Microstructure and Properties. In E. Arnold, Steels Microstructure and Properties** (pp. 71-92). London: Edward Arnold. (1981).

HORNBOGEN, E. (n.d.). **Physical Metallurgy of Steels. (1996).**

HUANG, J., POOLE, J., & MILITZER, M. **Austenite Formation during Intercritical Annealing. Metallurgical and Materials Transactions** (Vols. 35, n. 11, pp. 3363-3375). (2004).

HUMPHREYS, J. F., & HATHERLY, M. **Recrystallization and Related Annealing Phenomena.** Manchester, UK: Pergamon (Manchester University). Second Edition (2004).

IMAMURA, J., FURUKAWA, T. Nippon Steel Technical Report, Overseas, No. 10, 103. (1977).

IRIE, T. **Metallurgical Factors Affecting the Formability of Cold Rolled High Strength Steels.** (T. ISIJ, Ed.) Transactions ISIJ, Vol. 21, 1981, Vol. 21, pp. 793-801. (1981).

JONAS, J. J. **Effect of Deformation on the Austenite-Ferrite Transformation in Two High Silicon Dual-Phase Steel.** Montreal H3A, 2A7, Canada: Dept. of Metallurgical Engineering, McGill University. (1981) pp. 95 - 112. (1981).

KATO, T., HASHIGUCHI, K., TAKAHASHI, I., IRIE, T., OHASHI, N., & BRAMFITT, B. L. **Fundamentals of Dual-Phase Steels.** Warrendale. (1981).

KOO, J. Y., YOUNG, M. J., & THOMAS, G. **On the Law of Mixtures in Dual Phase** (Vol. 11A). (M. T. A, Ed.) Berkeley, California, USA: ASM and Metallurgical Societyof AIME. (1980).

KORIR, K. K., AMOLO, G. O., MAKAU, N. W., & JOUBERT, D. P. **First-Principle Calculation of the Bulk Properties of 4d Transition Metal Carbides and Nitrides in the Rocksalt Zincblende and Wurtzie Sgrucgure.** Diamond and Related Materials. Vol. 20. Issue 2. (pp. 157 - 164). (February 2011).

KRAUSS, G. **Steels: Heat Treatment and Processing Principles.** ASM Internacional Fourth printing. (1995).

KRAUSS, G. **Heat-Treated Low-Alloy Carbon Steels: The Benefits of Molybdenum. International Seminar on Applications of Mo in Steels**, pp 14-23. (2010, June 27th).

KRUPITZER, R. P., & HEIMBUCH, R. A. **Revolutionary steels are helping automakers produce stronger, more fuel-efficient and cost-effective vehicle structures**. Metalforming. (Apr 2005).

LEE, C. G., KIM, S.-J., LEE, T.-H., & OH, C.-S. **Effects of Tramp Elements on Formability of Low-Carbon TRIP-aided Multiphase cold-rolled Sheets.** ISIJ International, 44, pp 737-743. (2003, December 15).

LEE, S. J., MATLOCK, D. K., & VAN TYNE, C. J. **An Empirical Model for Carbon Diffusion in Austenite Incorporating Alloying Element Effects.** ISJI International, 51, pp 1903-1911. (2011, Nov.).

LESLIE, W. C. **Trans. TMS-AIME**, 221, pp. 982-989. (1961).

LLEWEUYN, D. T., HUDD, R. R,. **Steels: Metallurgy and Applications Third Edition** (Vol. 3). Oxford: Reed Educational and Professional Publishing Ltd. (1998).

LLEWEUYN, D. T., **Boron in steels.** The Institute of Materials. University College, Swansea. Vol. 20. N. 5. (pp. 338 - 343). (1993).

SOUZA, M. M. **Met.Trans,** Vol.13A, p. 575. (1982).

MEYRICK, G. WAGONER, R. H. **Steel Class Notes and Lecture Material for MSE 651.01.** Physical Metallurgy of Steels. The Ohio State University. (1998).

MIAO, B., NORTHWOOD, D. O., LIM, L. C., & LAI, M. O. **Microstructure of Tempered AISI 403 Stainless Steel. Materials Science and Engineering**. pp 21-23. (1993, May 18).

MILITZER, M. ; GIUMELLI, A. ; HAWBOLT, E.B. ; MEADOWCROFT, T.R. **AUSTENITE AND FERRITE GRAIN SIZE EVOLUTION IN PLAIN CARBON STEEL.** American iron and Steel Inst. Pittsburgh, PA, (United States). (pp. 1 - 28). (1995).

MOHANTY, R. R., GIRINA, O. A., & FONSTEIN, N. M. **Effect of Heating Rate on the Austenite Formation in Low-Carbon High-Strength Steels Annealed in the Intercritical Region.** Metall. Mater. Trans. A, 42, pp. 3680-3690. (2011).

NASCIMENTO, R. A. **Influence of Grain Refinement and Deformation on Ferrite Formation in a High Silicon Dual Phase Steel.** Mcgill University, Department of Mining and Metallurgical Engineering, Montreal. (1981).

NOURI, A., SAGHAFIAN, H., & KHEIRANDISH, S. **Effects of Silicon Content and Intercritical Annealing on Manganese Partitioning in Dual Phase Steels.** Journal of Iron and Steel Research International, 17(5), pp 44-50. (2010).

OGAWA, T., MARUYAMA, N., SUGIURA, N., & YOSHINAGA, N. **Incomplete Recrystalization and Subsequent Microstrutural Evolution during Intercritical Annealing in Cold-rolled Low Carbon Steels: ISIJ Int**., v.50, pp. 469-475. (2010).

OLIVEIRA, M. A., JORGE, A. M. & BALANCIN, O. **Influence of Deformation on the Kinetics of Phase Transformation in a Forging Steel During Warm Working.** Materials Research, 7, pp 247-253. (2004).

OSAWA, K., SUZUKI, Y., & TANAKA, S. **980 MPa Grade Low-Carbon Equivalent Type Galvannealed Sheet Steels with Superior Spot-Weldability.** (Vols. v. 48, pp 9-16). Kawasaki Steel Technical Report. (2003).

PADILHA, A. F., & SILICIANO, F. **Encruamento, Recristalização, Crescimento de Grão e Textura.** São Paulo, SP , Brazil: Associação Brasileira de Metalurgia e Materiais. (2005).

PETROV, L. **Iron Steel Inst. Jpn. Int. Recrystallization of a Cold Rolled Trip-assisted Steel during**, Vol. 41, pp. 883-890. (2001).

PICKERING, F. B. **High-Strength Low-Alloy Steels - A Decade of Progress**. Microalloying 75, pp 9-30. (1977).

PICHLER, A., TRAINT, S., ARNOLDNER, G., WERNER, E., PIPPAN, R., STIASZNY, P. **Phase Transformation During Annealing of a Cold-Rolled Dual-Phase Steel Grade.** VOEST-ALPINE STAHL LINZ GmbH. 42nd MWSP CONF. PROC. (pp. 573 - 593). (2000).

PORTER, D. A., EASTERLING, K. E., SHERIF, M. **Phase transformations in metals and alloys.** Boca Raton - FL: Taylor and Francis Group. Third Edition. (2004).

POTTORE, N. **A Family of 980 Mpa Tensile Strength Advanced High Strength Steels with Various Mechanical Properties Attributes.** (pp. 119–130). International Conf. on Advanced High Strength Sheet Steels for Automotive Applications, AIST. (2004).

POTTORE, N. E. **Effect of C, Mn, Si and Al Additions on the Mechanical Properties of 980 MPa Tensile Strength, Cold Rolled, Advanced High-strength Steel.** Iron and Steel Technology (Vols. v. 3, n. 9, pp 63-71). (2006).

POTTORE, N., GUPTA, I., & PRADHAN, R. **Effects of Composition & Processing in Cold-Rolled, Dual-Phase Steels for Automotive Applications.** Materials Science and Technology - Association for Iron and Steel Technology (Vols. v. 4, pp 721-732). (2006).

PURDY, G. R. **Acta Met.**, pp 487. (1978).

PUSHKAREVA, I. **Evolution microstruturale d'un aciere dual fase.** Optimisation de la resistance a l'endomage. Ecole des Mines de Nancy. (2009).

QIU, C. **Thermodynamic Analysis and Calculation of the Cr-Mo-C System** (Vol. 199). Stockholm, Sweden: Journal of Alloys and Compounds. (pp. 53 - 59). (1993).

RASHID, M. S. **GM 980X-A Unique High-Strength Sheet Steel with Superior Formability.** SAE Technical Paper 760206. (1976).

RAZZAK, M. A. **Heat Treatment and Effects of Cr and Ni in Low Alloy Steel.** Bull. Material Sci., 34, pp. 1439-1445. (2011, December 7).

REED-HILL, R. E. **Princípios de Metalurgia Física**. Second Edition (1982).

SHEN, P. P. **Effect of boron on the microstructure and tensile properties of dual-phase steel.** Metallurgical Transactions A, 21A, 25472553. (pp. 2547 - 2553). (1990, September).

SILVA DE OLIVEIRA, C. A. **Estudo do Processo de Revenimento de um Aço DIN 1.2714 Modificado pela Adição de Nióbio**. Dissertação de Mestrado, Pontifície Universidade Católica do Rio de Janeiro, Ciência dos Materiais e Metalurgia , Rio de Janeiro. (1985).

SILVA, A. L., & MEI, P. R. **Aços e Ligas Especiais. In Aços e Ligas Especiais** (pp. 196-203). Sumaré, São Paulo, Brazil: Eletrometal. (1988).

SONG, R., Ponge, D., Kaspar, R., & Raabe, D. **Grain boundary characterization and grain size measurement in an ultrafine-grained steel.** Düsseldorf, Germany: Z. Metallkd. pp. 95. (2004).

SOUZA, E. **Cinética e morfologia das transformações de fase em aços trip contendo teores variaveis de Si e Mn.** (SOCIESC, Ed.) Dissertação de Mestrado do Instituto Superior Tupy. (2009)

SOUZA, M. M., GUIMARAES, J. R., & CHAWLA, K. K. **Met.Trans,** Vol.13A, p. 575. (1982).

SPEICH, G. R. **Physical Metallurgy of Dual-Phase Steels. Fundamentals of Dual-Phase Steels** (pp. 3-45). Chicago, Illinois, USA: Metallurgical Society of AIME and the ASM/MSD. (1981).

SPEICH, G. R., Demarest, V. A., & Miller, R. L. **Formation of Austenite During Intercritical Annealing of Dual-Phase Steels.** Metall. Mater. Trans. A , 12, pp. 1419-1428. (1981).

SUN, X., & YONG, Q. T**he Roles and Applications of Molybdenum Element in Low Alloy Steels**. International Seminar on Application of Mo in Steels, pp. 61-73. (2010).

OGAWA, T. N., MARUYAMA, N. and YOSHINAG, N. **ISIJ Int**., v.50, pp.469-475. (2010).

TAKAKURA, K., & TAKAGI, K. **Application Development of Low Carbon Type 980 MPa High Strength Steel.** Nissan Motor Co. Ltd. Copyright. SAE International. (pp. 196 - 200). (2005).

TANAKA, T., NISHIDA, M., HASHIGUCHI, K., & KATO, T. **Structure and Properties of Dual-Phase Steel.** The Metallurgical Society of AIME, pp. 221-241. (1979).

TRAINT, S., PICHLER, A., SPIRADEK-HAHN, K., KREMPASZKY, C., & WERNER, E. **Microstructure Characterization of Cold-Rolled Dual-Phase Steels.** 35, pp. 448-456. (2004).

WATERSCHOOT, T., VANDEPUTTE, S., DE COOMAN, B. C., & HOUBAERT, Y. **The influence of P, Si and Mn on the mechanical properties and bake-hardening of ti-ulc steels.** In MWSP Conf. Proc. ISS (Ed.), 41st MWSP Conf. Proc. , XXXVII, pp. 425-433. (1999).

WEY, M. T. **Effect of Alloying Elements on the Grain Growth in Dual-Phase Stees.** ISIJ (Institute of Steel and Iron of Japan). (1981, 101st).

WU, J., WRAY, P. J., HUA, M., GARCIA, C. I., & DEARDO, A. J. **Austenite Formation and Decomposition.** Mater. Sci. Technol., A, pp. 291-309. (2003).

XIAO, B., XING, J. D., FENG, J., LI, Y. F., ZHOU, C. T., SU, W., et al. **Theoretical Study on the Stability and Mechanical Property of Cr₇C₃.** (Elsevier, Ed.) ScienceDirect, pp. 2273-2281. (2007, December 5).

XIE, J., CHEN, N., TENG, L., & SEETHARAMAN, S. **Atomistic study on the struture and thermodynamic properties of Cr7C3, Mn7C3, Fe7C3.** Beijng: Acta Materialia 53. (pp. 2727 - 2732). (2005).

YANG, D. Z. **Metall. Trans. A** (Vols. v. 16A, pp. 85-92). (1985).

YEFEI, L., GAO, B., XIAO, B., MIN, T., YANG, Y., MA, S., et al. **The electronic , mechanical properties and theoretical hardness of chromium carbides by first-principles calculations. Journal of alloys and Compunds**. pp. 5242 - 5249. (2011, February 23).

YEN, H. W., CHEN, P. Y., HUANG, C. Y., & YANG, J. R. **Interhase Precipitation of Nanometer-sized Carbides in a Titanium-Molybdenum-bearing Low-Carbon Steel.** (A. MATERIALIA, Ed.) ScienceDirect, 59, pp. 6264-6274. (2011).

ZHUKOV, A. A., & KRISHTAL, M. A. **Met. Sci. Heat Treat**. pp 17; 626. (1975).

APPENDIX A – Samples preparation (SEM)

Samples for metallography and scanning electron microscopy were cut from the region of tensile test specimen without defomation, according to the scheme shown in figure below.

Figure: Schematic profile of mechanical specimen used for take metallographic samples
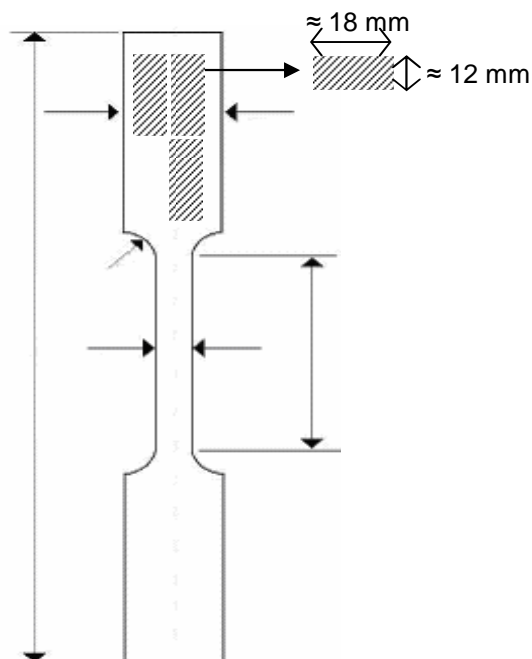
Source: Original.

Samples were withdrawn in dimensions of ≈ 18 x 12 mm using abrasive cutting disc (cut-off). Afterwards, they were cleaned in ultrasonic washer with acetone, before mounting in baquelite. This procedure aims to remove solid particles of dust, grease and others. Samples were hot mounted in baquelite using the press Buehler equipment (see parameters described in Table below).

Table of hot mounting parameters

Temperature (ºC)	Heating Time (min)	Cooling Time (min)	Mounting Press (Bar)
180	15	5	200

Source: Original.

The following figure shows the assembly of samples after hot mounting. Figure: Schematic figure showing a disc with the assembly of the samples in baquelite.
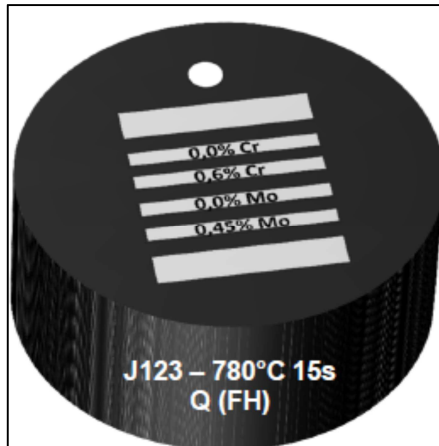
Source: Original.

Baquelite disc was manually grinded using a mechanical grinder Arotec APL-4D aiming to reach an adequate surface. The grinding directions should be changed by 90 degrees, according to figure below, to remove scratches from the previous process.

Figure: Positions of reference point of sample during grinding to prevent from scratches.
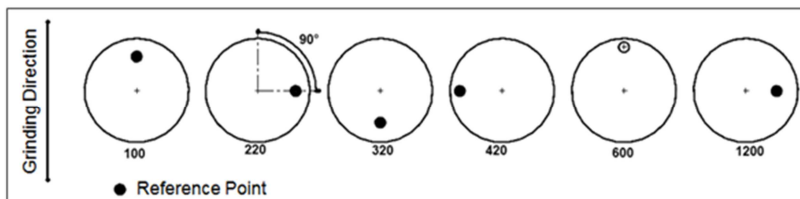
Source: Original.

The grinding procedure was carried out by using sequential steps of papers with the following grits 120, 320, 600, 800, 1200 meshes. Each step held 3 to 5 minutes.

The polisher device used was the Buehler Metaserv model 2000. Polishing process was divided in two steps, coarse and fine. Coarse polishing was carried using diamond paste 3 to 6 μm and the fine ones 0.5 to 1μm.

After the surface finishing stage, it was etched in 4 % Nital solution (Ethanol + Nitric Acid) for about 8 seconds aiming the revealing of phases.

After the metallographic preparation, the samples were observed in optical and scanning electron microscope.

The investigation of phases in the steel microstructures was carried out randomly along the ¼ and ½ of thickness (section) of the sample, as shown in schematic figure of section below. Microstructures in different magnifications like 500, 1000, 2500, 5000, 10000 and 15000 were obtained for support analysis.

Figure: Scheme of cross section of sample with positions used for microstructure analysis
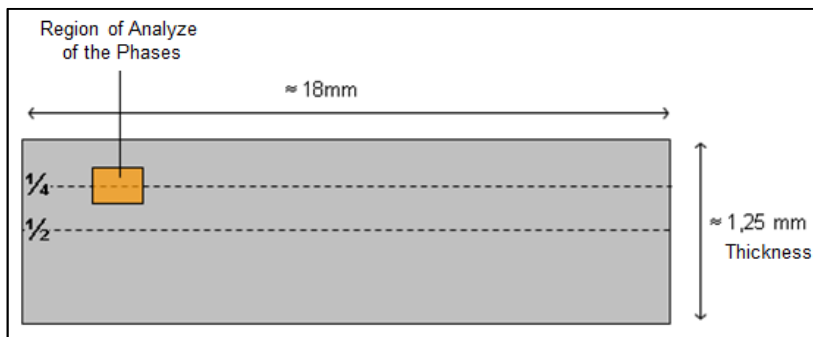
Source: Original.

APPENDIX B – Martensite quantification by grid

Martensite quantification was determined by the method of the grid of lines and intersection points: i) SEM micrographs were developed at a magnification of 2500x; ii) pictures of microstructure were open with the image analyze software (digital image); iii) grid was set up on the picture (grid = 980 points); iv) the intersection points of grid found inside the martensite were count, as shown in schematic figure of counting martensite below; v) calculus % of martensite = number of point within a intersected martensite.

Figure below displays the grid used for martensite counting. Points in the center of martensite island (white) on the boundary (green).

Figure: Grid for martensite counting
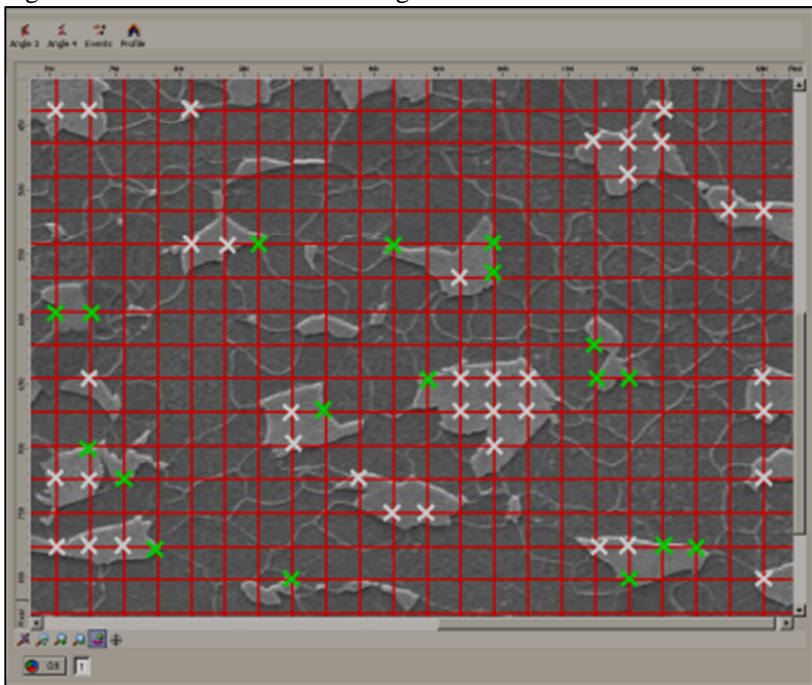
Source: Original.

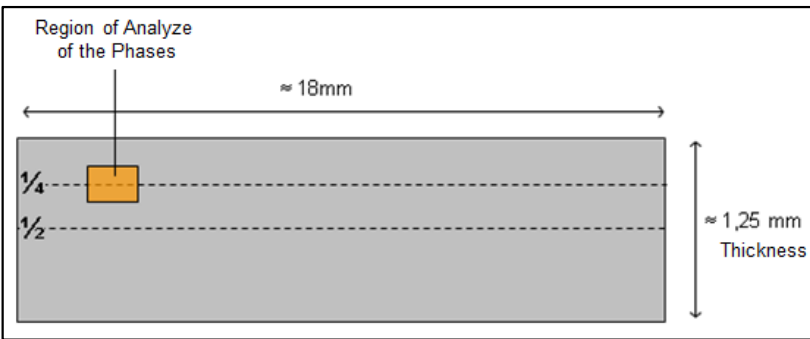Martensite volume fraction equation:

$$Martensite\% = \left(\frac{whitepoint + \left(\dfrac{green.points}{2} \right)}{920} \right) \times 100$$

Figure: Scheme representation of phases analyse method in steel microstructure

Source: Original.

APPENDIX C – Metallographic analyses samples, by TEM

Precipitates and phases were investigated also by transmission electron microscopy (bright and dark field) and diffraction of electrons. Carbon replica and thin film techniques were used to extract carbides and reveal constituents, respectively.

Extraction by replica of carbon

Samples cut from steels heat treated at 740 °C and 780 °C were prepared accordingly:

i)   mounting in baquelite disk, with rolling direction thickness to the face.

ii)   grinding on sequential grits 120, 300, 400, 600, 800 and 1200 mesh (for each grind time = 120 sec and rotation = 90 rpm).

iii) polishing mechanically (about 1cm * 1cm, up to 1/4 um diamond paste):

   a. First polishing: 3 µm (time = 90 s; rotation = 150 rpm).

   b. Second polishing: 1 µm (time = 120s; rpm= 100).

iv)   Electro-Chemical etching of samples in baquelite using (TMAC solution).

   a. Solution: AA solution (890 mL methanol + 100 mL acetylaceton + 10 g TetraMethyl Ammonium Chloride).

   b. Etching Time: 4~5 min

   c. Electro-chemical etching condition: 2 V, 0.03 mA (if possilble use current control).

v)   C-film coating: Hold baquelite with sample inside a vacuum evaporator for 4 minutes, and then 1.2 seconds for C film deposition.

vi) Make grid (2~3 mm), using sharp blade, in the C-film sticked on the samples and clear out edge region of sample.

vii) Electro-Chemical polishing (if possible, voltage control):

a. AA solution (C film, fine ppt.) : ~ 2 h, 2 V, 0.02 mA

b. 5 % Nital (Al film) : ~ 1 h, 2 V, 0.01~0.015 mA

c. 15 % Perchloric acid + 85 % ethanol (C film, large ppt.) : ~ 20 min., 2 V, 0.01~0.015 mA.

viii) Make sample using copper or Ni grid.

ix) Washing 2 times in ethanol at least.

x) Fishing in DI water.

xi) Storage in a squared sliding box.

Required Equipments/Materials

- Carbon (or Al) deposition machine
- Platinum electrodes for electro-chemical etching and polishing
- Chemicals for etching and polishing solutions

The carbon replicas were examined in a transmission electron microscope (TEM), Jeol JEM-2100 Electron Microscope operating at 200 kW. The TEM was equipped with an energy-dispersive spectroscopy (EDS) system.

Thin film

Samples size $\approx$ 20 mm x 20 mm were withdrawn by abrasive cutting disc. The preparation procedure was carried out on 4 steps as shown in figure of sequential steps below.

Figure: Sequential steps for preparation of samples for TEM
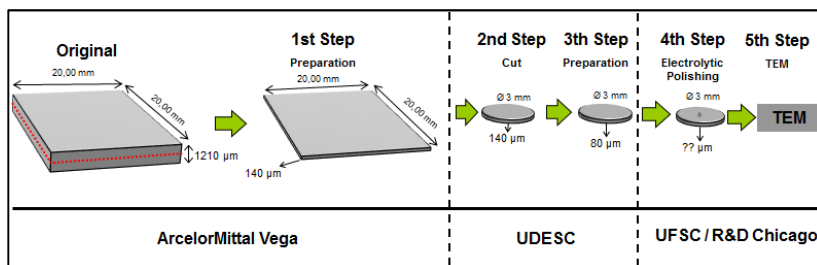
Source: Original.

The first step was the mechanical grind using the Mechanical grinder Arotec APL-4D.

Grinding on sequential grits 120, 320, 600, 800 1200 and 1500 mesh for about 5 minutes in each grind, in order to reduce the thickness of the sample to ≈ 140 µm in region of ¼ thickness (section), according to the scheme shown in the following.

Figure: Scheme representation of 1st step of grinding samples.
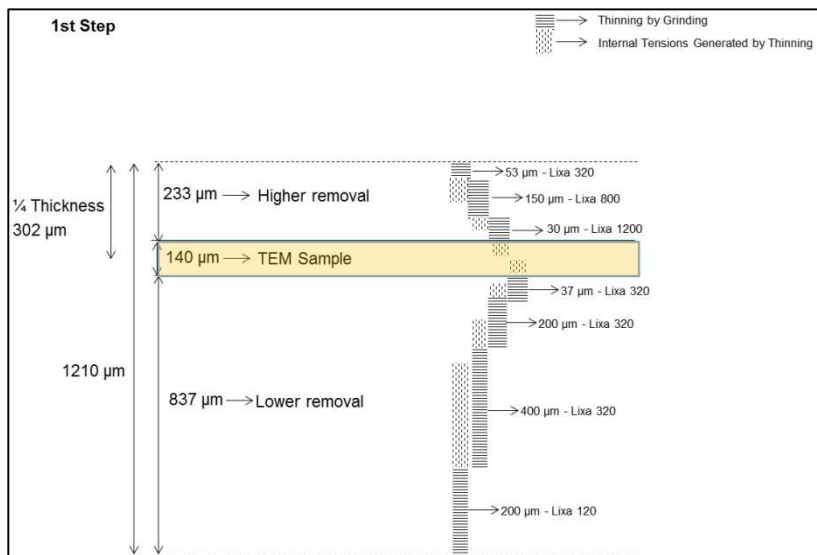
Source: Original.

The samples were cut off in discs shape of 3 mm diameter and thickness of ≈ 140 µm, then cut by disc Punch Gatan device, as shown in figure below.

Figure: Disc punch (model 659 Gatan)

1. Source: Original.

Afterwards, discs were set up in a disc grinder Gatan (Figure below) for reducing the thickness to ≈ 75 µm (3th Step).

Figure: Disc grinder (model 659 Gatan)
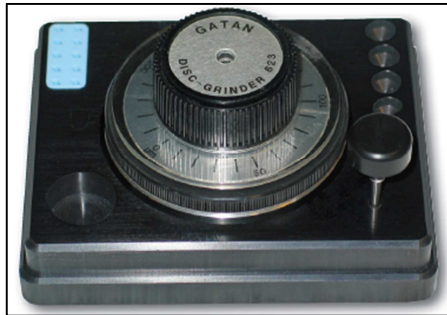
Source: Original.

This was electrolytically polished using the equipment TenuPol (see figure below) with A8 solution (950 ml acetic acid + 50 ml perchloric acid) at 12 ºC, in order to develop hole by anodic dissolution on the steel surface, as shown in figure below. Parameters controlled during tests: temperature, voltage, current and electrochemical solution.

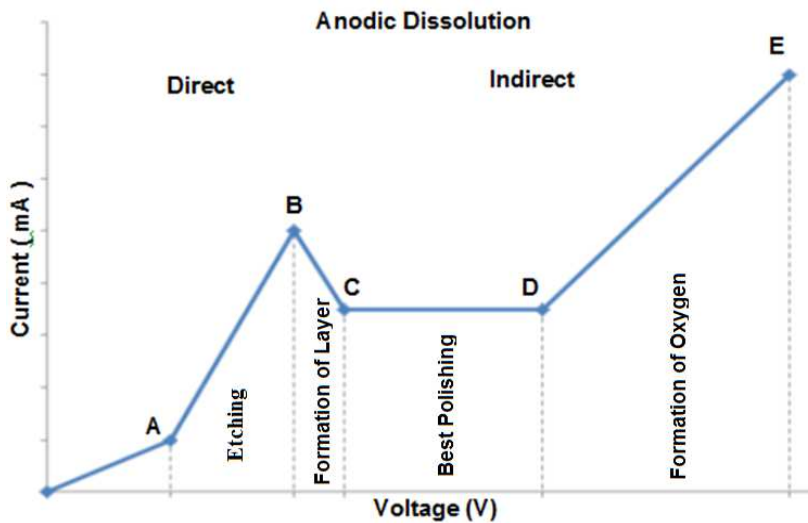Figure: TenuPol (Struers)

Source: Original.

The polishing occurs at an intermediate position of electrolytic polishing curve that in low voltages occurs chemical Etching and in high voltages occurs the corrosion of the sample.

APPENDIX D – Sample preparation (EBSD)

1. Next, it was withdraw samples with dimensions of ≈ 8.0 x 7,0 mm (L x L x h) by abrasive cutting disc (cut-off).
2. After withdrawer the sample, it was performed the cleaning in ultrasonic washer, with acetone, the same, before of the mounting operating. This is procedure to remove any solid particulate of dust, grease and others.
3. After the cleaning of the samples, the same was mounted by method to hot mounting with granulated bakelite, in mounting press Buehler equipment, with parameters described in the following Table.

Table: Parameters for hot mounting.

Temperature (ºC)	Heating Time (min)	Cooling Time (min)	Mounting Press (Bar)
180	15	5	200

Source: Original.

1. The Figure below shows the schematic photo of the samples after hot mounting.

Figure: Schematic photo of the samples after hot mounting
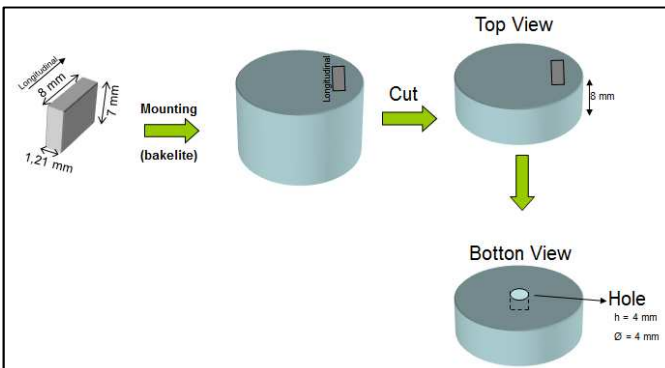
Source: Original.

2. After the samples mounted, it was held metallographic grinding procedure in mechanical grinder Arotec APL-4D, using manual grinding method.
3. The sequence of grind discs paper to grinding the steel samples is 120, 320, 800, 1200 and 1500 Mesh for about 5 minutes in each grind.
4. Next, it was held the polishing procedure, using a polisher Buehler device, with to purpose of obtain a plane surface, risk free and High reflectivity, that the polishing time can last a few minutes or hours.

Polishing procedure was divided into three steps: (i) rough, (ii) refined and (iii) ultra-refined polishing. Rough polishing was carried out using diamond paste range 3 to 6 μm; Refined polishing using diamond paste range 0.5 a 1 μm and Ultra-refined polishing used Colloidal Silica range 0.25 μm.

APPENDIX E – Table of compounds and d-spacing (TEM)

Table of compounds found in particles extracted on carbon replica and identified through the d-spacing (JCPDS). Particles were extracted from steels with 0.6 % Cr and Cr-free and heat treated at 720; 740 and 780 ºC.

T (ºC)	0.6 % Cr Steel					0 % Cr Steel				
	d-spacing by TEM (nm)	Compound identified on JCPDS files				d-spacing by TEM (nm)	Compound identified on JCPDS files			
		Fe_3C	$Cr_{23}C_6$	TiC	Cr_7C_3		Fe_3C	$Cr_{23}C_6$	TiC	Cr_7C_3
720	0.2590		$Cr_{23}C_6$			0.3536	Fe_3C			
	0.2493	Fe_3C		TiC		0.2736				
	0.2361		$Cr_{23}C_6$			0.2652				
	0.2257		$Cr_{23}C_6$		Cr_7C_3	0.2495	Fe_3C		TiC	
	0.2126	Fe_3C	$Cr_{23}C_6$		Cr_7C_3	0.1860				
	0.2124	Fe_3C	$Cr_{23}C_6$		Cr_7C_3	0.1821	Fe_3C			
	0.2130	Fe_3C				0.1809	Fe_3C			
	0.1997	Fe_3C	$Cr_{23}C_6$		Cr_7C_3	0.1798				
	0.1816	Fe_3C	$Cr_{23}C_6$		Cr_7C_3	0.1756				
	0.1632	Fe_3C	$Cr_{23}C_6$			0.1725				
	0.1489	Fe_3C			Cr_7C_3	0.1507	Fe_3C			
	0.1391	Fe_3C				0.1275			TiC	
						0.1260			TiC	
740	Non Analysed					0.2530	Fe_3C			
						0.2470			TiC	
						0.2469			TiC	
						0.2012	Fe_3C			
						0.1985				
						0.1585	Fe_3C		TiC	
780	0.3122		$Cr_{23}C_6$							
	0.2361		$Cr_{23}C_6$							
	0.2257		$Cr_{23}C_6$		Cr_7C_3					
	0.2239				Cr_7C_3	0.1595			TiC	
	0.1852				Cr_7C_3	0.1580			TiC	

Source: Original.